12-2017

Chemical Reactions in the Gas Phase, Solution Phase and at Interfaces to Facilitate Mass Spectrometric Analysis and Rapid Synthesis

Stephen T. Ayrton
Purdue University

CHEMICAL REACTIONS IN THE GAS PHASE, SOLUTION PHASE AND AT INTERFACES TO FACILITATE MASS SPECTROMETRIC ANALYSIS AND RAPID SYNTHESIS

by

Stephen T. Ayrton

A Dissertation

Submitted to the Faculty of Purdue University

In Partial Fulfillment of the Requirements for the degree of

Doctor of Philosophy

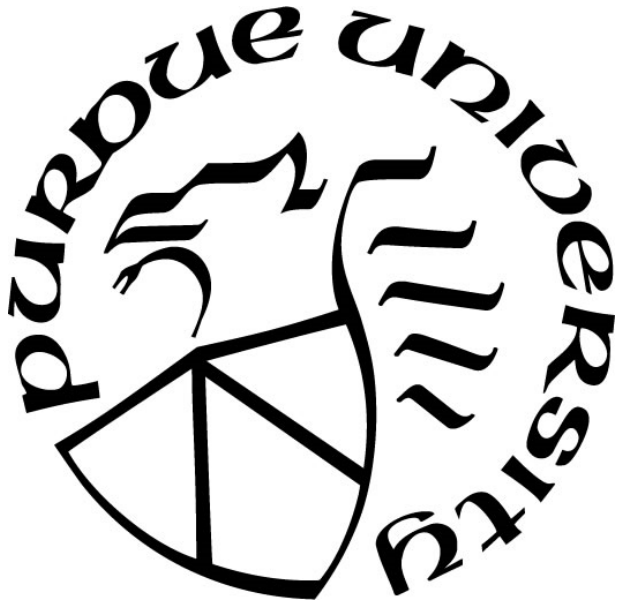

Department of Chemistry

West Lafayette, Indiana

December 2017

THE PURDUE UNIVERSITY GRADUATE SCHOOL

STATEMENT OF THESIS APPROVAL

Dr. R. Graham Cooks, Chair
Department of Chemistry
Dr. Mary Wirth
Department of Chemistry
Dr. Philip Low
Department of Chemistry
Dr. David Thompson
Department of Chemistry

Approved by:

Dr. Christine Hyrcyna
Head of the Departmental Graduate Program

To Isabelle

To Grandma Sylvia

To Mum

ACKNOWLEDGMENTS

I would not be where I am in life without the support of my family, particularly my Grandma, Sylvia, and my mother, Nicola. My gratitude and love for these two people will endure throughout my life and their contributions to who I am and what I have achieved cannot be overstated.

Lorna, my fiancée, who has had to endure our time apart has been an anchor to home. Our daughter, Isabelle, has brightened my life and is full of love, fun and games. Together, they make sure I have a reason to work towards the day I get to go home to them.

Another source invaluable of support was that of Dr. Richard Bowen, who during my formative years at Bradford University provided me with the foundation and education I needed to make a success of graduate school.

The graduate school experience is different for everyone in many ways and in others, it is very similar. The similarities and shared experiences include a love of science and a passion for discovery. Ryan Bain, Anyin Li and Josh Wiley are three people in particular who have served as inspiration and provided invaluable guidance. Adam Hollerbach was an indispensable ally on the project for Siemens Healthcare; working on that project with him cemented a great friendship which I value greatly. Recently Rob Schrader has has contributed in no small part to the work in this thesis on accelerated reactions in a rotary evaporator, for which I am very grateful.

Ben Martin, a fellow graduate student, has in one way or another shared my graduate school experience from day one. Without his friendship, graduate school would have been a far more difficult experience. Similar things can be said about my friendships with Ryan Bain, Patrick Fedick, and Kiran Iyer who made my last couple of years in graduate school far more enjoyable.

I thank the entire Aston Labs family. Brandy McMasters, Dalton Snyder, David Logsdon, Valentina Pirro, Karen Yannell, Bas Teunissen and Ryan Espy are all specific members of that family who have made the experience of working here great. Thank you all.

Finally, thank you to Dr. Cooks, who gave me the opportunity to study at Purdue, the resources to conduct my research and the stimulus to move outside of my comfort zone and tackle tough problems in the lab.

TABLE OF CONTENTS

LIST OF TABLES

LIST OF FIGURES

LIST OF SCHEMES

ABSTRACT

Author: Ayrton, Stephen T. Ph.D.
Institution: Purdue University
Degree Received: November 2017
Title: Chemical Reactions in the Gas Phase, Solution Phase and at Interfaces to Facilitate Mass Spectrometric Analysis and Rapid Synthesis
Major Professor: R. Graham Cooks

Chemical derivatization is the act of taking an analyte and transforming it into something with more desirable properties, typically for analytical purposes. In the cases presented here, the desirable properties are those which increase the ionization efficiency of the species of interest or those which facilitate the discrimination of isomers.

Nanoparticles are often utilized in biological assays, but unless they are made of metal such that they can be ionized directly by inductively coupled plasma (ICP) ionization, they are undetectable by mass spectrometry. Surface functionalization of silica nanoparticles (SiNPs) facilitates the reversible binding of highly ionizable molecules which can serve as reporters for the presence of the particle. This constitutes chemical derivatization. In this dissertation, the synthesis of imidazolium salts for use as chemical derivatization reagents (mass labels) is reported. They were designed to be synthesized quickly and cheaply and bind reversibly to amine and diol functionalized nanoparticles. The “pre-charged” (imidazolium) nature of the labels facilitates excellent limits of detection (1 nM). Binding and release of the mass labels from nanoparticles is demonstrated and analysis of the loading and release efficiency is conducted.

Isobaric amino acids in the backbone of a peptide are difficult to determine. The prime example of a problematic isobaric pair of amino acids is the coding aspartic acid (Asp) and the product of its post-translational modification, isoaspartic acid (isoAsp). Reported here is the use of a common reagent which binds carboxylic acids, substituted carbodiimide, to determine the

percentage of isoAsp in a sample of peptide. The carbodiimide is added to a solution of the peptide and it binds the carboxylate of the Asp or isoAsp residue. The resulting acylisourea (AiU) is ionzed and, in the gas phase, it rearranges via a 1-3 acyl shift to yield an *N*-acylurea (NAU). The AiU and NAU yield different fragment ions and so even though they are isobaric, they can be differentiated via collision induced dissociation (CID) product ion mass spectrometry. Importantly, the AiU derived from isoAsp rearranges more slowly to NAU than the AiU from derived from Asp. The rearrangement occurs on the timescale of the MS experiment (milliseconds) and so can be affected by the residence time of ions in the ion trap, the bandwidth of the isolation waveform, the potential offset applied to the transfer optics in the high-pressure region of the atmospheric pressure interface and the amplitude of the activation waveform.

Saturated alkanes are a third example of analytes which pose a problem to mass spectrometry. They are completely inaccessible to spray-based ionization methods and often require specialized equipment or niche methods for ionization. Field ionization persists as the gold-standard in hydrocarbon ionization and atmospheric pressure chemical ionization (APCI) continues to develop in the field. Typical products of APCI of saturated hydrocarbons are hydride abstraction ($[M-H]^+$), nitric oxide addition ($[M+NO]^+$) or electron abstraction ($M^{+\cdot}$). This dissertation reports the chemical derivatization of saturated hydrocarbons by selective fixation of nitrogen (to generate ions of the formula $[M+N]^+$) or oxygen (to generate ions of the formula $[M+O-H]^+$). The standard Waters APCI-Gas Chromatography (APGC) ion source was used to affect this chemistry. The oxidation process was shown to be regioselective and energetic enough to induce C-C bond cleavage. The off-line collection of ketones and aldehyde fragments of those ketones is reported. Subsequent analysis of the collected species shows that even outside of the mass spectrometry experiment, the chemistry is regioselective. The ion chemistry leading to

oxidation is elucidated as an ion/molecule reaction between charged hydrocarbons and neutral ozone.

Spray-based mass spectrometry has yielded interesting insights into the acceleration of reaction rates at the interface between small charged droplets and air. Other developments have included accelerated reactions in thin films. The phase of the reaction at the point of acceleration is explored in this dissertation by utilizing the Fischer Indole Synthesis under conditions which produce different products depending on the phase in which the reaction takes place.

Reaction acceleration has typically been conducted on the small-scale. Production of milligrams of material per hour has been demonstrated with spray-based ionization sources but this scale still does not represent synthetically useful quantities. Discussed herein is the scale-up of the accelerated Claisen-Schmidt and Katritzky reactions as well as the acceleration of ester hydrolysis and imine formation in a rotary evaporator. The Suziki reaction is also demonstrated to undergo reaction acceleration at the interface of chloroform and water; a biphasic system commonly encountered in a separating funnel during the normal workflow of the synthetic organic chemist.

.

CHAPTER 1. INTRODUCTION

1.1 Overview

As long as an analytical technique exists, there will be a drive to apply it to the analysis of difficult and apparently inaccessible analytes. Analytical chemists do battle with limits of detection on a daily basis, adapting and refining known methodologies to better serve the requirements of the study. Mass spectrometry (MS) has proven time and again to be an exceptionally sensitive technique, with good linear dynamic range. The analytical limits of detection achieved by MS are exceptional for most species, depending on the ionization method, reaching parts-per-billion levels routinely and its ability to provide information on chemical structure through the analysis of data produced by tandem mass spectrometry (MS/MS or MS^n) experiments is remarkable[1-2].

Collision induced dissociation, the technique which elevated mass spectrometry from niche analytical technique to widespread analytical tool, represented at the time a way to detect structural characteristics of ions which were otherwise undetectable by mass spectrometry[3-5].

The dissociation of ions led researchers to mix-and-match sector components in order to make a plethora of different measurements. Notably, thermochemical measurements became feasible[6-7]. Prior to this development, the ability to determine the energy associated with the cleavage of a bond within an ion represented a completely inaccessible measurement.

As the analytical challenges presented to mass spectrometry became more and more complex, so too did the instrumentation and the theory driving the research. Originally, sector instrumentation, which was relatively easy to understand but difficult to tune, was replaced with electrodynamic devices such as the quadrupole mass filter, which are difficult to understand but easy to tune (though only by virtue of the control software). In the same stroke, it took the mainstream of mass spectrometric analysis from the high mass accuracy of sectors to the low mass

accuracy of quadrupoles. The onward march to high resolution electrostatic analyzers led back to high mass accuracy; time of flight (ToF) and Orbitrap mass analyzers are now being used to detect the previously undetectable in the realms of proteomics[8-9], to name but one significant field of research.

Mass accuracy can contribute only so much, however, and detection of molecular properties such as chirality remained out of the reach of mass spectrometry until the kinetic method[10], which relies on the chemical association and subsequent fragmentation characteristics of metals and organic molecules, was appropriately applied. The resulting measurement is thermochemical in nature and has been refined and applied to monitoring chiral degradation[11] as well as the analysis of every naturally occurring hexose[12]; previously indistinguishable by MS.

Chemical cross-linkers, which report spatial relationships between the residues of a protein and preserve those relationships for detection after digestion, probably represent the most prolific field of research into chemical derivatization[13-14]. This is a clear example of the utility of clever chemical derivatization to detect the otherwise undetectable.

Electrospray ionization (ESI)[15], which serves to create a nebulous plume of charged droplets from a solution containing, usually, the polar analyte(s) of interest, represented a major breakthrough in the field of mass spectrometry. Understanding ESI has proven to be no easy task[16-19] and still, it is not fully understood. The efforts to derivatize reagents in preparation for electrospray-based MS analysis has received no small amount of attention, as a series of reviews by Van Berkel demonstrates[20-23].

One significant challenge that remains is the analysis of post translational modifications in proteins and peptides, specifically those which produce isobaric structural isomers. Often, isobaric peptides reside within a complex mixture of other peptides from a protein digest and can only be

ionized by ESI. Chapter 2 of this thesis deals with the determination of isoaspartate (which is almost always indistinguishable from its aspartate precursor[24]) in a peptide backbone.

Nanoparticles are ever more frequently being utilized for drug delivery[25] and bioassays[26-27], amongst a multitude of other things. The detection of naoparticulate matter in general will likely present itself as one of the major analytical challenges of the 21st century[28]. Mass spectrometry has the ability to report on metal nanoparticles when coupled with inductively coupled plasma ionization (ICP)[29], where metals of any kind are ablated to their oxidized constituent atoms. Though ESI-mass spectrometry is blind to silica nanoparticles, the paradigm of chemical derivatization may be able to facilitate their detection by mass spectrometry if an appropriate combination of chemistries is implemented. Chapter 3 of this dissertation demonstrates a new way of combining functionalized silica nanoparticles with appropriately designed small molecules to form the foundation of what could be used for nanoparticulate assays in the future.

The analysis of saturated hydrocarbon species poses a particular challenge to mass spectrometrists. Not only are hydrocarbon samples some of the most complex in nature[30], most of the components are not ionizable and ESI can only access the polar components[31]. There has been a plethora of ionization methods and derivatization chemistries reported for such samples[31-38], and many of these are very effective, but they are generally restricted to research laboratories.

So resistant is the problem of hydrocarbon analysis to general solution by mass spectrometry that the decades-old technique of field ionization (FI) is still considered to be the gold-standard of analysis[39-41]. Ambient plasmas are currently under study for their figures of merit with regard to the ionization of these difficult substrates, but carefully controlled conditions are necessary in order to generate reproducible results[42-43].

Chapter 4 of this dissertation details the oxidation of saturated hydrocarbons in a standard, commercial atmospheric pressure chemical ionization source with only one, simple, non-destructive addition to the setup; the addition of a line through which air can be leaked. The complex chemistry leading to oxidation is explored and reported in the hope that it provides a foundation for further understanding of the complex nature of the interactions between ambient plasmas and hydrocarbons.

After the development of electrospray ionization (ESI), the concept of ambient ionization was a sizeable step towards simplifying and making available ionization sources which were not only versatile, but cheap[2, 44]. From desorption electrospray ionization (DESI)[45] to paper spray ionization[44], fast analysis in the open air has become a paradigm of its own in mass spectrometry.

The observation of unusually fast reactions, first recorded using DESI[46], has provoked the study of such phenomena[46-52]. If reaction rates can be accelerated in a general sense, without the need of a specific chemical catalyst, then the synthesis of many important molecules might be done in a green and efficient fashion.

In some cases, the systems typically employed to accelerate reactions, such as thin films[53] and emulsions[54], could conceivably be found in the every-day workflow of the synthetic organic chemist, rather than in the niche, charged microdroplet environment. In a rotary evaporator, for instance, thin films are generated as solvent is removed under reduced pressure. In a separating funnel, temporary micro-emulsions are formed which constitute a system similar to that studied by Sharpless *et al.*[54]. Chapter 5 of this dissertation presents an initial exploration of reaction acceleration under such conditions, including the acceleration of the metal-catalyzed Suzuki reaction in an emulsion.

In summary, this dissertation covers reactions between chemicals in the gas phase, the solution phase, and at interfaces to facilitate chemical analysis of difficult substrates and fast chemical synthesis at scale.

1.2 References

1. Qu, M.; An, B.; Shen, S.; Zhang, M.; Shen, X.; Duan, X.; Balthasar, J. P.; Qu, J., Qualitative and quantitative characterization of protein biotherapeutics with liquid chromatography mass spectrometry. *Mass Spectrom. Rev.* **2017,** *36* (6), 734-754.

2. Ferreira, C. R.; Yannell, K. E.; Jarmusch, A. K.; Pirro, V.; Ouyang, Z.; Cooks, R. G., Ambient Ionization Mass Spectrometry for Point-of-Care Diagnostics and Other Clinical Measurements. *Clin. Chem.* **2016,** *62* (1), 99-110.

3. Cooks, R. G., Collision-nduced Dissociation: Readings and Commentary. *J. Mass Spectrom.* **1995,** *30*, 1215-1221.

4. Bozorgzadeh, M. H.; Morgan, R. P.; Beynon, J. H., Application of Mass-analysed Ion Kinetic Energy Spectrometry (MIKES) to the Determination of the Structures of Unknown Compounds. *Analyst* **1978,** *103*, 613-622.

5. Senko, M. W.; Speir, J. P.; McLafferty, F. W., Collisional Activation of Large Multiply Charged Ions Using Fourier Transform Mass Spectrometry. *Anal. Chem.* **1994,** *66*, 2801-2808.

6. Armentrout , P. B., Mass Spectrometry - Not Just a Structural Tool: The Use of Guided Ion Beam Tandem Mass Spectrometry to Determine Thermochemistry. *J. Am. Soc. Mass. Spectrom.* **2002,** *13*, 419-434.

7. Cooks, R. G.; Patrick, J. S.; Kotisho, T.; McLuckey, S. A., Thermochemical Determintations by the Kinetic Method. *Mass Spectrom. Rev.* **1994,** *13*, 287-339.

8. Yang, Y.; Franc, V.; Heck, A. J. R., Glycoproteomics: A Balance between High-Throughput and In-Depth Analysis. *Trends Biotechnol.* **2017,** *35* (7), 598-609.

9. Lamond, A. I.; Uhlen, M.; Horning, S.; Makarov, A.; Robinson, C. V.; Serrano, L.; Hartl, F. U.; Baumeister, W.; Werenskiold, A. K.; Andersen, J. S.; Vorm, O.; Linial, M.; Aebersold, R.; Mann, M., Advancing cell biology through proteomics in space and time (PROSPECTS). *Mol Cell Proteomics* **2012,** *11* (3), O112 017731.

10. Cooks, R. G.; Wong, P. S. H., Kinetic Method of Making Thermochemiclal Determinations: Advances and Applications *Acc. Chem. Res.* **1998,** *31* (7), 379-386.

11. Bain, R. M.; Yan, X.; Raab, S. A.; Ayrton, S. T.; Flick, T. G.; Cooks, R. G., On-line chiral analysis using the kinetic method. *Analyst* **2016,** *141* (8), 2441-6.

12. Nagy, G.; Pohl, N. L., Complete hexose isomer identification with mass spectrometry. *J. Am. Soc. Mass. Spectrom.* **2015,** *26* (4), 677-85.

13. Leitner, A., A review of the role of chemical modification methods in contemporary mass spectrometry-based proteomics research. *Anal. Chim. Acta* **2017,** *In Press*, 1-18.

14. Liu, F.; Heck, A. J., Interrogating the architecture of protein assemblies and protein interaction networks by cross-linking mass spectrometry. *Curr Opin Struct Biol* **2015,** *35*, 100-8.

15. Fenn, J. B., Electrospray wings for molecular elephants (Nobel lecture). *Angew. Chem. Int. Ed. Engl.* **2003,** *42* (33), 3871-94.

16. de la Mora, J. F., Electrospray ionization of large multiply charged species proceed via Dole's charged residue mechanism. *Anal. Chim. Acta* **2000,** *406*, 93-104.

17. Nguyen, S.; Fenn, J. B., Gas-phase ions of solute species from charged droplets of solutions. *PNAS* **2007,** *104* (4), 1111-1117.

18. Wong, S. F.; Meng, C. K.; Fenn, J. B., Multiple Charging in Electrospray Ionization of Poly(ethylene glycols). *J. Phys. Chem.* **1988,** *1988*, 546-550.

19. Iribarne, J. V.; Thompson, B. A., On the evaporation of small ions from charged droplets. *The Journal of Chemical Physics* **1976,** *64* (6), 2287-2294.

20. Quirke, J. M. E.; Adams, C. L.; Van Berkel, G. J., Chemical Derivatization for Electrospray Ionization Mass Spectrometry. 1. Alkyl Halides, Alcohols, Phenols, Thiols, and Amines. *Anal. Chem.* **1994,** *66*, 1302-1315.

21. Van Berkel, G. J., Derivatization for Electrospray Ionization Mass Spectrometry. 3. Electrochemically Ionizable Derivatives. *Anal. Chem.* **2998,** *70*, 1544-1554.

22. Van Berkel, G. J.; Asano, K. G., Chemical Derivatization for Electropray Ionixation Mass Spectrometry. 2. Aromatic and Highly Conjugated Molecules *Anal. Chem.* **1994,** *66*, 2096-2102.

23. Van Berkel, G. J.; Quirke, J. M. E.; Adams, C. L., Derivatization for electrospray ionization-mass spectrometry. 4. Alkenes and alkynes. *Rapid Commun. Mass Spectrom.* **2000,** *14*, 849-858.

24. Liu, M.; Cheetham, J.; Cauchon, N.; Ostovic, J.; Ni, W.; Ren, D.; Zhou, Z. S., Protein isoaspartate methyltransferase-mediated 18O-labeling of isoaspartic acid for mass spectrometry analysis. *Anal. Chem.* **2012,** *84* (2), 1056-62.

25. Dai, Y.; Xu, C.; Sun, X.; Chen, X., Nanoparticle design strategies for enhanced anticancer therapy by exploiting the tumour microenvironment. *Chem. Soc. Rev.* **2017,** *46* (12), 3830-3852.

26. Zhao, X.; Hillard, L. R. M., S. J.; Wang, Y.; Bagwe, R.; Jin, S.; Tan, W., A rapid bioassay for single bacterial cell quantitation using bioconjugated nanoparticles. *PNAS* **2004,** *101*, 15027-15032.

27. Li, H.; Xu, D., Silver nanoparticles as labels for applications in bioassays. *TrAC, Trends Anal. Chem.* **2014,** *61*, 67-73.

28. Yin, Y.; Tan, Z.; Hu, L.; Yu, S.; Liu, J.; Jiang, G., Isotope Tracers To Study the Environmental Fate and Bioaccumulation of Metal-Containing Engineered Nanoparticles: Techniques and Applications. *Chem. Rev.* **2017,** *117* (5), 4462-4487.

29. Montano, M. D.; Olesik, J. W.; Barber, A. G.; Challis, K.; Ranville, J. F., Single Particle ICP-MS: Advances toward routine analysis of nanomaterials. *Anal Bioanal Chem* **2016,** *408* (19), 5053-74.

30. Wu, Z.; Rodgers, R. P.; Marshall, A. G., Comparative Compositional Analysis of Untreated and Hydrotreated Oil by Electrospray Ionization Fourier Transform Ion Cyclotron Resonance Mass Spectrometry. *Energy Fuels* **2005,** *19*, 1072-1077.

31. Zhan, D.; Fenn, J. B., Electrospray mass spectroemtry of fossil fuels. *Int. J. Mass spectrom.* **2000,** *194*, 197-208.

32. Duan, P.; Fu, M.; Pinkston, D. S.; Habicht, S. C.; Kenttamaa, H. I., Gas-Phase Reactions of ClMN(H2O)+ with Polar and Nonpolar Hydrocarbons in a Mass Spectrometer. *J. Am. Chem. Soc.* **2007,** *129*, 9266-9267.

33. Fialkov, A. B.; Gordin, A.; Amirav, A., Hydrocarbons and fuels analyses with the supersonic gas chromatography mass spectrometry--the novel concept of isomer abundance analysis. *J. Chromatogr. A* **2008,** *1195* (1-2), 127-35.

34. Hsu, C. S.; Qian, K., CS2 Charge Exchange as a Low-Energy Ionization Technique for Hydrocarbon Characterization. *Anal. Chem.* **1993,** *65*, 767-771.

35. Roussis, S. G.; Fitzgerald, W. P.; Cameron, A. S., Low-energy Ionization of Hydrocarbons in the Quadrupole Ion Trap Mass Spectrometer. *Rapid Commun. Mass Spectrom.* **1998,** *12*, 373-381.

36. Wu, C.; Qian, K.; Walters, C. C.; Mennito, A., Application of atmospheric pressure ionization techniques and tandem mass spectrometry for the characterization of petroleum components. *Int. J. Mass spectrom.* **2015,** *377*, 728-735.

37. Wu, C.; Qian, K.; Nefliu, M.; Cooks, R. G., Ambient analysis of saturated hydrocarbons using discharge-induced oxidation in desorption electrospray ionization. *J. Am. Soc. Mass. Spectrom.* **2010,** *21* (2), 261-7.

38. Jjunju, F. P. M.; Badu-Tawiah, A. K.; Li, A.; Soparawalla, S.; Roqan, I. S.; Cooks, R. G., Hydrocarbon analysis using desorption atmospheric pressure chemical ionization. *Int. J. Mass spectrom.* **2013,** *345-347*, 80-88.

39. Hsu, C. S.; Green, M., Fragment-free accurate mass measurement of complex mixture componentd bu gas-chromatography/field ionization-orthogonal acceleration time-of-flight mass spectrometry: an unprecedented capability for mixture analysis. *Rapid Commun. Mass Spectrom.* **2001**.

40. Liang, Z.; Hsu, C. S., Molecular Speciation of Saturates by On-Line Liquid Chromatography-Field Ionization Mass spectrometry *Energy Fuels* **1998,** *12*, 637-643.

41. Scheppele, S. E.; Hsu, C. S.; Marriott, T. D.; Benson, P. A.; Detwiler, K. N., Field-Ionization Relative Sensitivities for the Analysis of Saturated Hydrocarbons from Fossil-Energy-Related Materials. *International Journal of Mass Spectrometry and Ion Physics* **1978,** *28*, 335-346.

42. Jin, C.; Viidanoja, J.; Li, M.; Zhang, Y.; Ikonen, E.; Root, A.; Romanczyk, M.; Manheim, J.; Dziekonski, E.; Kenttamaa, H. I., Comparison of Atmospheric Pressure Chemical Ionization and Field Ionization Mass Spectrometry for the Analysis of Large Saturated Hydrocarbons. *Anal Chem* **2016,** *88* (21), 10592-10598.

43. Xie, X.; Wang, Z.; Li, Y.; Zhan, L.; Nie, Z., Investigation and Applications of In-Source Oxidation in Liquid Sampling-Atmospheric Pressure Afterglow Microplasma Ionization (LS-APAG) Source. *J. Am. Soc. Mass. Spectrom.* **2017,** *28* (6), 1036-1047.

44. Ifa, D. R.; Wu, C.; Ouyang, Z.; Cooks, R. G., Desorption electrospray ionization and other ambient ionization methods: current progress and preview. *Analyst* **2010,** *135* (4), 669-81.

45. Takats, Z.; Wiseman, J. S.; Gologan, B.; Cooks, R. G., Mass Spectrometry Sampling Under Ambient Conditions with Desorption Electrospray Ionization. *Science* **2004,** *306*, 471-473.

46. Girod, M.; Moyano, E.; Campbell, D. I.; Cooks, R. G., Accelerated bimolecular reactions in microdroplets studied by desorption electrospray ionization mass spectrometry. *Chem. Sci.* **2011,** *2* (3), 501-510.

47. Yan, X.; Bain, R. M.; Cooks, R. G., Organic Reactions in Microdroplets: Reaction Acceleration Revealed by Mass Spectrometry. *Angew. Chem. Int. Ed. Engl.* **2016,** *55* (42), 12960-12972.

48. Lee, J. K.; Kim, S.; Nam, H. G.; Zare, R. N., Microdroplet fusion mass spectrometry for fast reaction kinetics. *Proc Natl Acad Sci U S A* **2015,** *112* (13), 3898-903.

49. Bain, R. M.; Pulliam, C. J.; Thery, F.; Cooks, R. G., Accelerated Chemical Reactions and Organic Synthesis in Leidenfrost Droplets. *Angew. Chem. Int. Ed. Engl.* **2016,** *55* (35), 10478-82.

50. Crawford, E. A.; Esen, C.; Volmer, D. A., Real Time Monitoring of Containerless Microreactions in Acoustically Levitated Droplets via Ambient Ionization Mass Spectrometry. *Anal Chem* **2016,** *88* (17), 8396-403.

51. Muller, T.; Badu-Tawiah, A.; Cooks, R. G., Accelerated carbon-carbon bond-forming reactions in preparative electrospray. *Angew. Chem. Int. Ed. Engl.* **2012,** *51* (47), 11832-5.

52. Badu-Tawiah, A. K.; Campbell, D. I.; Cooks, R. G., Accelerated C-N bond formation in dropcast thin films on ambient surfaces. *J. Am. Soc. Mass. Spectrom.* **2012,** *23* (9), 1461-8.

53. Yan, X.; Augusti, R.; Li, X.; Cooks, R. G., Chemical Reactivity Assessment Using Reactive Paper Spray Ionization Mass Spectrometry: The Katritzky Reaction. *ChemPlusChem* **2013,** *78* (9), 1142-1148.

54. Narayan, S.; Muldoon, J.; Finn, M. G.; Fokin, V. V.; Kolb, H. C.; Sharpless, K. B., "On water": unique reactivity of organic compounds in aqueous suspension. *Angew. Chem. Int. Ed. Engl.* **2005,** *44* (21), 3275-9.

CHAPTER 2. DETERMINATION OF ISOBARIC PEPTIDES

2.1 Introduction

Mass spectrometry dominates the field of peptide and protein sequencing, with the proteomics field basing its success on the chemical specificity and selectivity of the technique[1-3]. Isobaric amino acids pose particular analytical challenges to mass spectrometric analysis[4]. Their significance is clear; if protein structure and therefore function is to be understood, then the sequence of that protein must be known unambiguously. Isomers in general can confound accurate assignment of structure by mass spectrometry, particularly when they do not produce different spectral features upon fragmentation.

Isobaric amino acids don't only include coding residues such as leucine and isoleucine, but also include the precursor and product of one post translational modification; aspartate and isoaspartate, which is a non-coding β amino acid. This residue can pose significant problems to mass spectrometry; not only is it difficult to determine from its isomer, it is often present only at low abundance relative to aspartate.

In vitro and *in vivo* isomerization of aspartate (Asp) to isoaspartate (isoAsp) is one of the main routes to protein degradation. The spontaneous, post-translational generation of isoAsp poses an immediate problem to the development of biopharmaceuticals[4-5], where shelf-life and activity may be directly affected. In fact, isoAsp generation is one of the most common contributors to heterogeneity in protein-based drugs. Factors which promote the generation of isoAsp include pH, secondary and tertiary protein structure and method of formulation.

Methods for the detection of isoAsp vary in complexity. An enzymatic, fluorescence based assay has recently been reported by Puri *et al.*[6]; it has a significant time requirement. HPLC has been used to separate Asp/isoAsp containing peptides; the success of this method largely relies on

changes in the secondary structures of medium or large peptides associated with isomerization[7]. Circular dichroism, X-Ray crystallography and nuclear magnetic resonance are primary tools for the study of β peptides[8-9]. Mass spectrometric methods also not uncommon. Specifically, they include electron transfer dissociation (ETD), electron capture dissociation (ECD) and ^{18}O labeling. ETD[10] and ECD yield specific fragment ions for isoAsp, facilitating detection. Methods of ^{18}O labeling[4] involve the selective enzymatic conversion of isoAsp to the succinimide intermediate, followed by hydrolysis with $H_2{}^{18}O$.

Recently, matrix-assisted laser desorption/ionization mass spectrometry (MALDI-MS) has been utilized to differentiate beta peptides[11]. Utilizing in-source decay, a pseudo tandem mass spectrometry technique, Yu *et al.* were able to observe specific reaction and subsequent fragmentation of Asp/isoAsp with 1,5-diaminonaphthalene (1,5-DAN)[11]. This method yielded similar fragmentation to that of ETD, but did not require specialized equipment. Issues with MALDI include poor signal/noise in the low mass range and poor performance with regard to quantitation. High resolution ion mobility has also very recently been documented as a viable technique for the determination of aspartate and isoaspartate[12]. The results from this technique are apparently excellent, but the equipment is still not widely available.

One of the oldest questions in tandem mass spectrometry has been whether an ion undergoes a specific rearrangement before dissociation. McLafferty in 1959 reported the best-known version of this paradigm with the (subsequently) eponymous McLafferty rearrangement[13]. That example permitted the determination of the structural arrangements of functional groups in particular ions.

Rearrangements, if non-specific, can also be detrimental[13], for example deuterium scrambling can convolute isotope dilution experiments or the interpretation of fragmentation

pathways. Some of the more important rearrangements arise from fragmentation of intermediates known as ion-neutral complexes[14].

This study utilizes typical carboxylic acid coupling reagents, namely carbodiimides, to derivatize aspartate/isoaspartate bearing peptides. The discussion will focus on the use of 1-ethyl-3-(3-dimetylaminopropyl)carbodiimide (EDC). While this reagent is usually used to couple carboxylic acids with amines to form amides, it also exhibits by-product formation by rearrangement[15]. The major by-product of EDC-bound peptides (which are acylisoureas, AiUs) is *N*-acylurea (NAU) formed by O–N migration at the carboxylate to which EDC is bound.

Some groups have studied this rearrangement for synthetic purposes, while others have studied it because it interferes with the intended coupling reaction[15-24]. In the former case, some specific examples exist of the formation of isocyanates and amides as by-products under elevated temperatures in the condensed phase[23]. This reactivity has parallels to the results presented here. In any case, Studies of AiU are difficult because it is thought to exist kinetically as a steady-state intermediate in reactions in which it participates[18].

1-Ethyl-3-(3-dimethylaminopropyl)carbodiimide (EDC) was used in this work to label the carboxylate group of an aspartate/isoaspartate residue within a peptide backbone. The ionized molecule undergoes interconversion through a 1,3-acyl shift in the gas-phase. The AiU to NAU conversion is shown to occur at a higher rate for aspartate relative to iso-aspartate, facilitating semi-quantitative determination of the ratio of the isomeric residues in otherwise equivalent peptides.

2.2 Results and Discussion

2.2.1 Gas-phase Ion Chemistry to Determine isoAspartate in a Peptide Backbone

Peptides bearing an Asp residue have a very specific arrangement of functional groups relative to those bearing the isoAsp residue. IsoAsp is a β peptide while Asp is a naturally occurring α peptide. This difference changes the chemistry of the residue, particularly with regard to the sterics of the system.

Figure 2.1 shows the CID product ion mass spectra of Ala-Leu-Asp-Gly-Lys (ALDGK) and Ala-Leu-isoAsp-Gly-Lys (ALDisoGK), each bound to EDC.

Detected in the mass spectra is the ratio of isobaric fragments. AiU fragments differently to NAU, so even though they are isobaric, the ratio of the fragments can be used to calibrate the amount of each species present. The fragmentation pathways are shown in Scheme 2.1.

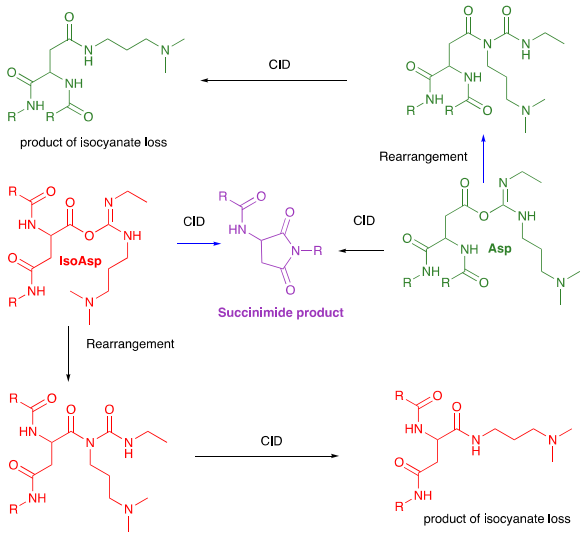

Scheme 2.1 Loss of urea from protonated AiU ions and loss of isocyanate from NAU ions. Red structures correspond to the isoAsp pathway. Green structures correspond to the Asp pathway. Purple structure is the common succinimide fragment. Blue arrows are the preferred reaction pathways

The two spectra shown in Figure 2.1 are distinctly different; that of the isoAsp containing peptide is dominated by the fragment of AiU to give a succinimide product at *m/z* 485, while the spectrum of the Asp containing peptide is dominated by the fragment of NAU to give an amide product ion at *m/z* 587. A less-dominant fragment ion signal corresponds to the loss of 3-dimethylaminopropylisocyanate (*m/z* 530), which simply corresponds to the fragment of NAU when the N-O migration sequesters the other available nitrogen in the EDC moiety.

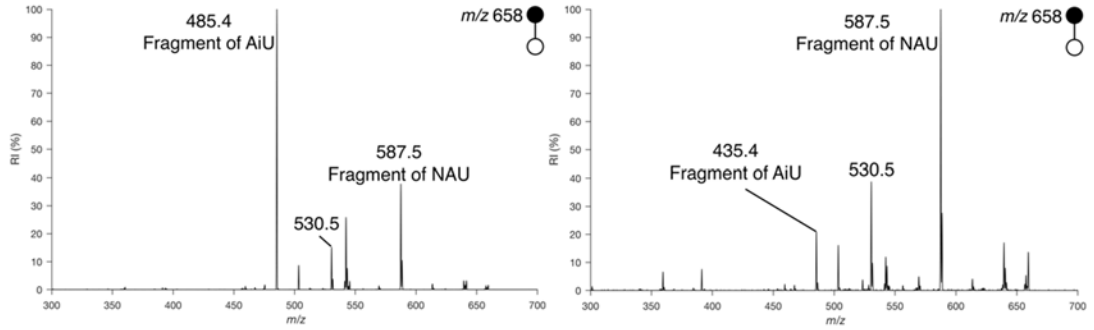

Figure 2.1 Product ion MS/MS spectra due to CID of the protonated peptides (left) Ala-Leu-isoAsp-Gly-Lys (ALDisoGK) and (right) Ala-Leu-Asp-Gly-Lys (ALDGK) giving characteristic fragment ions 1 (m/z 485) and 2 (m/z 587), respectively, the structures of which are shown in Scheme 1

It is possible that the EDC could bind the C-terminal of the peptide, and that it does so preferentially for either aspartate or isoaspartate. Fragmentation of the hypothetical AiU resulting from C-terminus binding of EDC could in principle produce an ion at *m/z* 485. This fragment would not be diagnostic, as it would not be the result of fragmentation of the isomeric residue, so it was necessary to obtain evidence of the structure of the ion which yields that signal.

The MS^3 spectrum of the postulated succinimide fragment ion (*m/z* 485) was recorded. In the full scan (i.e. from the bulk material in solution), a signal corresponding to the dehydrated peptide is also present at *m/z* 485. The MS^2 product ion spectrum of the dehydrated peptide in the

bulk solution was compared with the MS^3 spectrum recorded from the corresponding ion generated from the first stage of fragmentation of ALDGK-EDC. These two spectra are shown in Figure 2.2.

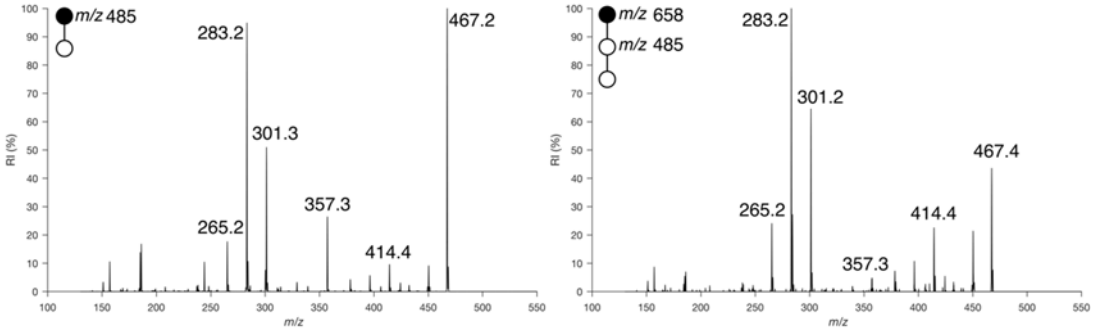

Figure 2.2: MS^2 spectrum of the ion corresponding to the mass of dehydrated peptide in the bulk ALDGK-EDC solution (left) and MS^3 spectrum of the ion corresponding to the mass of dehydrated peptide produced by fragmentation of carbodiimide bound ALDGK(right)

While the spectra are not identical, they share the same signals. In this case, where one of the spectra is produced by a second stage of fragmentation, the mismatch in spectral profiles is understandable. In all likelihood, these ions have the same structure. To probe the structure of the bulk-phase material (and so extrapolate to the structure of the fragment), phenylhydrazine was added to the solution. Phenylhydrazine was chosen as a reagent to open the succinimide according to Figure 2.3. The product ion mass spectrum of the reacted species was then recorded and interpreted.

The fragment ions at *m/z* 390 and 392 correspond to structures which contain a bond between phenylhydrazine and the carboxylate functional group of aspartate.

The only way these ions could be produced is via succinimide ring opening with phenylhydrazine. The ion at *m/z* 485 corresponds to ejection of the phenylhydrazine via re-formation of the succinimide and the ion at *m/z* 467 corresponds to subsequent fragmentation of that species, as do ions at *m/z* 301 and 283 (see MS^2 spectra in Figure 2.2).

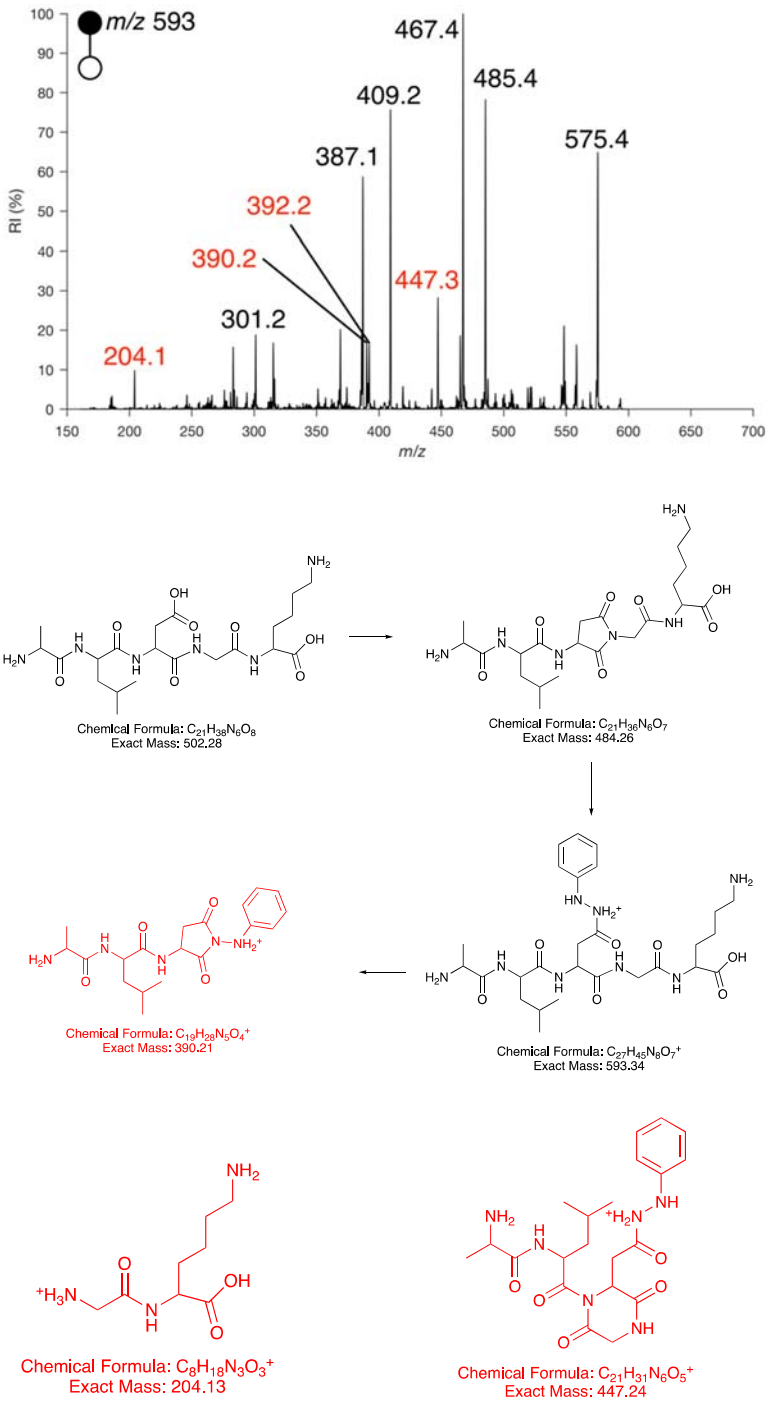

Figure 2.3 MS^2 spectrum of the phenylhydrazine derivatized, dehydrogenated peptide and important structures corresponding to the signals

The ion at *m/z* 204 corresponds to Gly-Lys, the two residues at the C-terminus of the peptide, which illustrates that phenylhydrazine was is not bound to the C-terminal of the peptide ion which produced this fragment. The ion at *m/z* 447 corresponds to the neutral loss of Lys, which is the C-terminal residue, which illustrates the same point.

The ion at *m/z* 409 is, in this case, non-diagnostic, as it corresponds to the loss of the *N*-terminal Ala-Leu residues from the phenylhydrazine-bound precursor ion, which would not exclude the possibility of phenylhydrazine binding to the C-terminus of the peptide.

Taken together, this evidence demonstrates that at least some portion of the population of ions which reacted with phenylhydrazine were the succinimide derived from the aspartate residue.

The difference in fragmentation ratios of EDC-bound peptides (as in Figure 2.1) can be recorded from a range of peptides, the data for which is presented in Table 2.1. Also included is data from a range of different carbodiimides, susch as dicyclohexyl- and diisopropyl-.

There remains the question of how the rearrangement from AiU to NAU takes place. In particular, it was necessary to determine whether it was a gas-phase or a solution-phase process and to what extent and by what means it could be controlled, and also why there was a difference between aspartate and isoaspartate derived AiU.

Figure 2.4 summarizes the effects of instrumental prarameters on the relative abundance of the fragment of AiU to the fragment of NAU. Three different MS operating parameters are used to vary the energy deposited in the EDC-bound pentapeptide ions.

The three parameters are: (i) The simplest and most common way to vary the energy deposition in ion trap CID experiments; the amplitude of the ac resonance signal used to excite the precursor ions. (ii) The isolation width used in the CID experiment; by decreasing the width of the isolation window, one is effectively heating the trapped ion population, a well-known effect. (iii)

The injection time (effectively the residence time of the ions before fragmentation); increasing this parameter allows the ions to undergo many more collisions and so obtain energy.

As the CID ac amplitude is increased in the case of the EDC adduct derived from ALDisoGK, the AiU fragment (giving *m/z* 485) is gradually matched in intensity by the NAU fragment (giving *m/z* 587). The same experiment with ALDGK shows that the fragment of NAU (*m/z* 587) is relatively competitive with the fragment of AiU (succinimide ion *m/z* 485) at any energy, i.e. it has appreciable abundance even at low ac amplitude, illustrating its greater propensity for rearrangement.

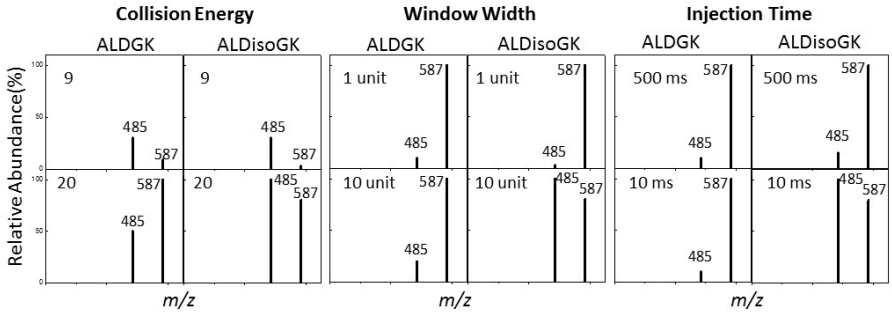

Figure 2.4 Relative formation of the two fragment ion m/z 485 and m/z 587 with repect to energy deposition varied by three instrunment parmeters 1) collison energy (arbitary CID energy), 2) isolation widow width, 3) injection time.

As the isolation width used in the MS/MS experiment is decreased, the ion population is expected to obtain more energy, though not enough to fragment, thereby facilitating rearrangement. Considering that the Asp containing peptide rearranges very efficiently regardless of the deposition of energy deposition, the effect of this parameter on peptides bearing that residue (as opposed to isoAsp) is relatively small (Figure 2.4). The effect of isolation width on the EDC-adduct of

ALDisoGK is pronounced, illustrating that the deposition of energy into that structure causes rearrangement of the ion population from AiU to NAU.

The result of changing the injection time parallel those of the other two methods; there is little effect on the Asp bearing peptide, as it rearranges so efficiently that it needs no encouragement, while the effect on isoAsp bearing peptides is profound. The final deposition of a large amount of energy into the structure to induce fragmentation facilitates the detection of the relative amount of AiU to NAU, which illustrates that the rearrangement takes place on a time scale far longer than that of a bond vibration.

The observation of strong influence of the reported operating parameters demonstrates that the rearrangement happens in the gas phase and that it happens on the timescale of the MS experiment (milliseconds), otherwise, such strong effects which differentiate Asp from isoAsp would not be encountered.

Mechanistically, there seems to be little to discriminate aspartate from isoaspartate as both can rearrange by a 1,3-acyl shift. Silverstein *et al.* have investigated this process and ruled out the production of NAU via a bimolecular reaction[15] (where an active carboxylic acid in AiU reacts directly with the nitrogen of another molecule of carbodiimide), which is supported in this experiment by the fact that it is highly unlikely that there would be effective collisions to generate such reactions between positively charged species in the ion trap, where the conversion between species can be affected. The apparent answer for the differential rate in the rearrangement of AiUs derived from Asp/isoAsp is sterics. Scheme 2.2 illustrates the steric argument. Simply put, there should be a higher steric barrier to the formation of NAU in the case of isoAsp, so AiU should be a more favorable structure, hence the observation of dominant fragments of AiU and the requirement of extra energy deposition to encourage conversion to NAU when isoAsp is present

in the peptide. In order to determine the validity of this hypothesis, different carbodiimides with different steric demands were used, and the effect recorded.

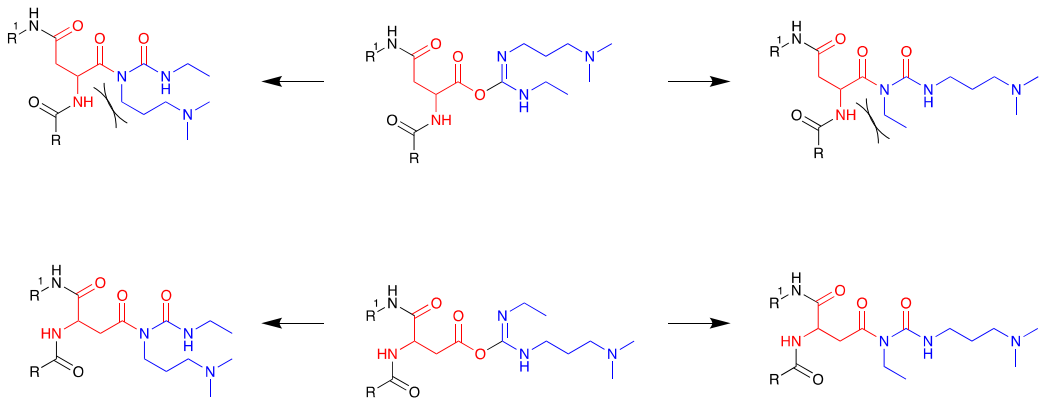

Scheme 2.2 Steric hindrance to rearrangement in isoAsp (top) and lack thereof in Asp (bottom)

Using the peptide system ALDGK, which by virtue of the aspartate residue should in this argument favor rearrangement without the requirement of extra energy deposition, and using instrumental conditions which provided the least opportunity for rearrangement (large isolation window, low injection time), the mass spectra of both EDC and DCC-bound ions were recorded. EDC-bound ions produced signals corresponding to the fragmentation of AiU and NAU, i.e. the ratio *m/z* 485 to *m/z* 587, was recorded. This ratio was about 1:5 (Figure 2.1). When DCC, a more sterically demanding carbodiimide, was used, the signal corresponding to the fragmentation of AiU was dominant in the mass spectrum; the recorded ratio was 1:0.22 in this case, on the order of a 10-fold difference (Table 2.1).

These results are interpreted as evidence that the more sterically demanding carbodiimide rearranges to the NAU less favourably. It should be noted that there was still a significant difference between the mass spectra of the DCC adducts of ALDGK and ALDisoGK, with the

fragments of the NAU ion in the Asp-bearing species being just under 10x that of the isoAsp-bearing species (Table 2.1).

Protonation is the typical route to positively charged ions. It was mechanistically interesting to determine if the proton was important to the differences in the kinetics of rearrangement. Protons, if properly situated, could promote rearrangement. One way to deal with positive ions without the need for protonation is to use the quaternary ammonium species. To do this the methiodide form of EDC (MIEDC) was tested and its behavior recorded to determine if a proton was necessary in the gas-phase rearrangement mechanism. In this case, the discrimination between Asp and isoAsp-bearing peptides was severely diminished. There are two possible explanations for this. The increased steric demand of the extra methyl group relative to EDC diminished the rearrangement to NAU in both cases or a proton is mechanistically required.

It is asserted that this experiment reveals the importance of a proton. The experiments with DCC show that the steric bulk of the substituents of the carbodiimide does not hinder the discriminating power of the method. Use of DCC showed a change in ratio of over an order of magnitude in the ion ratios produced from Asp/isoAsp, while with MEIDC, the difference in ion ratios was just over 2x. This trend persists for other peptide pairs (Table 2.1). Presumably, the proton must be bound close to the reactive site of the AiU moiety, i.e. it is likely to be associated with the nitrogen in the carbodiimide structure, which would also facilitate interaction with the reactive carbonyl in the 1,3-acyl shift which converts AiU to NAU.

If that carbonyl does indeed have a proton associated with it, in principle it would serve to enhance its lability towards nucleophilic attack; it would promote the formation of the succinimide which is the fragment ion associated with AiU. This activation presumably brings the relatively unfavourable succinimide formation into a regime where it effectively competes with

rearrangement to NAU but computation and further investigation would undoubtedly be required to confirm this hypothesis.

The observed processes, then, can be summarized as follows; AiU ions can rearrange to NAU ions quite favorably, with small differences in rate due to steric effects. Protonated AiU ions can also expel urea molecules by ring-closure to form a succinimide at a comparable rate to NAU formation.

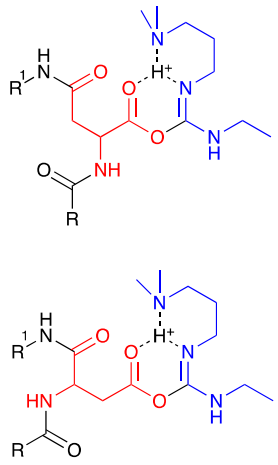

Scheme 2.3 Protonated ions considered to be important in the observed chemistry

The question remains; can the method be used for calibration? Figure 2.5 shows a calibration plot for the ALD(iso)GK system, the GD(iso)LLLK system and the ID(iso)A system. The percentage of isoaspartate to aspartate is calibrated in these plots.

The calibration illustrates that this method has strong semi-quantitative potential. In each case, the linearity of the plots is good but there are obvious deviations. These deviations are likely to be due to the fact that the system under study is highly dynamic, so changes in the atmosphere or in the timing of the experiment on the millisecond timescale (once the ions are born) can affect the result.

Table 2.1 shows the ratios of discriminating ions in the CID product ion mass spectra of peptides bound to different diimides (small peptides have different discriminating fragmentation pathways). The data shows that in all cases studied, the production of fragments of NAU is always preferred in the case of peptides bearing an aspartate residue, while fragments of AiU are preferred for isoaspartate bearing peptides.

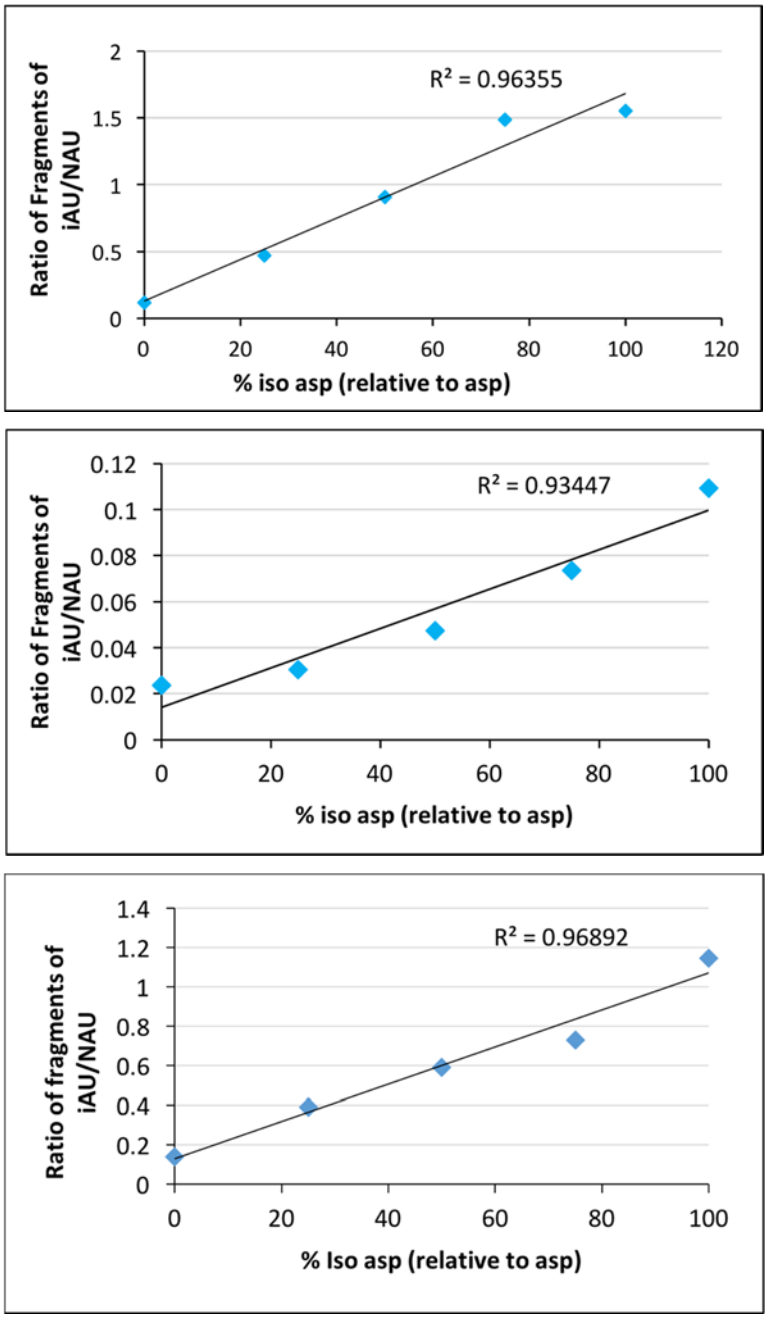

Figure 2.5 Calibration of ALD(iso)GK (top) ID(iso)A (middle) and GD(iso)LLLK (bottom) based on characteristic fragment ion ratio in MS/MS

Table 2.1 Ratio of fragment ions (iAU fragment/NAU fragment) for various peptide-diimide pairs

Peptide	**EDC**	**DCC**	**DIC**	**MEIDC**
DL	0:1	-	-	-
DisoL	1:0	-	-	-
LDA	1:1000	1:5	1:0.2	1:20
LDisoA	1:5.88	1:0.1	1:0.01	1:100
ALDGK	1:5	1:0.22	1:3.7	1:0.15
ALDisoGK	1:0.5	1:0.03	1:0.43	1:0.35
ALDEK	1:4.0	1:4.9	1:25.5	1:32.6
ALDisoEK	1:2.2	1:1	1:20	1:32.9
ADLGK	1:6.6	1:4.0	1:19	1:49
ADisoLGK	1:1.7	1:0.28	1:1	1:26
ALDGE	1:4.9	1:1.41	1:0.29	1:131
ALDisoGE	1:0.78	1:1.17	1:0.04	1:4
GLDLLK	1:2.3	1:19	1:30	1:96
GLDisoLLLK	1:0.39	1:3.3	1:4	1:26
GDLLLK	1:1.1	1:0.4	1:0.13	1:0.05
GDisoLLLK	1:0.2	1:0.3	1:2.1	1:0.4

There are limitations to the presented method. Due to the nature of the adduct of interest (it exists in low abundance), solutions of high concentration are required. Due to the fact that this method is geared towards the analysis of peptide maps, sample handling and preparation is controllable and so this should be taken into account during sample handling procedures.

A second limitation is the requirement of very strictly controlled ion source parameters for good calibration. Since this system is dynamic and is based on kinetics on the time scale of the MS experiment, there is low tolerance for variance of the MS parameters or ion source setup.

One further limitation is that of a limit on the length of the peptide that can be analyzed; while the definitive length has not been established, it has been observed that the method fails for a pentadecapeptide. This may be explained simply by the fact that the steric reasons for the differences in the rates of conversion of AiU to NAU are overwhelmed when the peptide chain is too long.

2.2.2 Gas-phase Ion Chemistry to determine isoAspartate at the Peptide *N*-terminus

Before mass spectrometry became the primary tool for peptide sequencing, the Edman degradation was the method of choice[25]. The Edman degradation exploits a reaction between the N-terminal residue in a peptide chain and phenylisothiocyanate, which induces cyclization and cleavage of that single residue to yield a phenylthiohydantoin analogue (Scheme 2.4), which is detectable by fluorimetry.

The selective addition of phenylisothiocyanate (PITC) to the *N*-terminus of the peptide and subsequent cyclization which utilizes the carbonyl function of the same residue is the process which facilitates Edman sequencing. It is apparent that the natural α arrangement of functional groups in the peptide backbone facilitates this reaction. It was hypothesized that if this arrangement were to be disturbed, i.e. if the peptide were a β peptide, the cyclization chemistry would occur with either far lower efficiency or not at all. It was also hypothesized that the reaction to produce the cleaved, cyclized species would proceed in the gas phase for α amino acid residues.

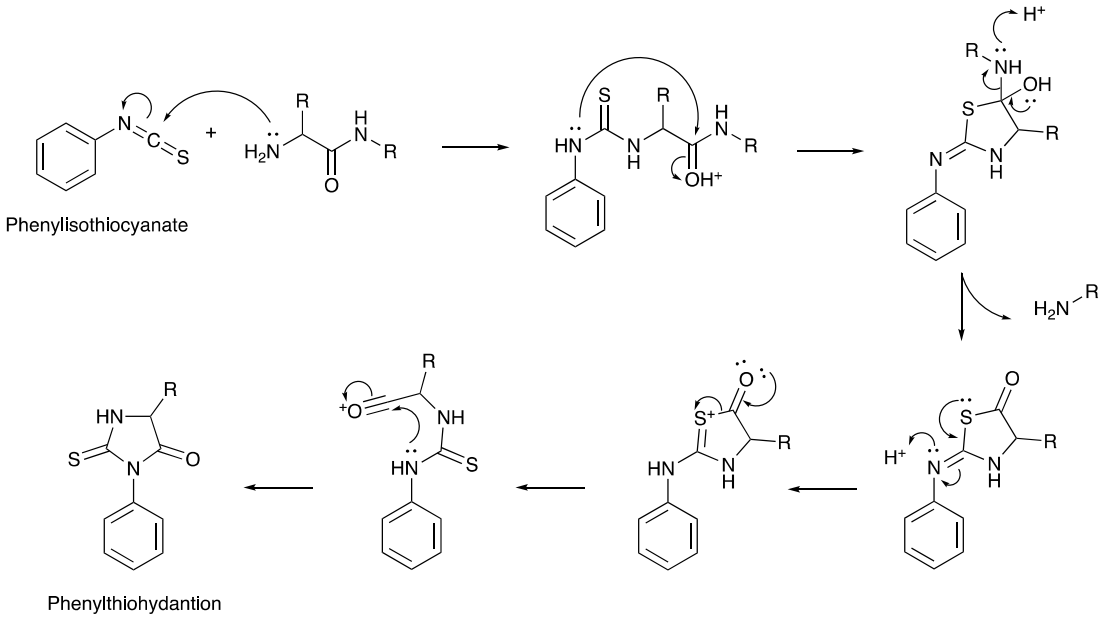

Scheme 2.4 Mechanism of the Edman degradation

To test these hypotheses, the Edman reagent needed to be adapted to facilitate mass spectrometric analysis. To increase the ionization efficiency of the adduct, PITC was switched for its pyridine analogue, pyridylisothiocyanate (PyITC). The aromatic heteroatom in this species facilitates ionization in the positive ion mode.

The isobaric adduct of each dipeptide with PydITC was ionized by nanoelectrospray ionization. The precursor ion was isolated and fragmented and the collision induced dissociation product ion mass spectrum was recorded (Figure 2.6).

The difference between the spectra is the additional peak in the case of the PyITC-DL adduct. This peak corresponds to a cleaved D residue from the dipeptide. Deposition of energy into the ion corresponding to the adduct of PyITC-DisoL did not affect the same cleavage reaction, instead, it cleaved across a C-N thiourea bond to yield the dominant ion at *m/z* 247, which is the protonated dipeptide (Scheme 2.5).

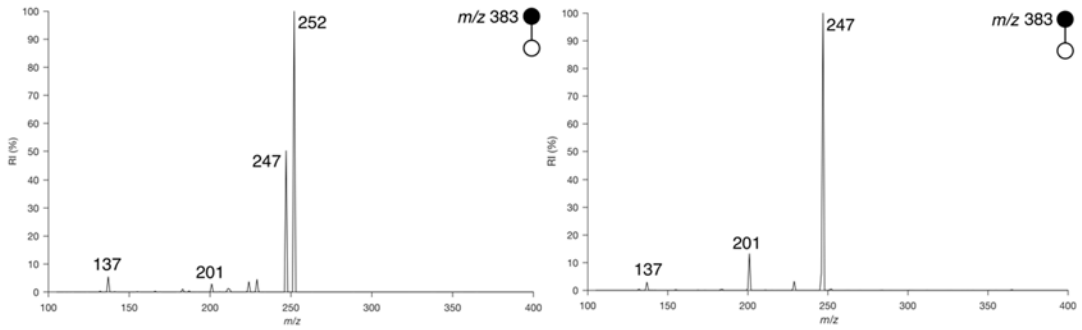

Figure 2.6 CID product ion mass spectra of the PyITC adduct of DL (left) and DisoL (right)

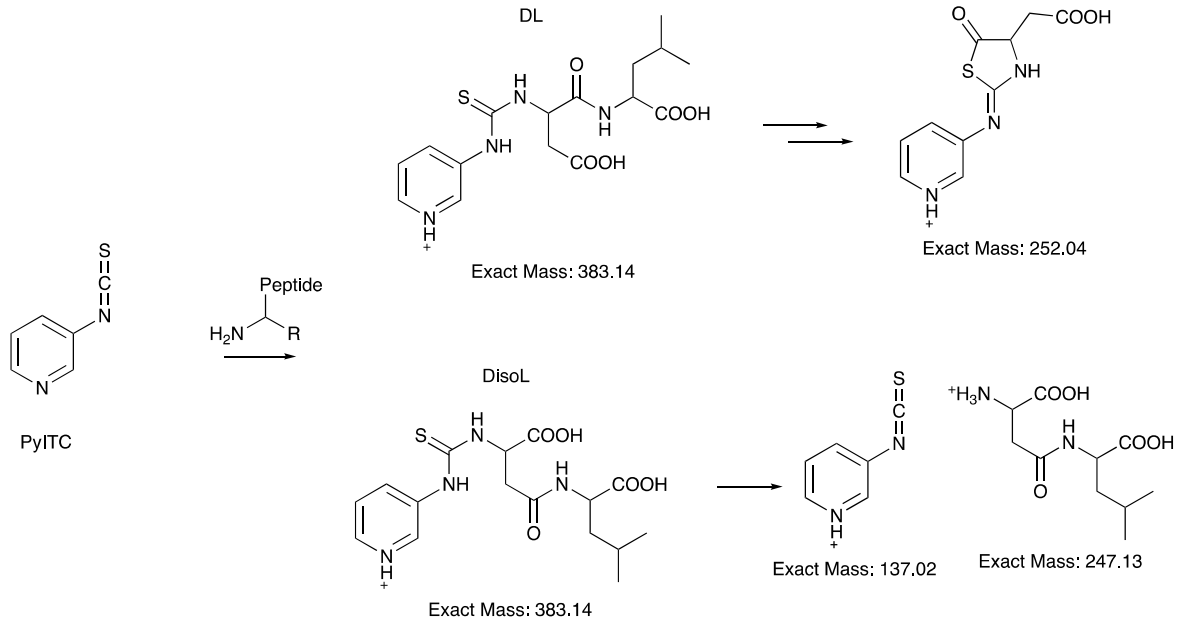

Scheme 2.5 PyITC was mixed at stoichiometric equivalence with DL or DisoL in a 1:1 methanol:water solution and subsequently analyzed by nanoelectrospray ionization. CID yielded the ions shown

The rationale for this is that in isoaspartae, a β peptide, the arrangement of functional groups does not facilitate Edman chemistry, so residue cleavage does not occur in the gas phase

(and likely not in the solution phase either). This constitutes a quick and easy test for *N*-terminal isoAspartate.

2.3 Experimental

EDC, MIEDC, DCC, phenylisothiocyanate and pyridylisothiocyanate were acquired from Sigma Aldrich and used as received. Ethanol was acquired from Makron fine chemicals LTD.. The peptide samples were purchased from Anaspec Inc. (Fremont, CA) and used as received. Nanoelectrospray emitters were prepared using a micropipette tip puller (Sutter instruments, Novato, CA). Analysis was conducted on a standard linear ion trap (LTQ, Thermo Scientific, San Jose CA) or an Orbitrap (LTQ-Orbitrap XL, Thermo Scientific, San Jose, CA) instrument.

2.3.1 General Method to Prepare and Analyze Peptide-Carbodiimide Conjugates

A stock solution of carbodiimide was prepared in (10 mM in 1:1 EtOH:H_2O). A sample of the peptide was prepared (1 mM in 1:1 EtOH:H_2O). Standard solutions for analysis by nanoelectrospray were prepared which contained both the peptide (500 μM, 1 eq.) and the carbodiimide (1 mM, 2 eq.). Analysis was conducted by loading a 10 μL sample into a nanoelectrospray emitter and then applying a potential of 1.5 kV.

The instrumental parameters for standard CID analysis were as follows: Capillary Voltage; 15 V, Tube Lens; 65 V, Capillary temperature; 150 °C, Maximum ion injection time; 10 ms, isolation width; 5 units, collision energy; 25 arb. It should be noted that these conditions are not necessarily suitable for every case/every instrument. The parameters with the most influence on the mass spectrum are ion injection time and ion isolation width.

2.3.2 General Method to Prepare and Analyze Peptide-PyITC Conjugates

A stock solution of PyITC (10 mM in ethanol) and peptide (10 mM in 1:1 ethanol:water) were prepared. 500 μL of each solution were combined in an Eppendorf tube and mixed using a vortex mixed for 10 seconds. The resulting solution was analyzed by nanoelectrospray ionization.

2.4 References

1. Liu, F.; Heck, A. J., Interrogating the architecture of protein assemblies and protein interaction networks by cross-linking mass spectrometry. *Curr Opin Struct Biol* **2015,** *35*, 100-8.

2. Yang, Y.; Franc, V.; Heck, A. J. R., Glycoproteomics: A Balance between High-Throughput and In-Depth Analysis. *Trends Biotechnol.* **2017,** *35* (7), 598-609.

3. Lamond, A. I.; Uhlen, M.; Horning, S.; Makarov, A.; Robinson, C. V.; Serrano, L.; Hartl, F. U.; Baumeister, W.; Werenskiold, A. K.; Andersen, J. S.; Vorm, O.; Linial, M.; Aebersold, R.; Mann, M., Advancing cell biology through proteomics in space and time (PROSPECTS). *Mol Cell Proteomics* **2012,** *11* (3), O112 017731.

4. Liu, M.; Cheetham, J.; Cauchon, N.; Ostovic, J.; Ni, W.; Ren, D.; Zhou, Z. S., Protein isoaspartate methyltransferase-mediated 18O-labeling of isoaspartic acid for mass spectrometry analysis. *Anal. Chem.* **2012,** *84* (2), 1056-62.

5. Manning, M. C.; Chou, D. K.; Murphy, B. M.; Payne, R. W.; Katayama, D. S., Stability of protein pharmaceuticals: an update. *Pharm. Res.* **2010,** *27* (4), 544-75.

6. Puri, A.; Quan, Y.; Narang, A. S.; Adams, M.; Gandhi, R.; Nashine, V. C., A Fluorescence-Based High-Throughput Coupled Enzymatic Assay for Quantitation of Isoaspartate in Proteins and Peptides. *AAPS PharmSciTech* **2017,** *18* (3), 803-808.

7. Winter, D.; Pipkorn, R.; Lehmann, W. D., Separation of peptide isomers and conformers by ultra performance liquid chromatography. *J. Sep. Sci.* **2009,** *32* (8), 1111-9.

8. Seebach, D.; Gardiner, J., b-Peptidic Peptidomics. *Acc. Chem. Res.* **2007,** *41*, 1366-1375.

9. Seebach, D.; Matthews, J. L., b-Peptides: a surprise at every turn. *Chem. Commun.* **1997,** *0*, 2015-2022.

10. Ni, W.; Di, S.; Karger, B. L.; Zhou, Z. S., Analysis of Isoaspartic Acid by Selective Proteolysis with Asp-N and Electron Transfer Dissociation Mass Spectrometry. *Anal. Chem.* **2010,** *82*, 7485-7491.

11. Yu, X.; Sargaeva, N. P.; Thompson, C. J.; Costello, C. E.; Lin, C., In-Source Decay Characterization of Isoaspartate and beta-Peptides. *Int. J. Mass spectrom.* **2015,** *390*, 101-109.

12. Zheng, X.; Deng, L.; Baker, E. S.; Ibrahim, Y. M.; Petyuk, V. A.; Smith, R. D., Distinguishing d- and l-aspartic and isoaspartic acids in amyloid beta peptides with ultrahigh resolution ion mobility spectrometry. *Chem Commun (Camb)* **2017**.

13. McLafferty, F. W., Molecular Rearrangements. *Anal. Chem.* **1959,** *31* (1), 82-87.

14. Bowen, R. D., Ion-Neutral Complexes. *Acc. Chem. Res.* **1991,** *24* (12), 364-371.

15. DeTar, D. F.; Silverstein, R., Reactions of Carbodiimides. I. The Mechanisms of the Reactions of Acetic Acid with Dicyclohexylcarbodiimide *J. Am. Chem. Soc.* **1966,** *85* (5), 1013-1019.

16. Carpino, L. A.; El-Faham, A., The Diisopropylcarbodiimide/1-Hydroxy-7-Azabenzotriazole System: Segment Coupling and Stepwise Peptide Assembly *Tetrahedron* **1999,** *55*, 6813-6830.

17. DeTar, D. F.; Silverstein, R., Reactions of Carbodiimides. II. Thre Recactiosn of Dicyclohexylcarbodiimide with Carboxylic Acids in the Presence of Amines and Phenols. *J. Am. Chem. Soc.* **1966,** *88* (5), 1020-1023.

18. DeTar, D. F.; Silverstein, R.; F., R. J. F., Reactions of Carbodiimides. III. The Reactions of Carbodiimides with Peptide Acids *J. Am. Chem. Soc.* **1966,** *88* (5), 1024-1030.

19. G., K. H., The Chemistry of Carbodiimides. *Chem. Rev.* **1953,** *53* (2), 145-166.

20. Giles, M. A.; Hudson, A. Q.; Borders Jr., C. L., Stability of Water-Soluble Carbodiimides in Aqueous Solution *Anal. Biochem.* **1990,** *184*, 244-248.

21. Iwasawa, T.; Wash, P.; Gibson, C.; Rebek Jr., J., Reaction of Introverted Carboxylic Acid with Carbodiimide. *Tetrahedron* **2007,** *63* (28), 6505-6511.

22. Kurzer, F.; Douraghi-Zadeh, K., Advances in the Chemistry of Carbodiimides *Chem. Rev.* **1967,** *62* (2), 107-152.

23. Nakajima, N.; Ikada, Y., Mechanism of Amide Formation by Carbodiimide for Bioconjugation in Aqueous Media. *Bioconjugate Chem.* **1955,** *6*, 123-130.

24. Schotman, A. H. M., Mechanism of reaction of carbodiimides with carboxylic acids. *Recl. Trav. Chim. Pays-Bas* **1991,** *110*, 319-324.

25. Edman, P.; Begg, G., A Protein Sequenator. *Eur. J. Biochem.* **1967,** *1* (1), 80-91.

CHAPTER 3. MOLECULAR LABELS FOR NANOPARTICLE DETECTION

3.1 Introduction

The use of antibody-bound nanoparticles (NPs) in immunochemical labelling methods for the detection of biological materials is relatively common[1-3]. *In-vitro* spectroscopic techniques have been used to detect nanoparticles on proteins, for instance[4]. In other work, inductively coupled plasma - mass spectrometry (ICP-MS) and laser ablation has been used to detect heavy metal atoms incorporated into tissues via staining procedures[5-6]. Such atoms (and their respective isotopic distributions) constitute highly specific mass labels[7-8]. Coinage metal NPs that were immunochemically linked to biological analytes have also been analyzed in a similar manner[9]. Cancer cells might be labelled with nanoparticles bound to specific antibodies which could facilitate the detection of circulating tumor cells[1]. Overall, the detection of biomaterials with methods such as these transposes itself from the detection of a complex biomaterial (bacterium, cell, protein etc.) to the detection of NPs. The rapid and specific detection of NPs in general, then, is a desirable goal.

Sometimes, an analyte to which a nanoparticulate label is bound is “rare”. A rare cell can be biologically relevant at a level of 10 in 10 mL of whole blood[10], for instance. Surface functionalization of nanoparticles is common and provides hundreds of thousands[1, 11] of chemical sites to which molecules can be bound. Utilizing this fact, one nanoparticle bound to one analyte could be engineered to yield hundreds of thousands of molecules for detection, effectively providing a basis for chemical “amplification”, which is already utilized in spectroscopy to a greater extent[12].

Compounds bearing a permanent charge (ammonium salts, for instance) have exceptional ionization efficiencies under spray based ionization conditions[13]. The use of quaternary amines (or other pre-charged compounds) as labels to improve ionization efficiency has precedent from the 1980's[14]. In the work of Busch *et al*.[15] amines were quaternized for analysis by SIMS. Similar work from the same decade utilized the Katritzky reaction to form pyridinium ions in the gas phase[16]. In 2007, Li *et al*. utilized the reaction between hydroxyl groups and betaine aldehyde to label diacylglycerols with a quaternary ammonium moiety for analysis by electrospray ionization (ESI)[17]. The work of Bachor *et al.*[18] and, separately, Kiderll *et al*.[19], documented peptides which were modified with tetraalkylammonium salts to improve their ionization efficiency.

Pre-charged molecules, in principle, could be designed to reversibly bind a nanoparticle. The molecules could be tailored serve as reporters for nanoparticles if they could be released under specific, pre-determined conditions. The major concept of this chapter is that with a particular set of labelled nanoparticles, an assay may be logically designed to utilize ideal analytes for mass spectrometry. This is a benefit rarely encountered in analytical chemistry.

Detailed here is the development of imidazolium salts which are pre-charged and therefore easy to detect by mass spectrometry. They are easy and cheap to synthesize and they bear an aldehyde residue which can be utilized in linkages which are cleavable by hydrolysis.

Due to the simple, two-step synthesis of the mass labels, it is straightforward to generate a range of compounds for the purpose of multiplexed analysis and/or internal standard generation. This highlights one of the main advantages of a mass spectrometric assay as opposed to a fluorimetric assay; labels can be designed to appear at unique *m/z* ratios across a range on the order of hundreds, while fluorescence is inherently limited by the emission bandwidth of fluorophores

to tens of signals[20]. A second advantage of mass spectrometry is its speed. An MS analysis can take seconds whereas analysis of rare biological materials by fluorescence may take longer[21-24].

The combination of the specific chemistry of the reported imidazolium mass labels, the simple chemical release process and the sensitivity and efficiency of mass spectrometry (MS) together have the potential to yield a highly specific and rapid assay.

3.2 Results and Discussion

3.2.1 Synthesis of the Mass Labels and Evaluation of Binding to Amines and Diols

The mass labels were synthesized according to Scheme 3.1. The synthesis is simple, cheap and fast. Salicylaldehyde is reacted with paraformaldehyde in concentrated hydrochloric acid to generate chloromethylsalicylaldehyde (1), which is subsequently reacted with an N-alkylimidazole to generate the mass label.

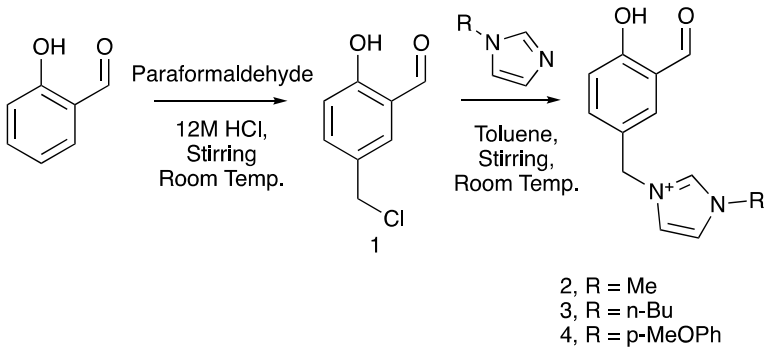

Scheme 3.1 General synthesis of mass labels

The mass labels were designed to fragment readily and yield only one or a few dominant product ions. The fragmentation of each of the mass labels reported here occurs via two analogous pathways. The CID product ion mass spectra of three of the mass labels are given in Figure 3.1.

As illustrated, the fragmentation is essentially a competitive two-channel process. This is advantageous for two reasons: it simplifies the spectrum and it preserves the intensity of the signals overall as the charge is only split two ways and the ratio of the two signals is characteristic of the mass label under fixed MS/MS conditions.

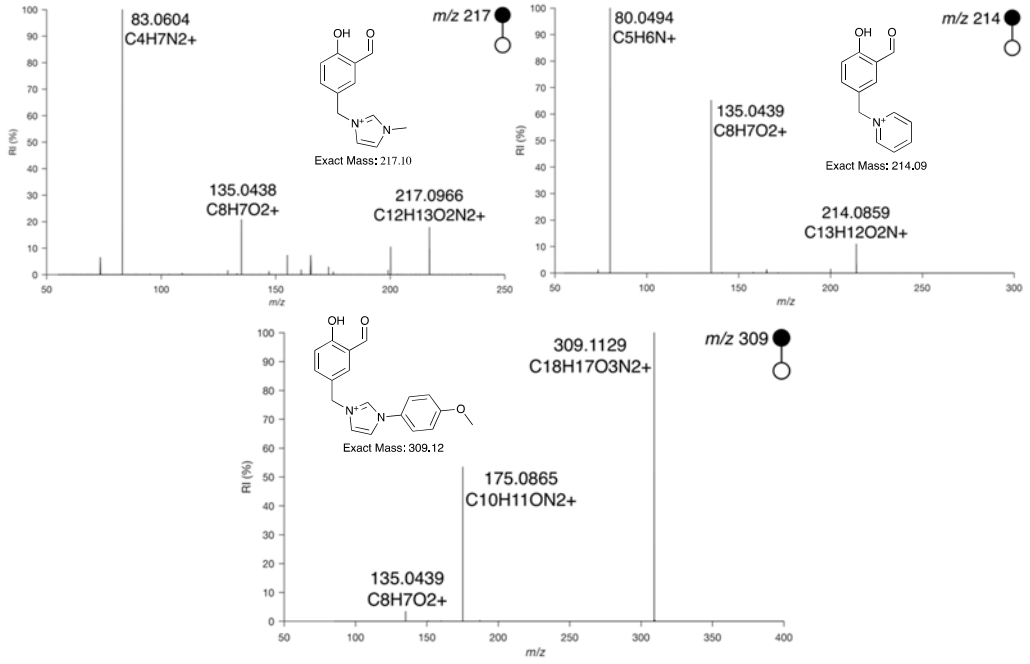

Figure 3.1 MS/MS product ion spectra of three of the imidazolium mass labels

The labels were originally designed to form stable imine bonds with propylamine. The nanoparticles utilized in this work were propylamine functionalized and commercially available. The mass spectra of the methylimidazolium mass label (Scheme 3.1) bound to and then released from propylamine are given in Figure 3.2.

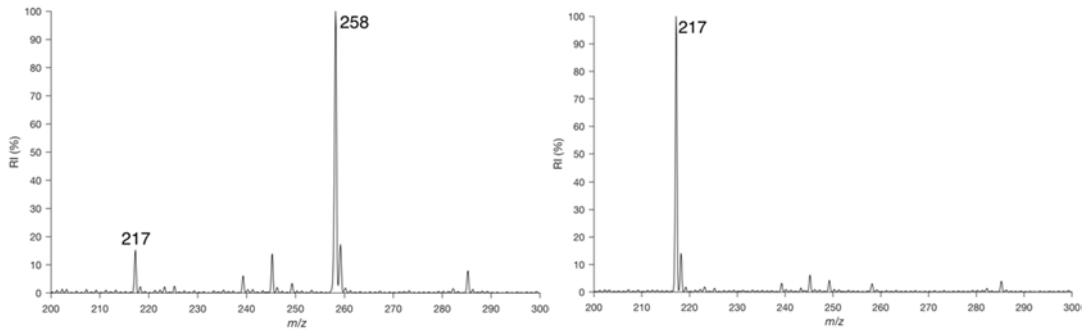

Figure 3.2 The mass label conjugated to propylamine (m/z 258) analyzed from methanol (left); The mass label released (m/z 217) from the propylamine conjugate imine analyzed from methanol:water, 1% formic acid (right)

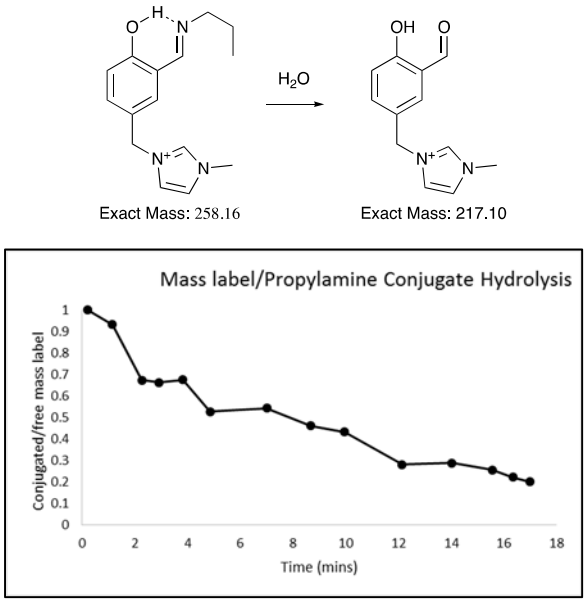

Figure 3.3 Hydrolysis of the propylamine conjugate imine over time in 1:1 PBS:methanol

Imine bonds are suitable for linkage under anhydrous conditions and the imine bond formed between these mass labels and an amine is a particularly stable one due to the proximal hydroxyl group (Figure 3.3), but the hydrolysis of the label in 1:1 aqueous buffer and methanol is still quite fast. For that reason, it would be an unsuitable linkage to use if this work were to be developed for biological purposes, where aqueous buffers are ubiquitous.

An acetal linkage was chosen as the ideal candidate for binding of the mass label to the propylamine functionalized SiNPs due to its greater stability towards hydrolysis. In order to conjugate the mass label to the propylamine functionalized NPs, chemical modification was necessary.

To develop the chemistry, free propylamine was used as a model for the nanoparticles. It was reacted with β-hydroxy-γ-butyrolactone (Scheme 3.2) (a modification of literature procedure[25]) to generate an amide with a 1,2-diol structure (Scheme 3.2; 5). The reaction proceeded with neat reagents quantitatively and so was adopted as the method of choice for nanoparticle derivatization.

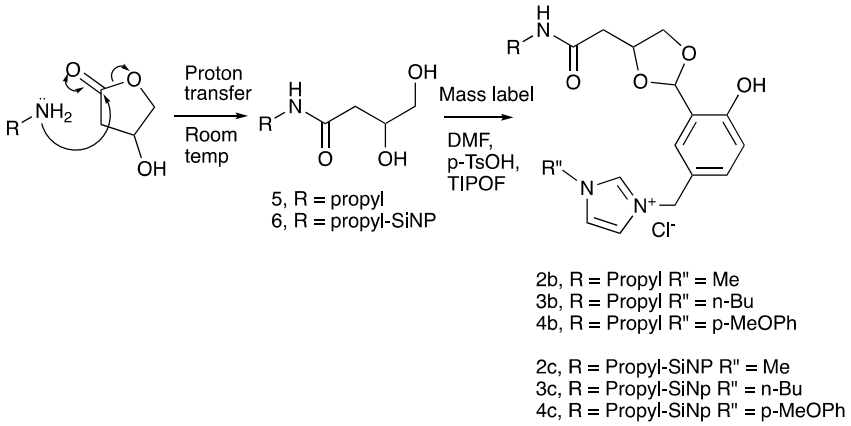

Scheme 3.2 Reaction between either propylamine or propylamine-functionalized silica nanoparticles and β-hydroxy-γ-butyrolactone to produce the diol functionality required for acetal-based conjugation to the mass label. The first reaction proceeds with neat materials. (TIPOF = triisopropylorthoformate)

3.2.2 Loading and Release of the Mass Label from the Model Diol

The product, 3, 4-dihydroxy-N-propylbutyramide (Scheme 3.2, 5), served as a solution-phase model diol for the nanoparticles participating in an acetal linkage. The acetalization reaction appeared to proceed with only 13% efficiency to produce the bound mass label (Scheme 3.2).

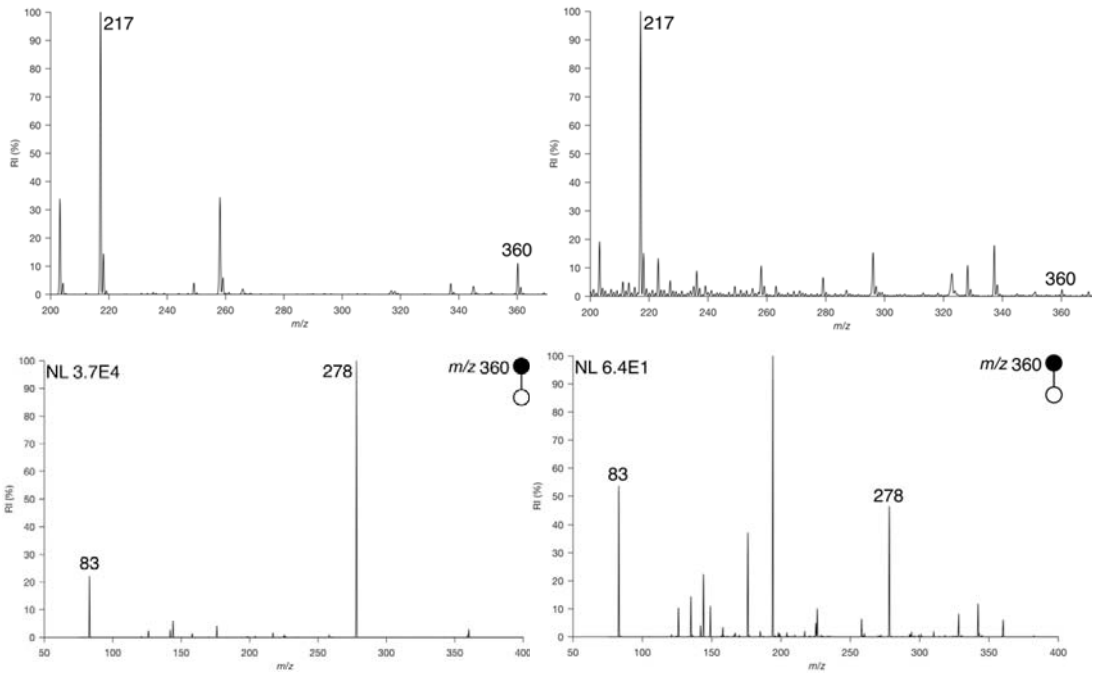

Figure 3.4 Top – Left top – full scan mass spectrum of solution with bound mass label; Left bottom – CID product ion mass spectrum of bound mass label; Right top – full scan mass spectrum of solution after release of mass label; Right bottom – CID product ion mass spectrum showing depletion of bound mass label

The approximation of the yield of the acetalization reaction of the methylimidazolium mass label with 3,4-dihydroxy-N-propylbutyramide was done by comparing the relative intensities of the signal related to the product of the reaction to the signal corresponding to the starting material. No internal standard was used in the traditional sense.

In order for this approximation to be valid, the ionization efficiency of both species must essentially be the same. A second necessary assumption is that there is no competitive reaction or degradation of the starting material. Due to the nature of the ions (imidazolium), it is assumed that they do have essentially the same ionization efficiencies. Due to the nature of the reaction (the lack of harsh conditions), it is assumed that no degradation occurs and competitive reaction of the

starting material via some other pathway is unlikely so the ratio of the signals in the mass spectrum should provide a reasonable (but not perfect) approximation of reaction yield.

The reason that the experiment was conducted in this manner was due to the difficulty of isolation of either the product or starting material from DMSO, which was the solvent in which the reaction was conducted. This problem is negated in the case(s) where nanoparticles are involved in the reaction because the product (derivitized Silica NPs, SiNPs) is isolated by centrifugation.

It was found that the rapid release of the acetal could be accomplished by hydrolysis in 4:1 MeOH:H_2O with a 1% spike of trifluoroacetic acid (TFA), this solution is termed the release solution hereafter. The spectrum of the conjugated material after exposure to the release solution is given in Figure 3.4.

Figure 3.4 also compares CID data obtained from the ions at *m/*z 360, which corresponded to the bound mass label, both before and after exposure to the release solution. The intensity of the product ion MS/MS spectrum of the conjugated material dropped by nearly three orders of magnitude after exposure to the release solution and the ratios of the fragment ions changed significantly when compared to the same spectrum obtained from the bound material. This suggests that the bound material is essentially absent from the spectrum after exposure of the conjugate to the release solution. Changes in the background ions in the full scan mass spectrum were expected as the solvent system was changed: the bound material was ionized from anhydrous methanol, whereas the released material was analyzed from the release solution.

The ability to store conjugated NPs is important. The ability to expose the NPs to a buffered solution without the release of the mass label is also important. An investigation into the stability of the mass label bound to the model diol (Scheme 3.2, 5) was conducted. The study consisted of

a temporally resolved experiment conducted over the course of 20 minutes, as this is conceivably the length of time that the nanoparticles would be exposed to buffer solution during an assay. Briefly, a solution of the bound mass label (Scheme 2, 2b) was analyzed from a solution of 1:1 methanol:PBS at 1.5 minute intervals. The ratio of the ions representing the free and bound mass labels were compared and the stability was excellent (Figure 3.5).

A second experiment was carried out using ethylene glycol as the second reagent for acatalization to test the general stability of the linkage and validate the first result. It was found that the stability of this conjugate was also excellent in buffered solution at 2 ºC over the course of one week.

This data is shown in Figure 3.5 as the change in the ratio of the signals for the conjugated and un-conjugated mass label over time in the full scan mass spectrum. Based on this dataset, hydrolysis of the mass label was very limited, suggesting that the acetal linkage was indeed suitably stable under buffered aqueous conditions.

A change of 10 % in the ratio of free/bound mass label in Figure 3.5 would correspond to a 5% release of mass label because the signal for the free mass label increases linearly with the decrease in the signal of the bound material.

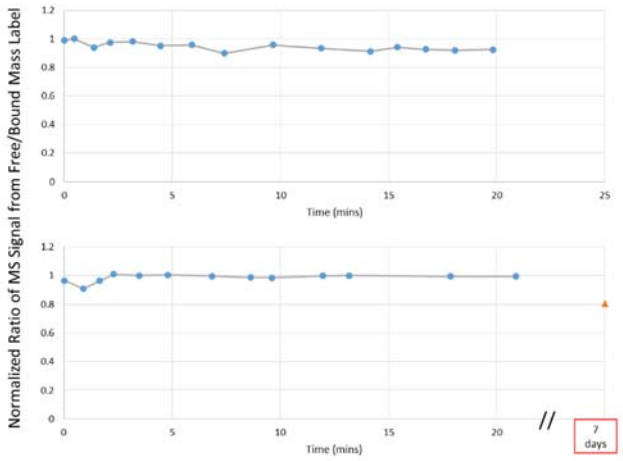

Figure 3.5 Plots of the change in the ratio of the signals corresponding to the acetylated and free mass label where the acetal was formed between 3, 4-dihydroxy-N-propylbutyramide (top) and ethylene glycol (bottom). Triangle = after storage for 7 days at 2ºC in 1:1 MeOH:PBS buffer.

3.2.3 Loading and Release of the Mass Label from Diol Functionalized SiNPs

Diol functionalized silica nanoparticles were prepared from propyliamine functionalized silica nanoparticles by exposure to β-hydroxy-γ-butyrrolactone (Scheme 3.2, 6). The diol functionalized NPs were loaded with mass label as described in the experimental section. With the observed efficiency of conjugation of the model system (13 %) in mind, diol modified NPs were exposed to a vast excess of the mass label during conjugation. This demand is economically viable considering the low cost of the mass label synthesis.

Cleaning of the NPs before releasing the mass labels was not fully efficient. Some signal from the free mass label was obtained from the supernatant of the final wash. The stability studies reported here (Figure 3.5), suggest that dissociation of the conjugate in the presence of methanol is unlikely. The signal at m/z 217 (and the relevant fragment ions in the CID spectrum) was almost negligible compared to the signal intensity obtained from the mass label after it was released from the nanoparticles, which was just over two orders of magnitude greater (Figure 3.3) The release

solution is also ideal for spray based ionization methods and it was the solvent of choice for the quantitative studies conducted in this work.

It was found that the concentration of the mass label upon release into the release solution was $2x10^{-4}$ M via the calibration curve (Figure 3.3). The total mass of nanoparticles that contributed to the release of the material was less than the initially weighed amount because some mass was inevitably lost during the washing steps. The mass of the nanoparticles was 3 mg (measured as 3.3 mg on a scale with uncertainty on the .1 mg regime) This was established after washing the remaining nanoparticles with acetone and allowing them to dry in the open air whereupon they were weighed. It is possible that there was a small amount of excess water weight in the measurement.

With these numbers, the loading efficiency of the mass label was estimated. According to Lu[26], the concentration of amines present on the surface of nanoparticles of average diameter of 183 nm is 0.32 mmol/g. The number of free amines present in 3 mg ($5.78x10^{17}$) was calculated by multiplying the moles of amine on 3 mg of NPs by Avogadro's number.

A background of $2x10^{-6}$ M mass label was found in the final aliquot of methanol used to wash the nanoparticles (before release, see Figure 3.3. This number was considered to be the background contribution to the measured concentration. Taking this into account, the concentration of released mass label was $2.2x10^{-4}$ M (triangle, Figure 3.3). This corresponded to $1.3x10^{17}$ molecules released into the solution, implying an overall efficiency (i.e. overall efficiency of conjugation and release) of 23%.

The mass label was released into a relatively large volume of solution; far greater than that needed for analysis by mass spectrometry. Using a small volume of solution to release the mass label would inevitably lead to a higher concentration of mass label in that solution and therefore

stronger signal in the mass spectrum. The important aspect of this is the fact that the mass label could be detected from a lower absolute amount of material. Figure 3.3 shows the quantitative data obtained from the release of the mass label from the nanoparticles.

The calibration curve was generated from product ion MS/MS spectra with the methylimidazolium (Scheme 3.1, 2) mass label as the analyte using the pyridinium analogue (pyridinium instead of methylimidazolium) as an internal standard. The major fragment from each ion was *m/z* 83 (protonated methylimidazole) and *m/z* 80 (protonated pyridine), respectively. The ratio of the integrated intensity of these two signals over 0.2 minutes was used to generate the data points for the calibration curve shown in Figure 3.3. An illustrative mass spectrum recorded using the internal standard is also given in Figure 3.3. Each data point is the average of three replicates. The maximum RSD was 11% and the minimum was 0.9%. The average RSD was 6.5%.

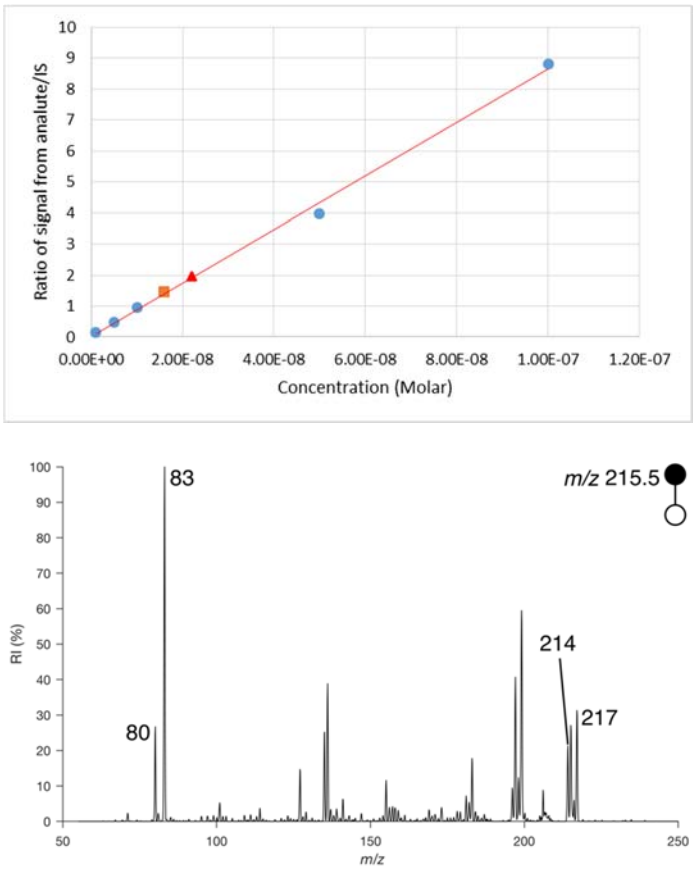

Figure 3.6 Concentration of the mass label released into the release solution using a calibration curve. The sample (triangle) was diluted by four orders of magnitude prior to measurement. The supernatant from the final wash before release (square) was also analyzed after a dilution of two orders of magnitude prior to measurement. The mass spectrum of the standard at an analyte concentration of $5x10^{-8}$ M is also shown

It was important to establish the limit of detection for the mass label. The experiment was carried out according to the general procedure described in the experimental section and the mass label was ionized with excellent efficiency, facilitating its detection at a concentration of 1 nM (the signal to noise ratio in the MS^2 product ion mass spectrum at this concentration was 3.01).

3.3 Experimental

3.3.1 Instrument Parameters and Materials

Unit resolution mass spectra reported here were recorded on a bench-top linear ion trap mass spectrometer (LTQ, Thermo Scientific, San Jose, CA) and high-resolution mass spectra were recorded on an LTQ Orbitrap XL (Thermo Scientific). The high resolution MS data is in the Supplementary Information. Collision-induced dissociation (CID) product ion mass spectra were collected typically using the following parameters: spray voltage; 1.5 kV, capillary voltage; 15 V, tube lens voltage; 65 V, parent ion isolation width; 1.5 Th, fragmentation energy; 20 arb., active Q (well depth); 0.25 arb., ion injection time 150 ms.

Methanol, dichloromethane, pyridine and N, N-dimethylformamide were purchased from Macron Fine Chemicals (Center Valley, PA). Propylamine functionalized silica nanoparticles and paraformaldehyde were acquired from Sigma Aldrich (St. Louis, MO). β-hydroxy-γ-butyrolactone, triisopropyl orthoformate, *p*-toluenesulphonic acid monohydrate, N-(n-butyl)imidazole and N-(p-methoxyphenyl)imidazole were acquired from Alfa Aesar (Heysham, Lancashire, UK). N-methylimidazole was acquired from TCI Chemicals (USA). All chemicals were used as received.

3.3.2 General Procedure for the Synthesis of Mass Labels

Paraformaldehyde (0.8 g) was dissolved in 12 M HCl (5 ml). Salicylaldehyde (0.7 g) was added dropwise over the course of 10 mins. The solution first adopted a yellow tint whereafter it lost its color. The reacting solution was left to stir overnight (*ca*. 12 h), during which time a white precipitate formed. Chloromethyl salicylaldehyde was collected as a white precipitate by filtration under gravity and washed with de-ionized water (3 x 20 ml). The typical yield was 80%. The product was used in the next step without further purification.

Chloromethyl salicylaldehyde (0.5 g, 1 eq.) was dissolved into dichloromethane and N-methylimidazole (0.37 g, 1.5 eq.) was added dropwise. The product of the reaction from methylimidazole (Scheme 1, 2) was precipitated as an off-white salt and was washed multiple times with dichloromethane to remove residual imidazole. The product of the reaction with n-butylimidazole (Scheme 1, 3) was isolated as a viscous yellow ionic liquid after removal of the solvent under vacuum. The reaction proceeded essentially quantitatively (>98% yield) in all cases. The above synthesis has literature precedent[27-28]. Step two of this general two-step procedure was adapted such that different N-alkyl imidazoles were introduced to the reaction vessel, thus generating different mass labels. These variants include the N-(p-methoxyphenyl) and N-(n-butyl) analogs of the imidazolium label (see Supplemental Information). In one case, pyridine was added instead of an imidazole analog. In the case of the N-(n-butyl)Imidazolium analogue of the mass label, the product was an oil. Because of this the procedure was adapted slightly, such that N-(n-butyl)imidazole was added to chloromethylsalicylaldehyde at stoichiometric equivalence. It was against the pyridinium mass label that the limit of detection (LOD) study (see below) was conducted.

3.3.3 General Procedure for the Determination of the LOD of a Typical Mass Label

The methylimidazolium mass label was prepared in 5-fold serial dilutions over the range 1E-9M to 1E-7M. The internal standard (the pyridinium analog of the mass label) was spiked into each standard at a concentration of 1E-8M. Both of the parent ions (m/z 214 and 217) were isolated in a single isolation event and fragmented simultaneously, yielding one signal corresponding to fragmentation of the analyte (*m/z* 83) and one signal corresponding to fragmentation of the internal standard (*m/z* 80). The ratio of these two signals was used to calibrate the method.

3.3.4 Synthesis of 3, 4-dihydroxy-N-propylbutyrolactone (5)

Synthesis of free 3, 4-dihydroxy-N-propylbutyramide was carried out by mixing β-hydroxy-γ-butyrolactone with propylamine in equimolar quantities, neat. The reaction proceeded quantitatively with a strong exotherm to produce an orange semi-solid wax. Characterizsation data can be found in the Supporting Information.

3.3.5 General Procedure for the Acetalization of Mass Labels with 3, 4-dihydroxy-N-propylbutyrolactone (Scheme 2; 2b, 3b, 4b)

The mass label (0.3 g, 1 eq.) was weighed into a round bottomed flask. N, N-dimethylformamide (10 ml) was added. 3, 4-dihydroxy-N-propylbutyrolactone (0.12 g, 1.2 eq.) was added to the flask with stirring along with a catalytic amount of p-toluenesulphonic acid and triisopropylorthoformate (1 eq.). The reaction was left to stir for 2 hours. Typical yields were 11-15% as suggested by the mass spectrum obtained from the crude reaction mixture and the relative intensities of the free and acetalated mass label (see Supplemental Information for further discussion).

3.3.6 General Procedure for the Derivatization of Propylamine Functionalized Silica Nanoparticles to give 3, 4-dihydroxy-N-propylbutyramide Functionalized Silica Nanoparticles (Scheme 2; 6)

Propylamine functionalized silica NPs (1-3 mg) were weighed into an Eppendorf tube. The NPs were covered with neat β-hydroxy-γ-butyrolactone and the suspension was agitated and left to react for 3 hours. The suspension was diluted with methanol and centrifuged whereupon the supernatant was removed. The particles were re-suspended and this washing procedure was repeated three times.

3.3.7 General Procedure for the Conjugation of the Mass Label to a Functionalized NP via an Acetal Linkage (Scheme 2; 2c, 3c, 4c)

A saturated solution of the mass label (*ca*. 15 mg/mL) in N, N-dimethylformamide was prepared. The saturated solution (1 ml) was added to diol modified propylamine functionalized silica nanoparticles (Scheme 2; 6, 1-3 mg) in an Eppendorf tube. A catalytic amount of *p*-toluenesulphonic acid was added along with two drops of triisopropyl orthoformate from a Pasteur pipette. The system was agitated frequently for one hour whereupon the suspension was left to react overnight. The suspension was subsequently separated via centrifugation, the supernatant was discarded and a fresh portion of N, N-dimethylformamide (1 mL) was added to the tube. The particles were re-suspended and centrifuged again. The nanoparticles were washed in this manner twice more with N, N-dimethylformamide and three subsequent times with anhydrous methanol in order to remove as much of the un-bound mass label as possible.

3.3.8 General Procedure for the Release of the Mass Label from the Acetal Linkage and Quantitation of Release Efficiency

In order to release and quantitate the mass label from the nanoparticles, the particles on of were suspended in 1 ml of a solution of 4:1 methanol:water with a 1% trifluoroacetic acid spike. After 1 minute, the suspension was separated by centrifugation whereupon a 1 μl aliquot of the supernatant was diluted into 999 μl of 4:1 methanol:water with a 0.1% formic acid spike. This sample was diluted by one further order of magnitude (total 4 orders of magnitude dilution) and the internal standard was spiked into the final solution. The solution was analyzed by nano-electrospray ionization.

3.4 Further Work

The amine functionalization of the nanoparticles studied herein lends itself to biochemical transformation. Immunochemical binding to amines is trivial and many commercialized kits for amine binding to proteins are available. The chemistry here was originally developed to report on isolated biological systems, such as circulating tumor cells which have been isolated.

By modifying the chemistry slightly, such as by using mercaptoaniline as a reagent for modification with beta-hydroxy-gamma-butyrolactone or use as an amine binding partner for imine linkage, coinage metal nanoparticles may be labelled and analyzed by the reporter labels detailed herein. Conjugation of the mass label to mercaptoaniline and release from that substrate is demonstrated by mass spectrometry in Figure 3.6. This unproven concept could lead to interesting developments in the field of nanomaterial detection by mass spectrometry if implemented with care.

The electron density of mercaptoaniline also improves the stability profile of the conjugate imine between it and the mass label (Figure 3.7) ,which is evidenced by the hydrolysis profile over time in buffered aqueous solution (compare to Figure 3.3)

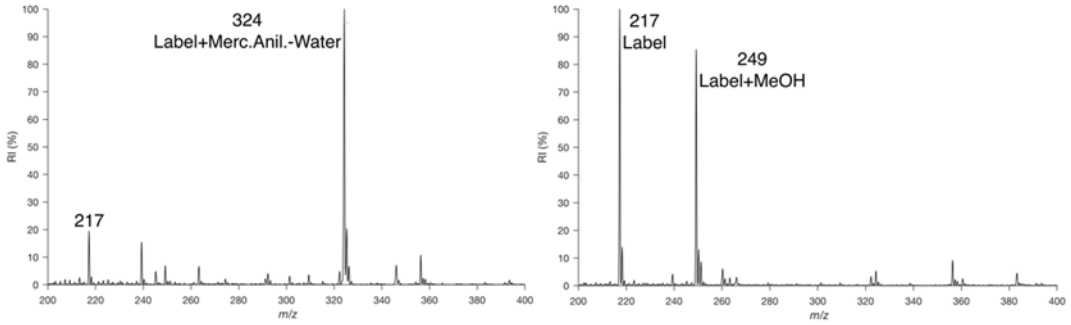

Figure 3.7 The mass label conjugated to mercaptoaniline (m/z 324), analyzed from neat methanol (top), The mass label released (m/z 217) from the mercaptoanilinie conjugate imine as well as the resulting methanol hemi-acetal (m/z 249) analyzed from methanol:water, 1% formic acid (bottom)

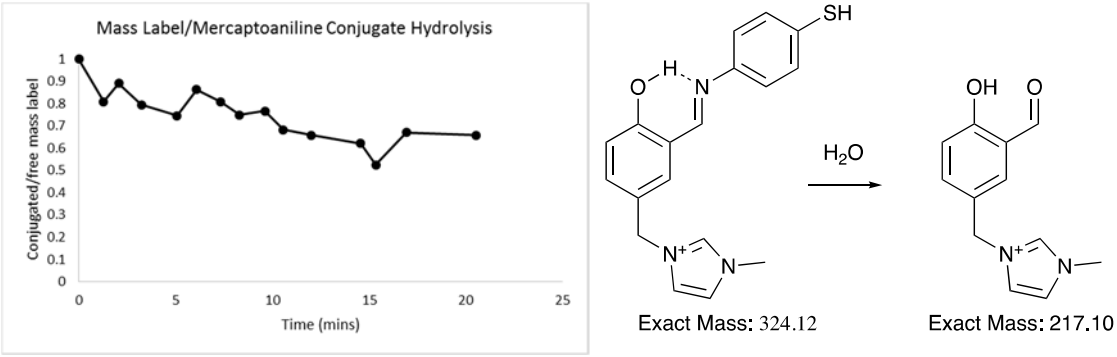

Figure 3.8 Hydrolysis of the mercaptoaniline conjugate imine over time in 1:1 PBS:methanol

3.5 References

1. Chinen, A. B.; Guan, C. M.; Ferrer, J. R.; Barnaby, S. N.; Merkel, T. J.; Mirkin, C. A., Nanoparticle Probes for the Detection of Cancer Biomarkers, Cells, and Tissues by Fluorescence. *Chem Rev* **2015,** *115* (19), 10530-74.

2. Bagwe, R. P.; Zhao, X.; Tan, W., Bioconjugated Luminescent Nanoparticles for Biological Applications. *Journal of Dispersion Science and Technology* **2003,** *24* (3-4), 453-464.

3. Santra, S. Z., P.; Wang, K.; Tapec, R.; Tan, W., Conjugation of Biomoleucles with Lumiphore-Doped Silica Nanoparticles for Photostable Biomarkers *Anal. Chem.* **2001,** *73*, 4988-4993.

4. Wang, H.; Li, G.; Zhang, Y.; Zhu, M.; Ma, H.; Du, B.; Wei, Q.; Wan, Y., Nanobody-Based Electrochemical Immunoassay for Ultrasensitive Determination of Apolipoprotein-A1 Using Silver Nanoparticles Loaded Nanohydroxyapatite as Label. *Analytical chemistry* **2015**.

5. Tata, A.; Zheng, J.; Ginsberg, H. J.; Jaffray, D. A.; Ifa, D. R.; Zarrine-Afsar, A., Contrast Agent Mass Spectrometry Imaging Reveals Tumor Heterogeneity. *Analytical chemistry* **2015,** *87* (15), 7683-9.

6. Sussulini, A.; Becker, J. S., Application of laser microdissection ICP-MS for high resolution elemental mapping in mouse brain tissue: a comparative study with laser ablation ICP-MS. *Talanta* **2015,** *132*, 579-82.

7. Bandura, D. R.; Baranov, V. I.; Ornatsky, O. I.; Antonov, A.; Kinach, R.; Lou, X.; Pavlov, S.; Vorobiev, S.; Dick, J. E.; Tanner, S. D., Mass Cytometry: Technique for Real Time Single Cell Multitarget Immunoassay Based on Inductively Coupled Plasma Time-of-Flight Mass Sepctrometry. *Analytical chemistry* **2009,** *81*, 6813-6822.

8. Tanner, S. D.; Baranov, V. I.; Ornatsky, O. I.; Bandura, D. R.; George, T. C., An introduction to mass cytometry: fundamentals and applications. *Cancer Immunol Immunother* **2013,** *62* (5), 955-65.

9. Lin, Y.; Hamme, A. T., 2nd, Gold Nanoparticle Labeling Based ICP-MS Detection/Measurement of Bacteria, and Their Quantitative Photothermal Destruction. *J Mater Chem B Mater Biol Med* **2015,** *3* (17), 3573-3582.

10. Tang, M.; Wen, C. Y.; Wu, L. L.; Hong, S. L.; Hu, J.; Xu, C. M.; Pang, D. W.; Zhang, Z. L., A chip assisted immunomagnetic separation system for the efficient capture and in situ identification of circulating tumor cells. *Lab Chip* **2016,** *16* (7), 1214-23.

11. Han, J.; Michel, A. R.; Lee, H. S.; Kalscheuer, S.; Wohl, A.; Hoye, T. R.; McCormick, A. V.; Panyam, J.; Macosko, C. W., Nanoparticles Containing High Loads of Paclitaxel-Silicate Prodrugs: Formulation, Drug Release, and Anticancer Efficacy. *Mol Pharm* **2015**.

12. Jaras, K. T., A. A.; Ressine, A.; Soukka, T.; Marko-Varga, G.; Bjartell, A.; Malm, J.; Lilja, H., ENSAM: Europium Nanoparticles for Signal Enhancement of Antibody Microarrays on Nanoporous Silicon. *Journal of Proteome Research* **2008,** *7*, 1308-1314.

13. Jjunju, F. P.; Li, A.; Badu-Tawiah, A.; Wei, P.; Li, L.; Ouyang, Z.; Roqan, I. S.; Cooks, R. G., In situ analysis of corrosion inhibitors using a portable mass spectrometer with paper spray ionization. *The Analyst* **2013,** *138* (13), 3740-8.

14. De Pauw, E.; Pelzer, G.; Marien, J., Hydrophobic Reverse Derivitization for Secondary Ion Mass Spectrometry/Fast Atom Bombardment. *Org. Mass Spectrom.* **1985,** *20* (11), 692-693.

15. Busch, K. L. U., S. E.; Vincze, A.; Cooks, R. G.; Keough, T., Desorption Ionization Mass Spectrometry: Sample Preparation for Secondary Ion Mass Spectrometry, Laser Desorption, and Field Desorption. *J. Am. Chem. Soc.* **1982,** *104*, 1507-1511.

16. Busch, K. L. H., B.; Wood, K. V.; Cooks, R. G. ; Schwarz, C. G.; Katritzky, A. R., Characterization of Organic Cations of Synthetic Interest by Desorption Ionization and Tandem Mass Spectrometry *Journal of Organic Chemistry* **1984,** *49*, 764-769.

17. Li, Y. L.; Su, X.; Stahl, P. D.; Gross, M. L., Quantification of Diacylglycerol Molecular Species in Biological Samples by Electrospray Ionization Mass Spectrometry after One-Step Derivitization. *Anal. Chem.* **2007,** *79*, 1569-1574.

18. Bachor, R.; Cydzik, M.; Rudowska, M.; Kluczyk, A.; Stefanowicz, P.; Szewczuk, Z., Sensitive electrospray mass spectrometry analysis of one-bead-one-compound peptide libraries labeled by quaternary ammonium salts. *Mol Divers* **2012,** *16* (3), 613-8.

19. Kidwell, D. A. R., M. M.; Colton, R. J., Sequencing of Peptides by Secondary Ion Mass Spectrometry. *Journal of the Americal Chemical Society* **1984,** *106*, 2220-2222.

20. Wilson, R.; Cossins, A. R.; Spiller, D. G., Encoded microcarriers for high-throughput multiplexed detection. *Angewandte Chemie* **2006,** *45* (37), 6104-17.

21. Stott, S. L. L., R. J.; Nagrath, S.; Yu, M.; Miyamoto, D. T.; Ulkus, L.; Inserra, E. J.; Ulman, M.; Springer, S.; Nakamura, Z.; Moore, A. L.; Tsukurov, D. I.; Kempner, M. E.; Dahl, D. M.; Wu, C.; Ifrate, A. J.; Smith, M. R.; Tompkins, R. G.; Seqiust, L. V.; Toner, M.; Haber, D. A.; Maheswaran, S. , Isolation and Characterization of Circulating Tumor Cells from Patients with Localized and Metastatic Prostate Cancer *Science Translational Medicine* **2010,** *2* (25), 1-11.

22. Min, H.; Jo, S. M.; Kim, H. S., Efficient capture and simple quantification of circulating tumor cells using quantum dots and magnetic beads. *Small* **2015,** *11* (21), 2536-42.

23. Lim, L. S.; Hu, M.; Huang, M. C.; Cheong, W. C.; Gan, A. T.; Looi, X. L.; Leong, S. M.; Koay, E. S.; Li, M. H., Microsieve lab-chip device for rapid enumeration and fluorescence in situ hybridization of circulating tumor cells. *Lab Chip* **2012,** *12* (21), 4388-96.

24. Marganski, W. A.; El-Sirgany Costa, V.; Kilpatrick, M. W.; Tafas, T.; Yim, J.; Matthews, M., Digitized microscopy in the diagnosis of bladder cancer: analysis of >3000 cases during a 7-month period. *Cancer Cytopathol* **2011,** *119* (4), 279-89.

25. Ella-Menye, J. R.; Sharma, V.; Wang, G., New synthesis of chiral 1,3-oxazinan-2-ones from carbohydrate derivatives. *The Journal of organic chemistry* **2005,** *70* (2), 463-9.

26. Lu, H.-T., Synthesis and characterization of amino-functionalized silica nanoparticles. *Colloid Journal* **2013,** *75* (3), 311-318.

27. Luo, R.; Zhou, X.; Chen, S.; Li, Y.; Zhou, L.; Ji, H., Highly efficient synthesis of cyclic carbonates from epoxides catalyzed by salen aluminum complexes with built-in "CO2 capture" capability under mild conditions. *Green Chemistry* **2014,** *16* (3), 1496.

28. Razi, S. S.; Ali, R.; Srivastava, P.; Misra, A., A selective quinoline-derived fluorescent chemodosimeter to detect cyanide in aqueous medium. *Tetrahedron Letters* **2014,** *55* (5), 1052-1056.

CHAPTER 4. SELECTIVE DERIVATIZATION OF HYDROCARBONS WITH NITROGEN OR OXYGEN IN AN AMBIENT PLASMA

4.1 Introduction

The analysis of hydrocarbon samples persists as a significant challenge in mass spectrometry. Many inventive methods have been demonstrated for this purpose, including chemical transformations and new types of ionization. Electrospray ionization (ESI) was reported by Zhan and Fenn to be of potential importance to the analysis of petrochemiclas and it is indeed excellent for the analysis of suitably polar components[1]. Electron ionization (EI) has also proven to be useful but it doesn't cleanly produce molecular ions at the energies typically utilized (70 eV), so some researchers have studied low-energy[2-3] or low temperature EI[4]. Charge exchange under low energy EI conditions (essentially a form of chemical ionization) has also been investigated[5].

Softer ionization methods, such as field ionization (FI) and, more recently, atmospheric pressure chemical ionization (APCI) have been explored in some detail for the purpose of ionizing hydrocarbons[6]. Field ionization has been a staple of hydrocarbon analysis for many years[6-7]. "Typical" signals seen for hydrocarbons under the conditions of atmospheric pressure plasmas include the products of hydride abstraction ($[M-H]^+$), electron abstraction ($M^{+\cdot}$) or adducts $(M+NO)^+$, though variants of APCI (specifically, atmospheric pressure solids analysis probe, or ASAP), have also produced data which demonstrates that hydrocarbons can undergo chemical transformation to produce ions in atmospheric pressure plasmas[8].

Chemical transformation of hydrocarbons in the gas-phase with metal species[9] or adduction of metal cations to hydrocarbons[10] has been recognized as a particularly effective contribution which requires specialized equipment, but the fact remains that it is difficult to derivatize saturated hydrocarbons; both C-H and C-C bonds are not easy targets for chemical reaction[11-12].

Nitrogen fixation has previously been demonstrated as an effective way to conduct hydrocarbon analysis[8, 13-14]. It has been shown to work on non-standard (albeit simple) ion sources in an academic laboratory. Oxygen fixation (oxidation) of hydrocarbons has been reported in the presence of catalysts, again on non-standard instrumentation[15], or under conditions of desorption electrospray ionization (DESI) when operated under unusual conditions which produced a discharge[16]. Oxidation of hydrocarbons as a mode of ionization hasn't been reported under the conditions of standard APCI.

Other forms of heteroatom fixation include oxygen fixation (rather than simple oxidation). Notably, Badal et al. recently demonstrated the insertion of oxygen into benzene[17], which induced the ejection of a CH unit to form pyrilium. This chemistry was shown to occur under conditions of a helium:oxygen flowing atmospheric pressure afterglow (FAPA), which is a DC plasma.

This work reports the use of a commercially available ion source to reproducibly and selectively incorporate nitrogen or oxygen into a saturated hydrocarbon sample, thereby efficiently ionizing the material. No sample preparation or catalyst is required and the experiment is conducted with standard instrumentation. The switch between the incorporation of oxygen or nitrogen is affected by simply changing the corona current of the APCI source at a constant supplementary flow of air into the ionization region, or changing the flow of air leaked into the ionization region while keeping the corona current constant.

4.2 Results and Discussion

4.2.1 Oxidation of Hydrocarbons for Analysis

The ability to switch between derivatization products, simply by switching the parameters of an ion source, is desirable and useful; the acquisition of data for both derivatives serves as a

complimentary set of data, which would arguably bolster the assignment of a molecular formula. Also, the ability to either oxidize saturated hydrocarbons or not highlights the very different chemical environments that can be generated in the APGC ion source depending on corona current and/or gas composition. Furthermore, the oxidation and dehydrogenation of hydrocarbons to ketones without a catalyst is remarkable.

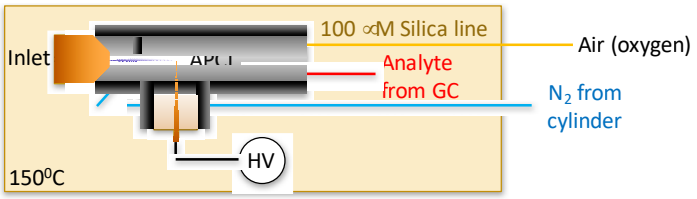

Figure 4.1 Illustration of the ion source fitted with a silica air line

Air was leaked into an otherwise sealed ion source via a fused silica capillary; the setup is illustrated in Figure 4.1. The flow of air can be approximated using Equation 4.1; the Hagen-Poiseuille equation. In this approximation, D is the diameter of the capillary in meters, P is the pressure drop across the capillary in pascals, μ is the dynamic viscosity of air in Pascal seconds and x is the length of the silica line. Laminar flow is assumed and the value of the dynamic viscosity of air at room temperature is used, so the calculated value of the flow rate through the capillary is rough. The pressure in the source has been determined internally at Waters to be about 94% of ambient pressure. Through the 90 cm, 250 μm internal diameter line, the flow was calculated to be approximately 0.8 liters/hour. The gas supplied to the source region by the instrument was set to flow at 200 liters/hour, so the air leak constituted approximately 0.4% of the overall gas flow.

The other gas flows, supplied through the instrument, were fed by a high purity nitrogen cylinder. Nitrogen fixation was found to be dominant at low (1 uA and below) corona currents. Setting the corona current above this threshold switched the dominant process to oxidation.

$$Q = \frac{\pi D^4 * \Delta P}{128\mu * x}$$

Equation 4.1 Hagen-Poiseuille equation for flow through a pipe

Nitrogen gas flow rates, ion source temperature and concentration of the analyte were all varied and their effect on the speciation of the mass spectra, recorded. These variables were not found to have a significant impact on the outcome of the experiment (Tables 4.1-4.4). The I.D. (inner diameter) of the silica line used to deliver air to the ion source was varied and the effect this had on the data was pronounced. Thinner capillary yielded less oxidation (Figure 4.2). Figure 4.3 shows the spectra of nonane and tetradecane, each recorded at a corona current of 10 μA and a current of 1 μA, having passed through the GC column.

The first and most obvious thing to note about the spectra is the speciation of the peaks of highest intensity. The low-current plasma generates the nitrogen fixation product, $[M+N]^+$ and its dehydrogenated analogue, $[M-2H+N]^+$, while the high-current plasma generates the oxidized species $[M-H+O]^+$ and its dehydrogenation products

Table 4.1 the effect of concentration on the speciation of the mass spectra at a corona current of 10 μA

Concentration (% in hexane)	**M+O-H:M+O-3H:M+O-5H**
10	1:0.67:0.41
1	1:0.65:0.42
0.1	1:0.82:0.67
0.01	1:1.4:1.1
0.001	1:1.25:1.15 (low signal)

Table 4.2 the effect of concentration on the speciation of the mass spectra at a corona current of 1 μA

Concentration (% in hexane)	**M+N:M+N-2H**
10	1:1.1
1	1:0.98
0.1	1:0.92
0.01	1:0.9
0.001	Not detectable

Table 4.3 the effect of temperature on the speciation of the mass spectra at a corona current of 10 μA

Temperature (ºC)	**M+O-H:M+O-3H:M+O-5H**
150	1:0.67:0.41
100	1:0.65:0.42
50	1:0.82:0.67

Table 4.4 the effect of temperature on the speciation of the mass spectra at a corona current of 1 μA

Temperature (ºC)	**M+N:M+N-2H**
150	1:1.1
100	1:0.98
50	1:0.92

To test the general nature of the observed phenomenon, tetradecane (Figure 4.3), octadecane (Figure 4.4) and a polywax (GC trace Figure 4.5 and mass spectra Figure 4.6) standard were also analyzed at different corona currents under a nitrogen atmosphere with an air leak. Each of these standards exhibited the same chemistry as nonane; the signals for oxidized materials exhibited the same dependence on corona current as the nonane standard.

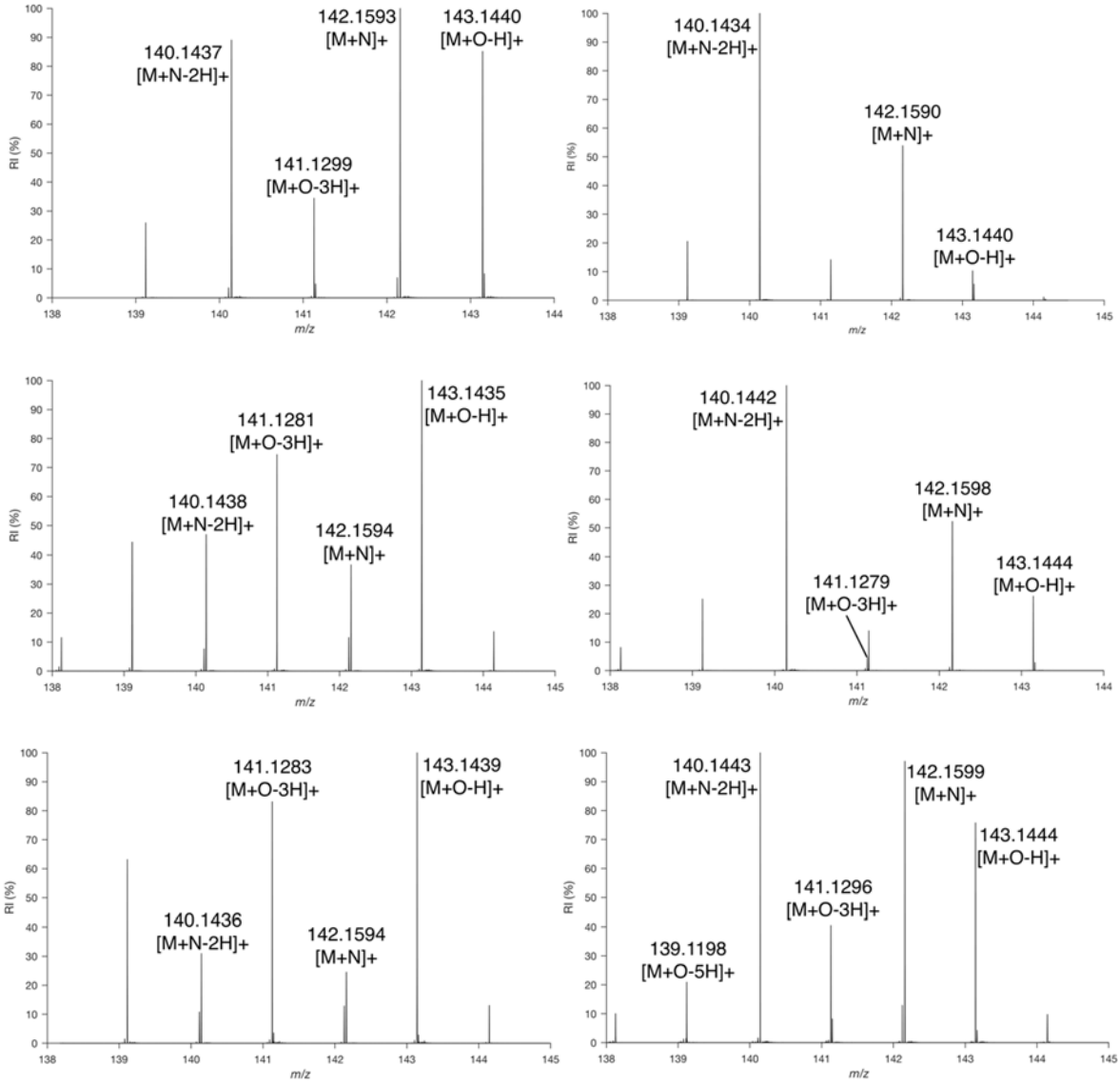

Figure 4.2 The effect of the inner diameter (I.D.) of the capillary used to carry air to the ionization region. Top- 100 μm I.D. fused silica line at 10 μA and 1 μA corona current; Middle- 250 μm I.D. fused silica line at 10 μA and 1 μA corona current; Bottom - 320 μm I.D. fused silica line at 10 μA and 1 μA corona current

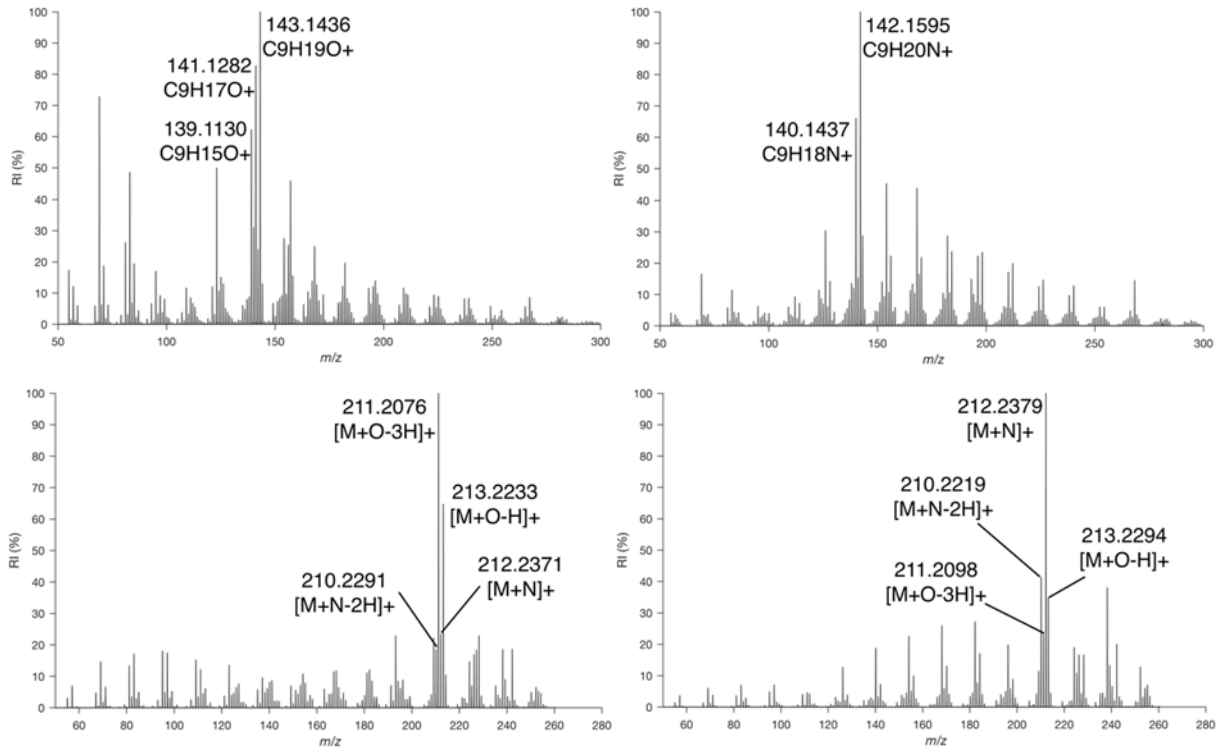

Figure 4.3 Clockwise from top left, Full scan mass spectrum of; nonane recorded at 10 μA, nonane recorded at 1 μA, tetradecane recorded at 1 μA and recorded at 10 μA

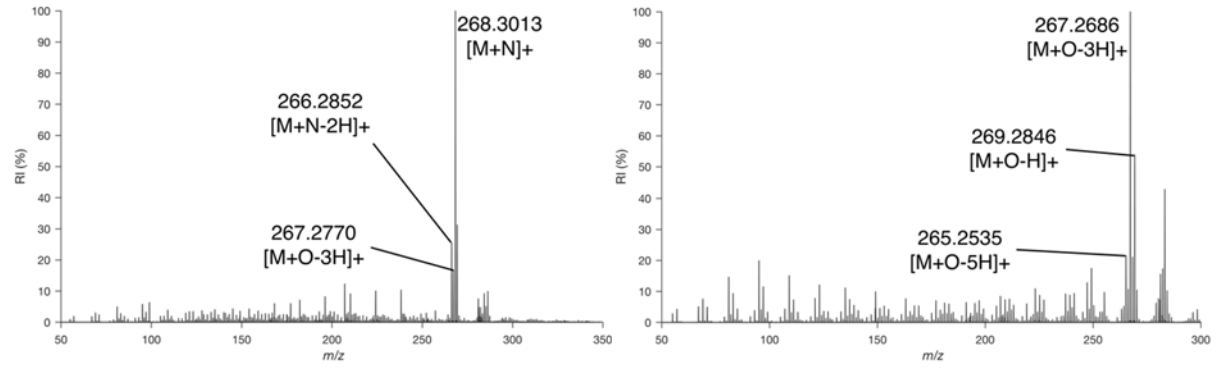

Figure 4.4 Mass spectrum of octadecane recorded at low corona current (left) and high corona current (right)

The polywax standard revealed an interesting aspect of the nitrogen fixation chemistry, specifically with regard to the competition between the observable M-H^+ signal and the products of oxidation or nitrogen fixation as a function of chain length. There is a sharp transition from

chain length C34 to C36, where M-H^+ appears. This seems to suggest that there is a saddle point of stability, where the product of hydride abstraction becomes stable enough to survive in high enough abundance to compete with the intensity of the product of nitrogen fixation or oxidation. This point will be referred to later in this chapter, when the ion chemistry is explored in detail.

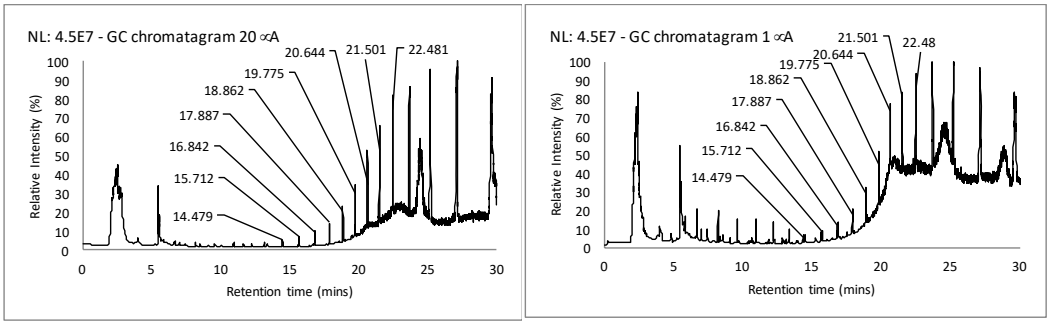

Figure 4.5 GC trace of the polywax standard recorded at high corona current (left) and low corona current (right)

It has previously been proposed that the production of highly reactive N_3^+ in the corona discharge is responsible for the conversion of hydrocarbons to imines ($[M+N]^+$), as this highly reactive nitrogen species may insert itself between C-C bonds and so react with otherwise inert material. In this case, the N_3^+ reagent ion was not directly observed; however, this is likely to be due to the relatively low transmission of low mass species in the TOF instrumentation. For the same reason, it was difficult to detect any potentially reactive oxygen species which may be responsible for oxidation; the only thing that was detected that may be considered to be notably reactive was charged molecular oxygen, which itself may not be likely to oxidize hydrocarbons.

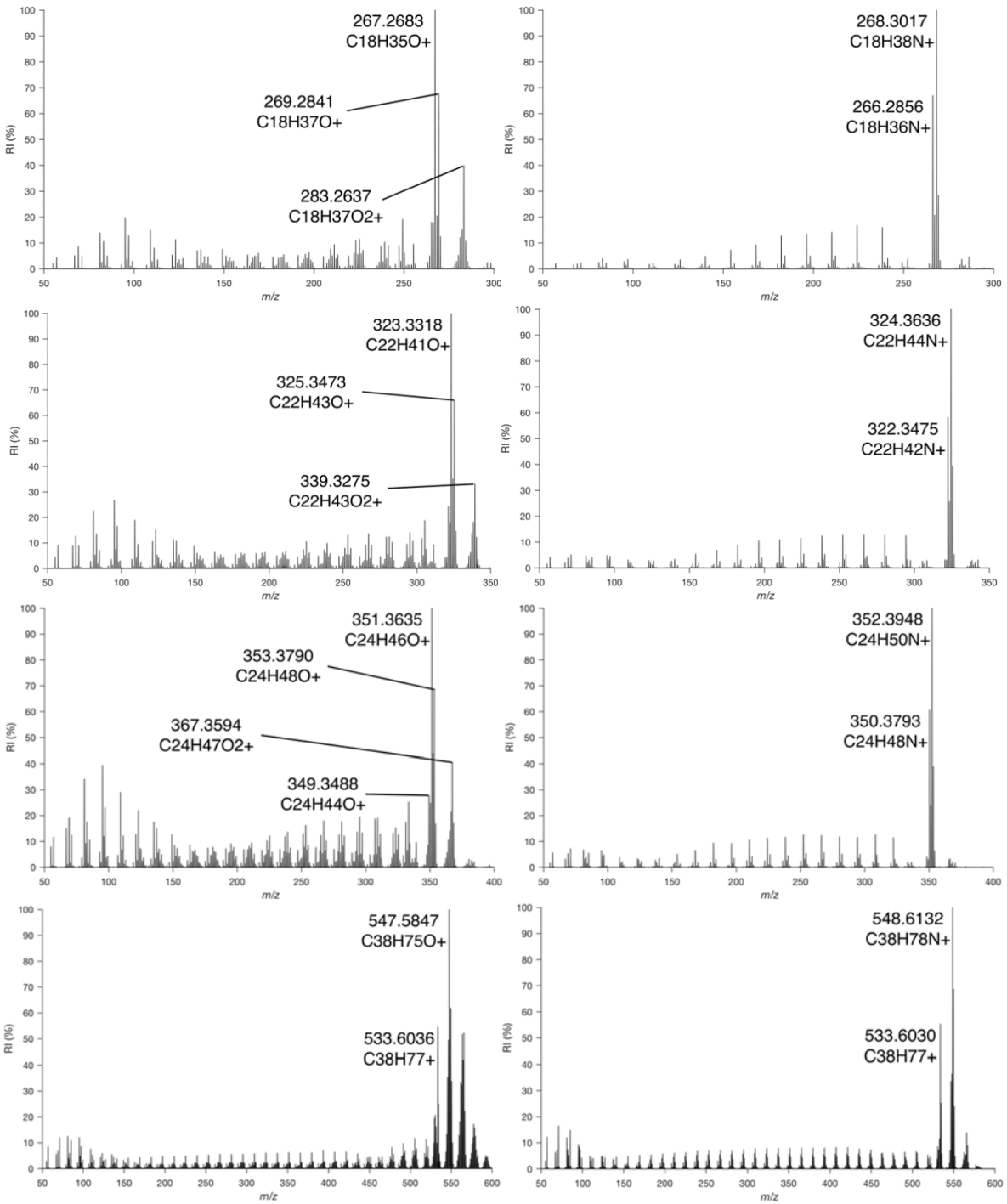

Figure 4.6 Representative mass spectra from the polywax sample obtained at high (left) and low (right) corona current

Regardless of this, the behavior of the APGC ion source was highly reproducible with regard to the ability to insert nitrogen, or oxidize the hydrocarbon chain, selectively.

Due to the observed fragmentation in the full scan mass spectra, it is reasonable to say that the corona discharge in the APGC source is relatively "hot", even though it is an atmospheric pressure corona discharge. The reasons for this fragmentation are assigned as by-products of the ion chemistry which produces the main species of interest in the spectra (see section 4.2.2). Of the series that are produced both above and below the pseudo-molecular ions, many are distributions comprising hydrocarbons with both oxygen and nitrogen fixation, though the latter is highly dominant. Also in the lower range, hydrocarbon fragment ions are present. The observation of a series of ions at higher mass, produced at reasonably high intensity from pure nonane suggests that not only does the APGC source cause fragmentation, but that the fragments are suitably reactive for recombination reactions to take place. Looking in detail at the spectrum of nonane, recorded at both low and high APCI currents, the recombination peaks bear only a single heteroatom (either nitrogen or oxygen), determined by accurate mass measurement. The hydrocarbon fragments in the lower range are charged carbocationic species. It is therefore proposed that the recombination is that of the reaction between the neutral product of nitrogen fixation at the terminus of the molecule (or an external imine on the chain, if formed) or the neutral product of oxidation and the lighter carbocationic species. These possibilities are summed up in Scheme 4.1.

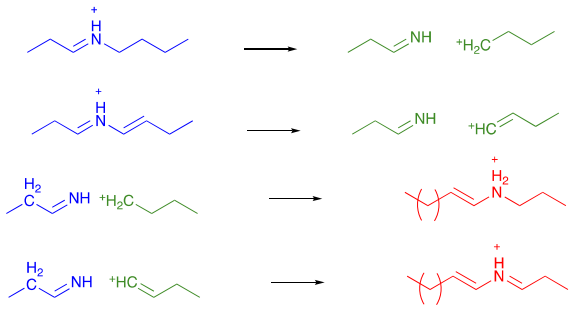

Scheme 4.1 Products of ionization (blue) fragment to reactive species (green) which may recombine with pseudomolecular ions to produce species of higher mass (red)

Labelled spectra based on this hypothesis can be found Figure 4.7. It is evident from these spectra that the carbon chain length of recombined species does not measurably progress past two times the chain length of the molecular ion; nonane does not produce a recombined ion above 18 carbons in length, for instance.

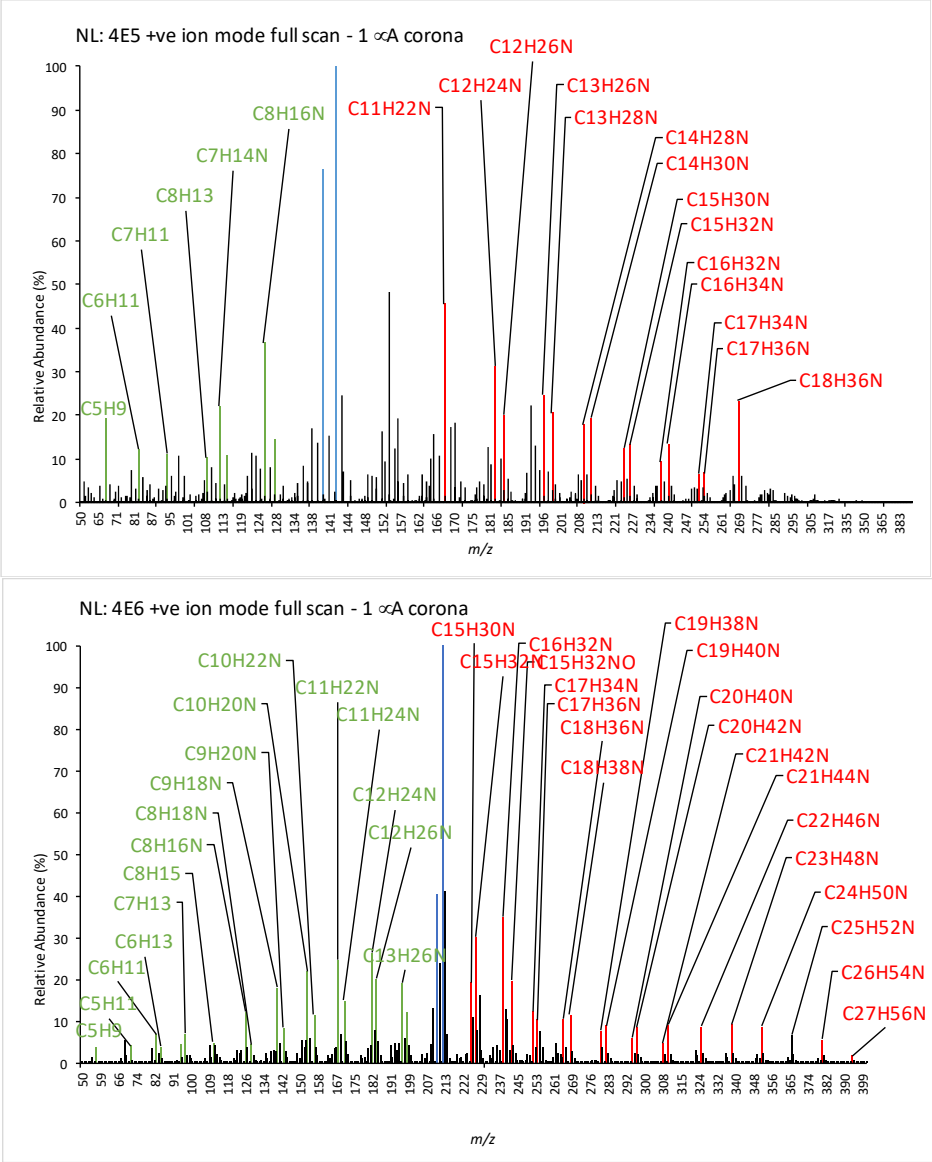

Figure 4.7 Analysis of the fragments and recombined ions present in the spectrum of nonane (top) and tetradecane (bottom)

Interestingly, this recombination drops off sharply as the hydrocarbon chain length increases (see octadecane and polywax spectra in Figures 4.4 and 4.6) implying steric barriers to recombination. The ion-molecule recombination is also hindered when the concentration of the analyte is very low (Figure 4.8). This provides further evidence of the nature of the recombination

process as a gas-phase ion molecule reaction which requires sufficient number density of analyte. The oxidation and/or recombination of hydrocarbons in plasmas is not new, but in previous reports, a catalyst for the transformation has always been documented[18-19].

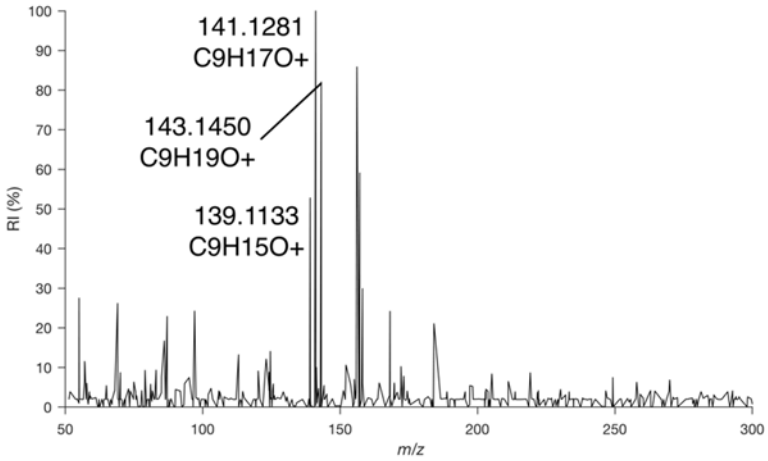

Figure 4.8 718 femtograms of nonane analyzed under oxidizing conditions

The fact that the addition of a small amount of air was required in order to see the oxidized products was demonstration enough that the ion source effectively excluded atmospheric oxygen under normal conditions. Conversely, using only pure nitrogen from a cylinder precluded oxidation and, under these conditions, ionization at any corona current yielded only nitrogen fixation products (Figure 4.9). The introduction of water to the ion source by putting a small vial of water into the source region (held at 150ºC) and feeding it into the ionization region via a 100 μM inner diameter fused silica capillary did not change the speciation of the spectrum; signals corresponding to nitrogen fixation were dominant in the mass spectrum while oxidation was absent (Figure 4.10).

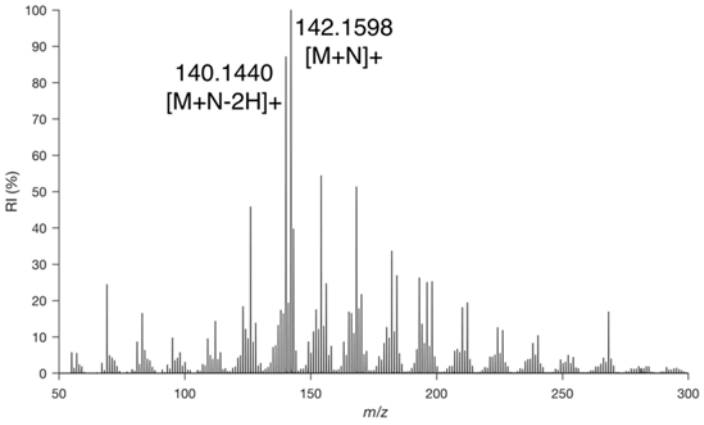

Figure 4.9 The mass spectrum of nonane recorded at high corona current in pure N_2

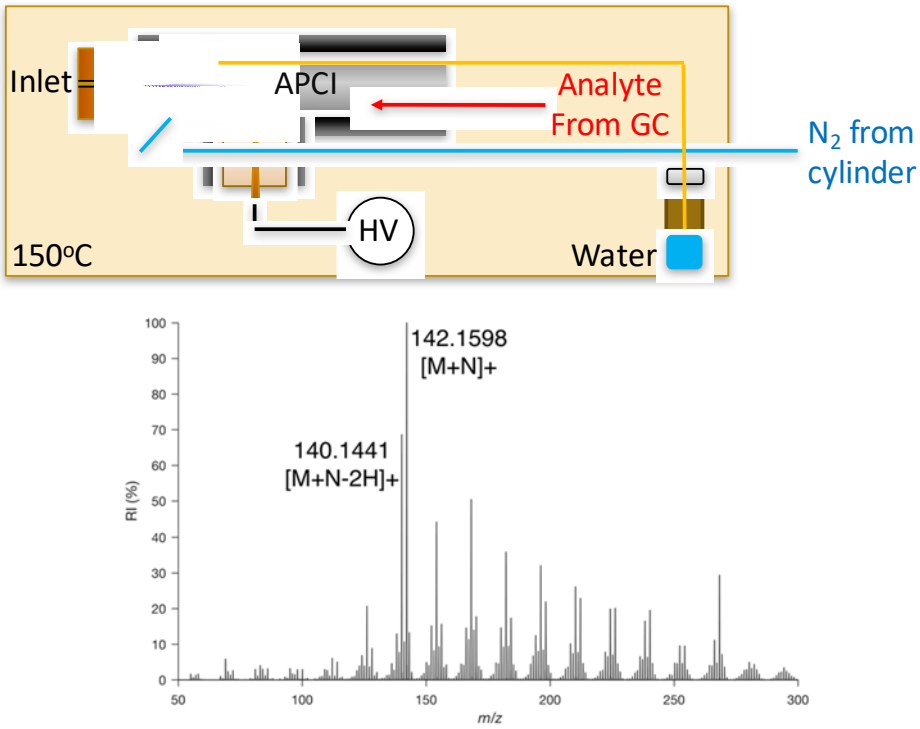

Figure 4.10 Experimental setup to introduce water to ion source and the spectrum of nonane recorded under these conditions

When pure oxygen from a cylinder was allowed to flow through the "air" line into the source at a pressure of 1 bar, nitrogen fixation was entirely quenched. The dominant signal in the spectrum was oxidized nonane ($[M+O-5H]^+$), which was accompanied by the dehydrogenated

form of the ion, $[M+O-3H]^+$ and the ketone $[M+O-H]^+$ (Figure 4.11). This profile persisted at both low and high corona current. A needle valve was used to restrict the flow of oxygen to below the measurable rate by a commercial flow meter yet still, the presence of pure oxygen in the ion source proved to be too overwhelming to permit nitrogen fixation with any set of variables.

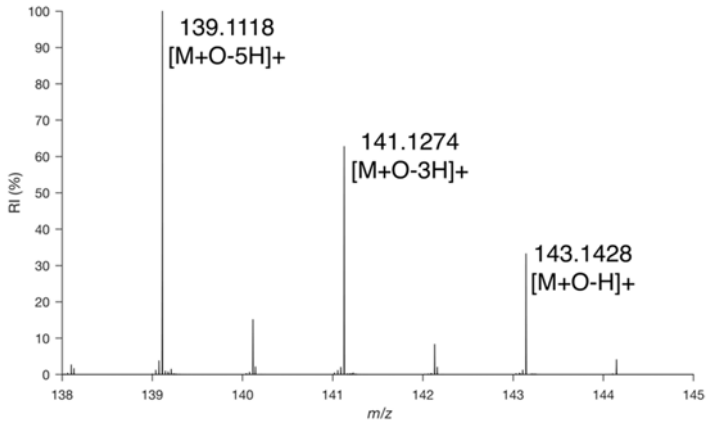

Figure 4.11 The spectrum of nonane recoded in the presence of a leak of pure oxygen from a cylinder at low corona current

4.2.2 Exploration of the Ion Chemistry Involved in Oxidation

In order to identify the oxidized product of nonane (and therefore extrapolate the result to other hydrocarbon species), a modified version of the APGC source, configured to run independently of the mass spectrometer in the open air, was used to generate and collect ions on a surface. This is illustrated in Figure 4.12.

A high voltage power supply was used to apply 4 kV to the corona pin, and the ground from the same supply was in electrical contact with the main barrel of the ionization source, so as to emulate the on-line setup. A stable corona current of less than 10 microamps was established. Nonane vapor was fed into the source from a heated vial of nonane liquid through a silica line for three hours. The sides of the barrel were subsequently washed with 100 microliters of hexane,

which was then diluted five-fold in order to make the volume of liquid accessible to the autosampling system of the GC-MS. The collected material was analyzed by and compared to standard materials.

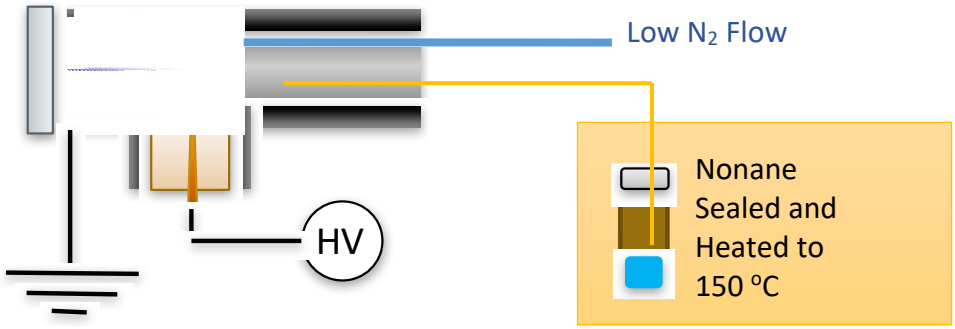

Figure 4.12 Illustration of a modified APGC source configured for collection of ions on a surface

The primary product of this process was 3-nonanone, as confirmed by the chromatography retention time and the full scan spectrum (Figure 4.13). The retention times of 4- and 5- nonanone were so similar as to be ambiguous. There were, however, spectral differences that facilitated the identification of the product as 5-nonanone (Figure 4.14).

3-nonanone and the lesser product, 5-nonanone, seemed to exist as the only ketone products. The hypothesis that ozone is implicated in the mechanism fits this data. A bent, 3-membered chain of oxygen atoms would be able to bridge and therefore interact with carbons in a chain separated by a methylene (Scheme 4.2). This hypothesis appears to be supported in the literature, especially in the recent work of Lee *et al.*[20]. In that work, the reaction between neutral, saturated hydrocarbon species and ozone was computed. What was shown was a complex pathway which may proceed via a neutral, ionic or radical route to generate the trihydroxide adduct of the hydrocarbon, with preference for the radical route in the gas phase. Following this, a series of reaction pathways were

computed which resulted in C-C fragmentation as well as the formation of ketones. The truncated form of the reaction scheme is given in Scheme 4.2.

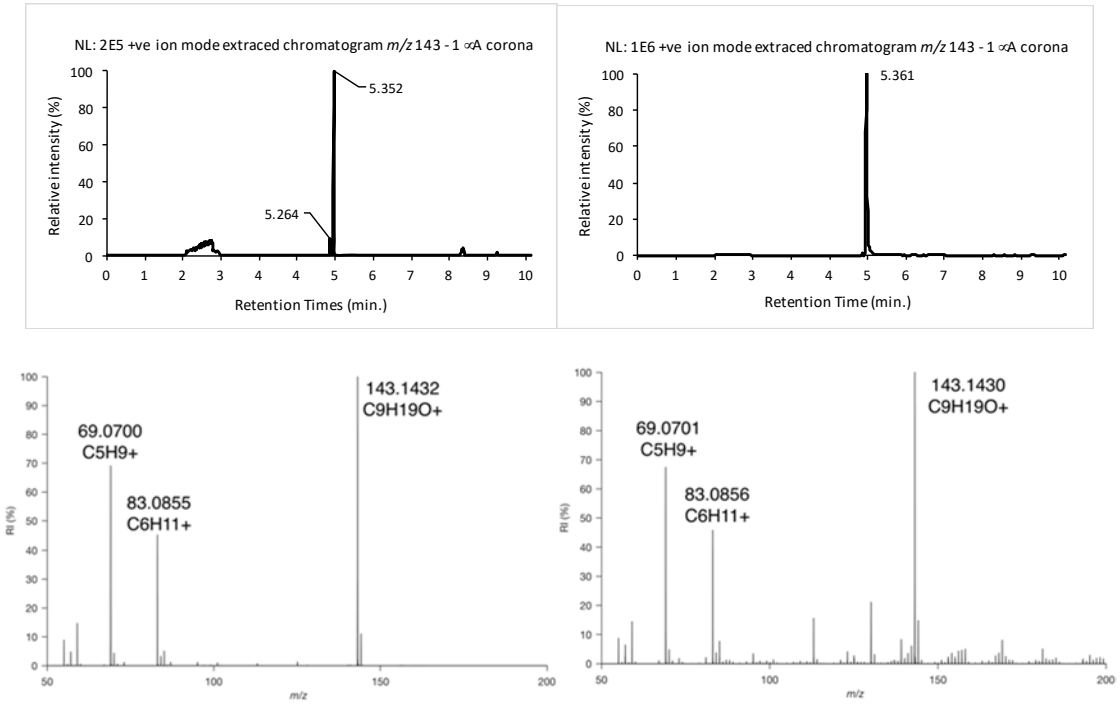

Figure 4.13 Top right – extracted ion chromatogram (XIC) of *m/z* 143.14 from the collected nonane product. Top left – XIC of *m/z* 143.14 from pure 3- nonanone. Bottom left – Full scan mass spectrum of product of nonane collection. Bottom right – full scan mass spectrum of 3-nonanone

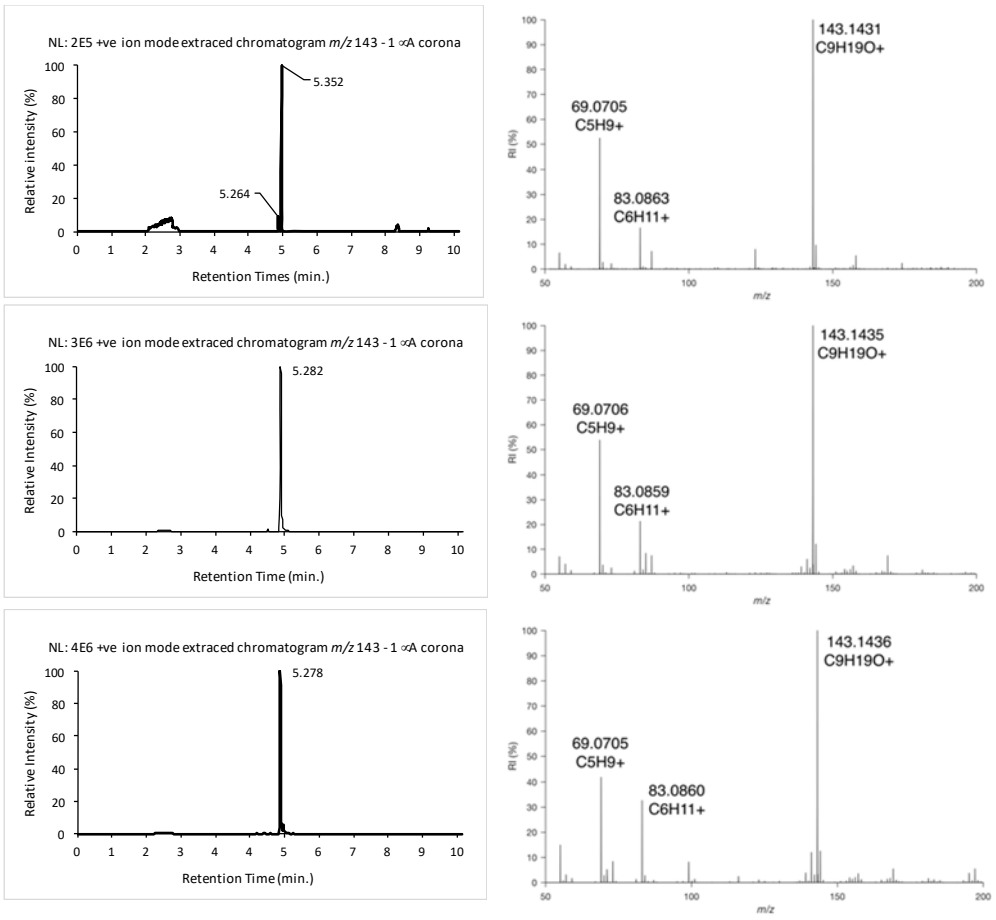

Figure 4.14 The retention time of 4 and 5 nonanone (top), the full scan mass spectra of 4 and 5 nonanone (middle) and the full scan mass spectrum of the minor component collected from nonane ionization (bottom)

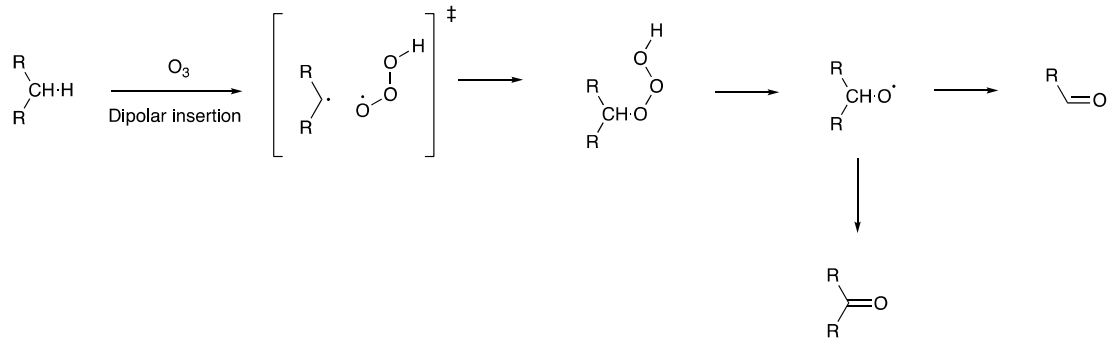

Scheme 4.2 Computed reaction pathway (truncated) between ozone and neutral saturated hydrocarbon molecules

As well as oxidation, routes to dehydrogenation were also computed in Lee's work[20], though they were considered to be unfavorable reaction pathways at least between neutral molecules. This is one indication that the energy landscape in the plasma forces the chemistry to diverge from previous observation. Evidence of ozone as the important species is in the fact that oxidation increases as a function of corona current; It is known that the volume of ozone produced from oxygen is dependent on the discharge current[21-22]. The voltage required to induce the currents in this experiment was over the range of 2.2 kV to 5 kV. Further evidence of the importance of Ozone will be discussed later.

In order to investigate the regioselectivity in more detail, a modified reflux condenser was constructed according to Figure 4.15. This condenser incorporated a pin-barrel corona discharge module in the neck of the reflux condenser, which facilitated interaction between vapor-phase hydrocarbon and the discharge.

Over the course of a number of hours, the hydrocarbon was left to boil through the system. Subsequently, nonane was replaced with heptane and treated in the same manner. In both cases, the conversion of hydrocarbon to oxidized product was minimal, presumably because the flux of hydrocarbon vapor overwhelmed the small plasma source. The residual liquid which was trapped between the steel barrel and the neck of the reflux condenser was dissolved in methanol and analyzed by mass spectrometry. The recorded spectrum is given in Figure 4.16. both species in the spectra corresponded to the dehydrogenated, oxidized materials.

The dehyderogenation products are readily observed in all mass spectra recorded using an APCI ion source under the conditions reported here, but they are typically flanked by peaks which are not dehydrogenated ($[M+O-H]^+$), as well as doubly-dehydrogenated ($[M+O-5H]^+$). This

experiment was performed on a different APCI setup, away from the mass spectrometer and the chemical selectivity clearly favors the singly dehydrogenated material.

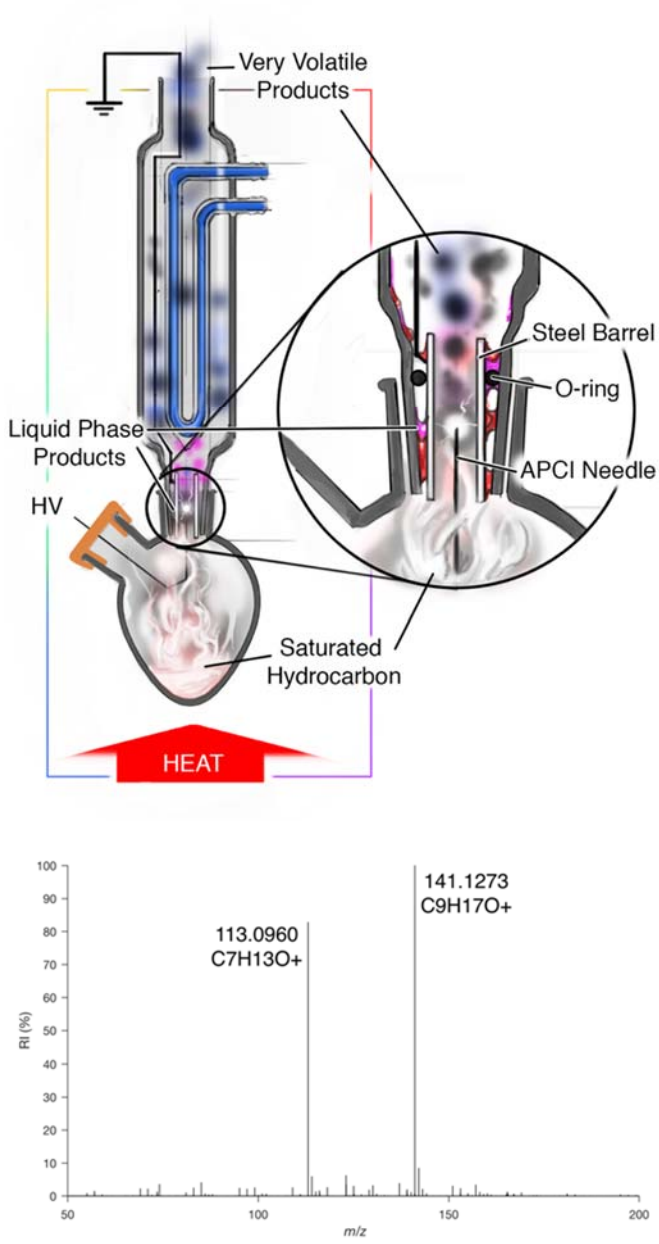

Figure 4.15 Modified reflux apparatus to expose hydrocarbon vapor to corona discharge and the species produced from heptane and nonane in this apparatus

During the experiment illustrated in Figure 4.15, an odor was emitted from the top of the reflux condenser, which suggested that inefficient condensation was occurring and some material was escaping. In order to determine what these vapors were, a second apparatus was constructed which was designed to transfer the vapor-phase chemicals from a hot vessel directly into a chilled vessel via an APCI discharge source (Figure 4.17).

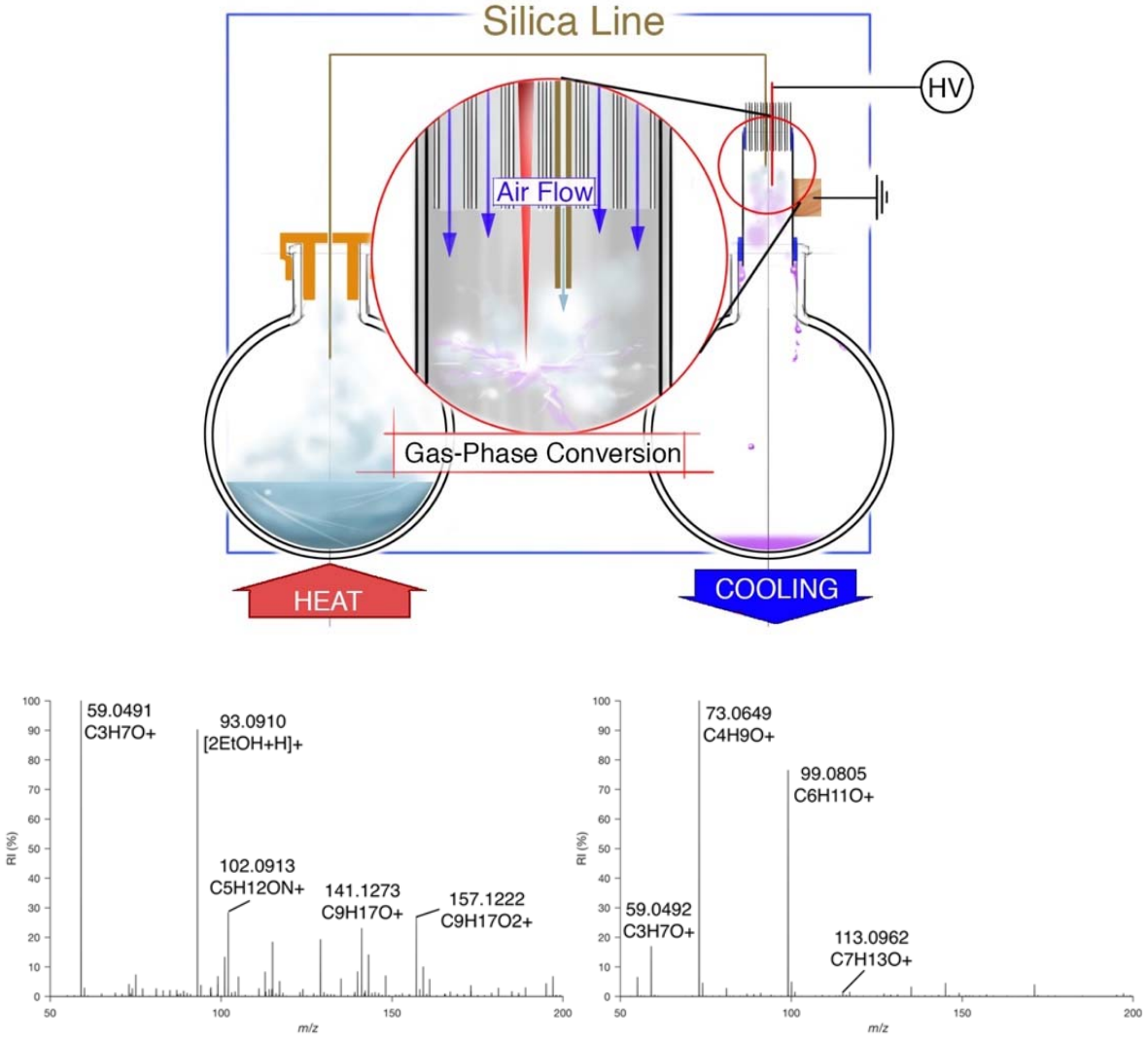

Figure 4.16 Illustration of the apparatus used to collect the volatile produts of hydrocarbon oxidation; A-Collected fragmented products from nonane. B – Collected fragmented products from heptane

In this experiment, nonane was boiled in the first flask which forced it through the silica transfer line and into the region of corona discharge. The resulting spectrum showed a dominant ion with the chemical formula C_3H_7O (Figure 4.16). This observation parallels the initial assignment of the major product of nonane oxidation in the corona discharge; 3-nonanone. The interpretation of this data is that upon exposure to the corona discharge, the small amount of material that was transferred was efficiently oxidized and then fragmented to yield propionaldehyde. This molecule was then collected by efficient condensation, though in low abundance.

The experiment was repeated with heptane and two prominent ions were observed. These ions had the molecular formula, C_4H_9O and $C_6H_{11}O$ (Figure 4.16). In this case, as with nonane, the two recorded structures provided a report on the position of oxidation in the chain. The formula of the two ions indicated that, as in the case of nonane, the position of oxidation was separated by a methylene unit. The regioselectivity of the reaction is suggested by this observation.

In order to observe both low and high-mass products from the same setup, but separated, a modified distillation-type apparatus was set up according to Figure 4.17 and nonane was exposed once again to the plasma. This setup was designed to facilitate condensation of the oxidized molecule, as well as its low mass fragment ions. By analyzing residual material in the distillation head, oxidized, dehydrogenated ions were found, while analysis of the collected material revealed the propionaldehyde fragment, illustrating the link between the two species.

With regard to the utility of this chemistry, the way in which hydrocarbons can be converted to their oxidized analogues in an otherwise un-catalyzed fashion is interesting. At low flow rates of hydrocarbon vapor (as in the initial GC-MS experiment), the chemistry that occurs in the APCI ion source is apparently very efficient. This is demonstrated by the fact that no

appreciable signal was observed for residual nonane after the collection experiment was conducted, i.e. all the hydrocarbon was converted efficiently.

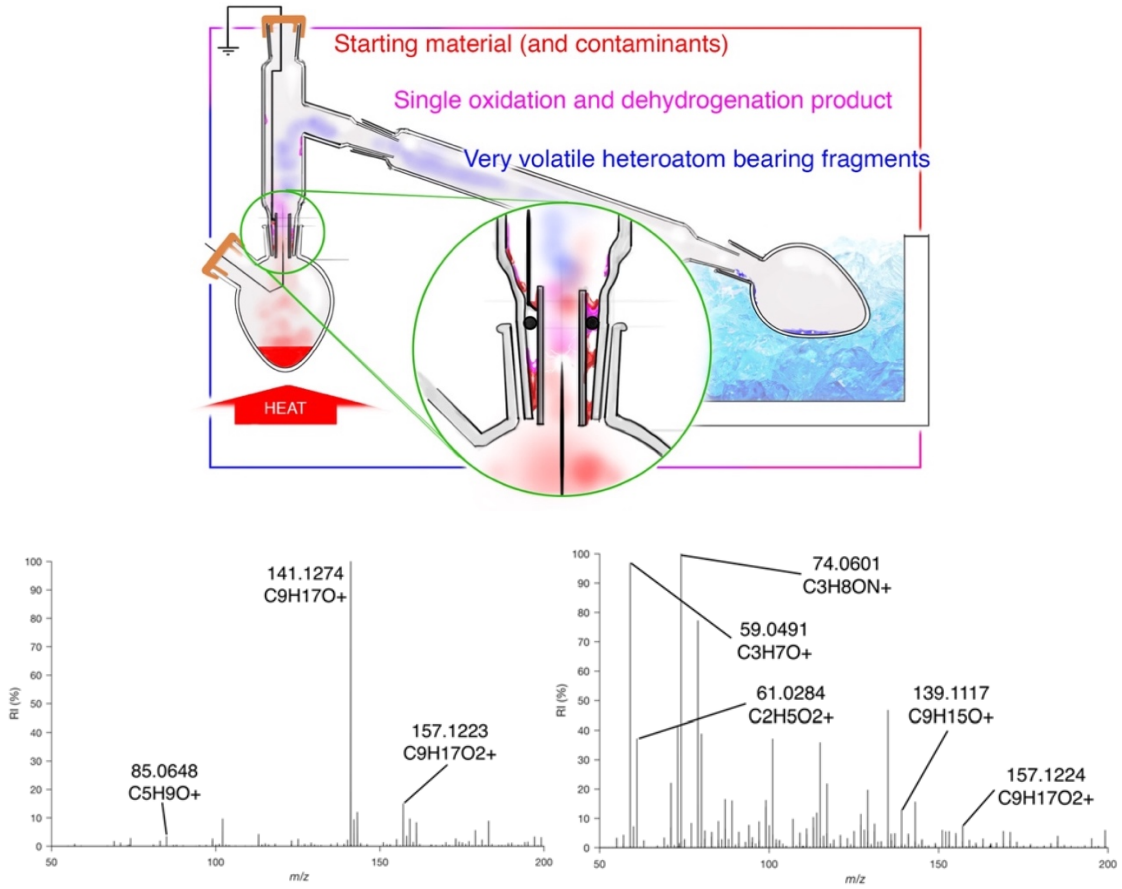

Figure 4.17 Illustration of the apparatus used to collect both non-volatile and volatile products of nonane oxidation (top) and the spectra from the residual liquid in the distillation head and the cooled collection flask (bottom)

Probe APCI was utilized to ionize heptane, nonane and hexadecane. Under these high-concentration conditions, it was possible to directly record fragmentation spectra of the ozone adducts of hydrocarbon species (Figure 4.18). The ozone adducts were present in series, corresponding to $[M+O_3-H]^+$ and $[M+O_3+H]^+$, the former of which is interpreted as the protonated

form of the initial product of addition of ozone to a neutral hydrocarbon computed by Lee *et al.*[20]. The latter is interpreted as the product of an ion-molecule reaction between hydride abstracted hydrocarbon and neutral ozone.

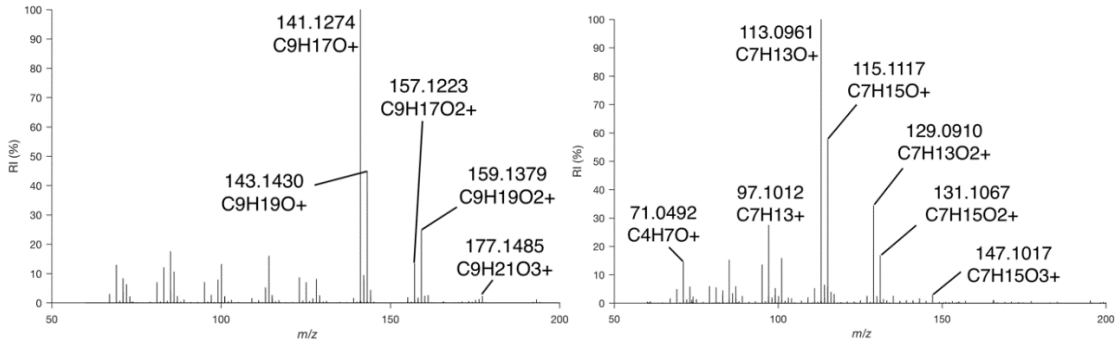

Figure 4.18 Full scan probe APCI mass spectra of nonane (left) and heptane (right)

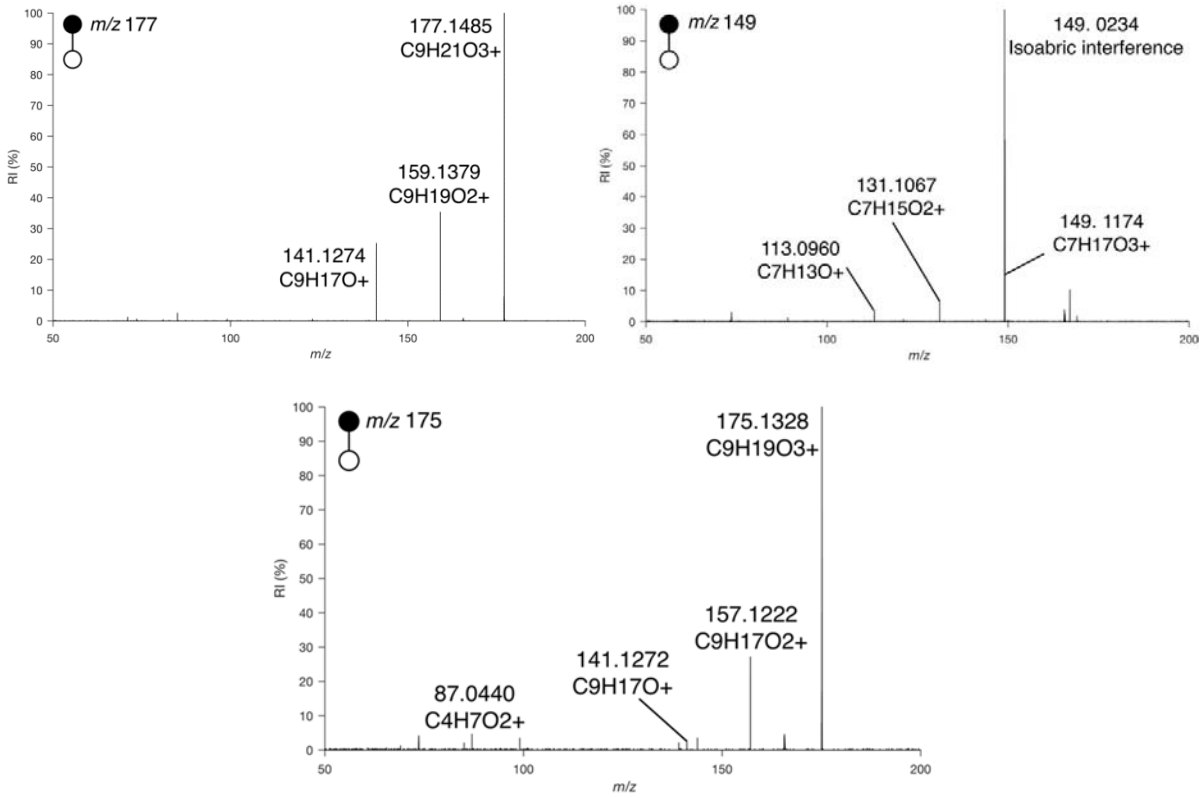

Figure 4.19 CID product ion mass spectrum of the protonated ozone adduct of nonane (left), heptane (right) and hydride abstracted ozone adduct of nonane (bottom)

Postulated fragmentation mechanisms of the protonated and hydride abstracted ozone adducts of hydrocarbons are presented in Schemes 4.3-4.5. These schemes make use of very similar mechanistic pathways to explain all of the observed behavior of the species in the data presented here, which takes into account the delicate nature of the balance between the observed species; energetically, the pathways to the many products are likely to be similar. This diverges from the computed data for the neutral species, which is justified by the consideration that these are gas-phase ions.

It is proposed that the hydride abstracted ozone adduct quickly rearranges to desaturate the hydrocarbon chain which facilitates the first loss of water recorded in the fragmentation spectrum of that adduct. The protonated ozone adduct is set up to lose water without rearrangement and so it does. Subsequent water loss from both types of adduct require further desaturation of the hydrocarbon chain, which is proposed to occur in both cases by essentially the same mechanism, involving a series of sigmatropic rearrangements (hydride shifts).

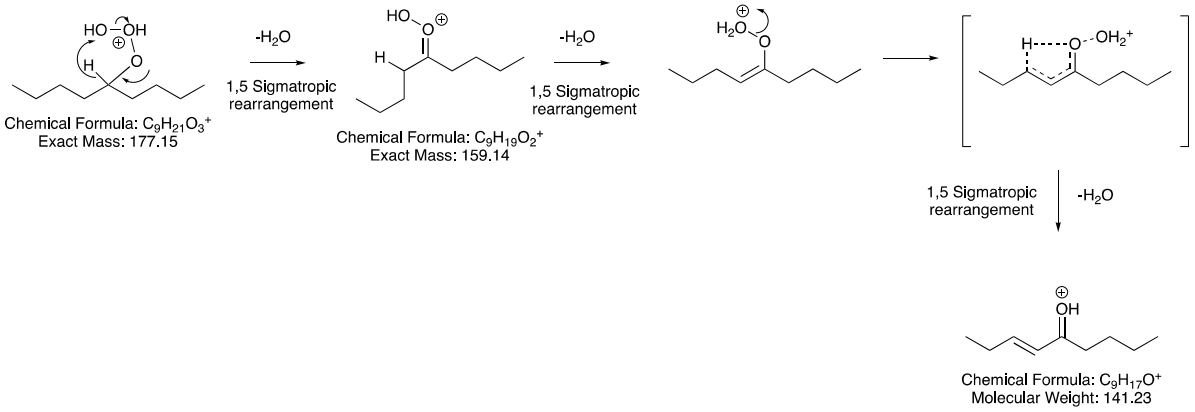

Scheme 4.3 Postulated route to protonated, dehydrogenated ketones from the protonated ozone adduct of nonane

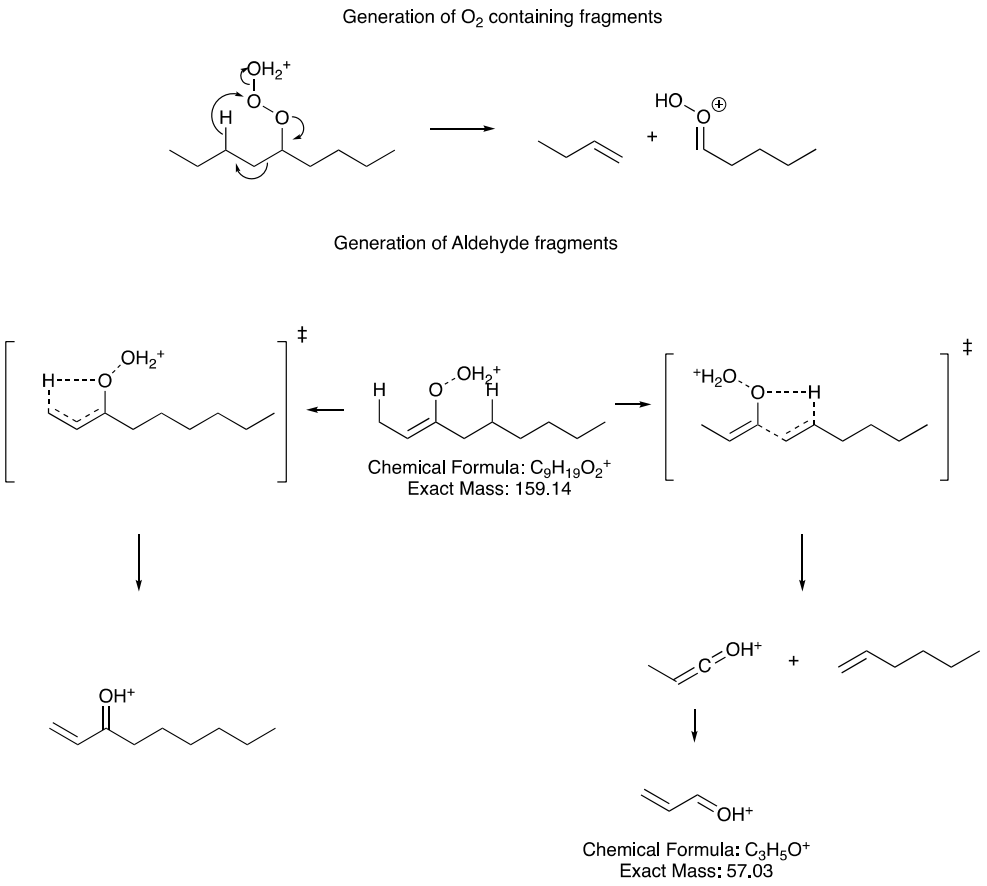

Scheme 4.4 Generation of peroxide-like fragments and the generation of desaturated aldehydes via sigmatropic rearrangement and a McLafferty-like mechanism respectively

The mechanisms of degradation presented here are attractive as they share apparently stable transition states, all of which invoke 5- or 6- membered conformations. These mechanisms also resemble transitions traditionally accepted for gas phase ions, such as the McLafferty rearrangement, which is also essentially a sigmatropic rearrangement.

Scheme 4.4 postulates why, when the oxidation site is at the 3-position of nonane, the primary product is the dehydrogenated propionaldehyde fragment. The rearrangement essentially has a “choice” of proton to affect rearrangement; a proton bound to a primary carbon or a proton bound to a secondary carbon. It should be more energetically favorable to invoke the latter.

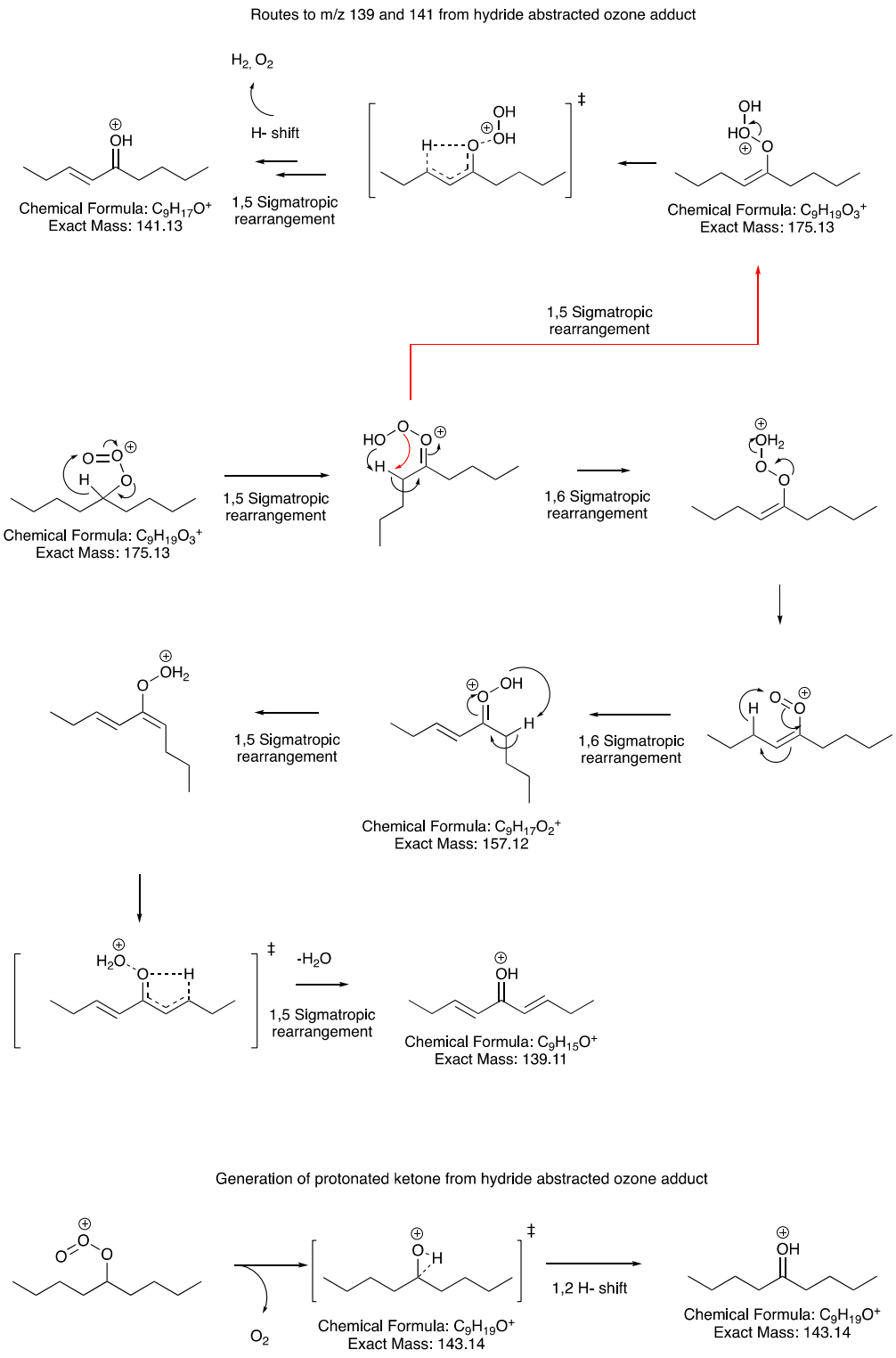

Scheme 4.5 Postulated mechanism for the formation of doubly-, singly- and non-dehydrogenated ketones from the hydride abstracted ozone adduct of nonane

4.3 Experimental

4.3.1 General Gas Chromatography Method

Gas chromatography was conducted on an Agilent A7890, using an RXI-5sil MS 30m x 0.25 mm GC column with a film thickness of 0.25 μm (Restek Inc.). The GC was equipped with an autosampler. The front inlet was operated at 180 ºC in splitless mode. The transfer line from the GC to the MS was held at 180 ºC.

For pure hydrocarbon samples (nonane, tetradecane and octadecane), 1 μL of sample (varying concentration in hexane) was injected onto the column at an initial temperature of 35ºC, which was ramped at 25ºC/min to 260º-C with a hold time of 0.2 mins. (total run time 10.2 mins.).

For the polywax standard material, 1 μL of the standard was injected onto the column at an initial temperature of 140 ºC, which was ramped at 15 ºC/min to 320 ºC, with a hold time of 10 mins (total run tome 30 mins.).

Ionization and analysis was conducted using an APGC interface with a QToF mass analyzer (Synapt G2 Si, Waters Corporation).

4.3.2 Analysis of Collected Hydrocarbon Reaction Products

In all cases, pure hydrocarbon liquid was loaded into the flask of the reflux apparatus without solvent. The hydrocarbon was heated to reflux for between three and eight hours. Subsequently, the apparatus was washed with ethanol to collect polar products. The washings were analyzed by nanoelectrospray ionization. Nanoelectrospray emitters were pulled from borosilicate glass capillary (Sutter Instrument Co.) using a micropipette tip puller (Sutter Instrument Co.) to a tip size of less than 10 μm. High voltage was applied to the solution within the emitter via a steel electrode to generate an electrospray.

Analysis was conducted using an LTQ XL-Orbitrap hybrid instrument (Thermo Scientific) with a standard atmospheric pressure interface.

4.3.3 Probe APCI

Pure hydrocarbon sample was deposited onto a steel wire. 4 kV was subsequently applied to the wire, which was held within 5 cm of the inlet of the mass spectrometer to facilitate a corona discharge.

Analysis was conducted using an LTQ-Orbitrap XL hybrid mass spectrometer (Thermo Scientific).

4.4 References

1. Zhan, D.; Fenn, J. B., Electrospray mass spectroemtry of fossil fuels. *Int. J. Mass spectrom.* **2000,** *194*, 197-208.

2. Roussis, S. G.; Fitzgerald, W. P.; Cameron, A. S., Low-energy Ionization of Hydrocarbons in the Quadrupole Ion Trap Mass Spectrometer. *Rapid Commun. Mass Spectrom.* **1998,** *12*, 373-381.

3. Guan, S.; Marshall, A. G.; Scheppele, S. E., Resolution and Chemical Formula Identification of Aromatic Hydrocarbons and Aromatic Compounds Containing Sulfur, Nitrogen, or Oxygen in Petrolium Distillates and Refinery Streams. *Anal. Chem.* **1996,** *68* (1), 46-71.

4. Fialkov, A. B.; Gordin, A.; Amirav, A., Hydrocarbons and fuels analyses with the supersonic gas chromatography mass spectrometry--the novel concept of isomer abundance analysis. *J. Chromatogr. A* **2008,** *1195* (1-2), 127-35.

5. Hsu, C. S.; Qian, K., CS2 Charge Exchange as a Low-Energy Ionization Technique for Hydrocarbon Characterization. *Anal. Chem.* **1993,** *65*, 767-771.

6. Jin, C.; Viidanoja, J.; Li, M.; Zhang, Y.; Ikonen, E.; Root, A.; Romanczyk, M.; Manheim, J.; Dziekonski, E.; Kenttamaa, H. I., Comparison of Atmospheric Pressure Chemical Ionization and Field Ionization Mass Spectrometry for the Analysis of Large Saturated Hydrocarbons. *Anal Chem* **2016,** *88* (21), 10592-10598.

7. Beckey, H. D., Determiantion of the Structures of Organic Molecules and Quantitative Analysis with the Field Ionization Mass Spectrometer. *Angewandte Chemie International Edition* **1969,** *8* (9), 623-688.

8. Wu, C.; Qian, K.; Walters, C. C.; Mennito, A., Application of atmospheric pressure ionization techniques and tandem mass spectrometry for the characterization of petroleum components. *Int. J. Mass spectrom.* **2015,** *377*, 728-735.

9. Duan, P.; Fu, M.; Pinkston, D. S.; Habicht, S. C.; Kenttamaa, H. I., Gas-Phase Reactions of ClMN(H2O)+ with Polar and Nonpolar Hydrocarbons in a Mass Spectrometer. *J. Am. Chem. Soc.* **2007,** *129*, 9266-9267.

10. Grace, L. I.; Abo-Riziq, A.; deVries, M. S., An in situ silver cationization method for hydrocarbon mass spectrometry. *J. Am. Soc. Mass. Spectrom.* **2005,** *16* (4), 437-40.

11. Schwarz, H., Chemistry with methane: concepts rather than recipes. *Angew. Chem. Int. Ed. Engl.* **2011,** *50* (43), 10096-115.

12. Shiov, A. E.; Shul'pin, G. B., Activation of C-H Bonds by Metal Complexes. *Chem. Rev.* **1997,** *97*, 2879-2893.

13. Li, G.; Li, X.; Ouyang, Z.; Cooks, R. G., Carbon-carbon bond activation in saturated hydrocarbons by field-assisted nitrogen fixation. *Angewandte Chemie International Edition* **2013,** *52* (3), 1040-3.

14. Li, X.; Yan, X.; Cooks, R. G., Functionalization of saturated hydrocarbons using nitrogen ion insertion reactions in mass spectrometry. *Int. J. Mass spectrom.* **2017,** *418*, 79-85.

15. Jjunju, F. P. M.; Badu-Tawiah, A. K.; Li, A.; Soparawalla, S.; Roqan, I. S.; Cooks, R. G., Hydrocarbon analysis using desorption atmospheric pressure chemical ionization. *Int. J. Mass spectrom.* **2013,** *345-347*, 80-88.

16. Wu, C.; Qian, K.; Nefliu, M.; Cooks, R. G., Ambient analysis of saturated hydrocarbons using discharge-induced oxidation in desorption electrospray ionization. *J. Am. Soc. Mass. Spectrom.* **2010,** *21* (2), 261-7.

17. Badal, S. P.; Ratcliff, T. D.; You, Y.; Breneman, C. M.; Shelley, J. T., Formation of Pyrylium from Aromatic Systems with a Helium:Oxygen Flowing Atmospheric Pressure Afterglow (FAPA) Plasma Source. *J. Am. Soc. Mass. Spectrom.* **2017,** *28* (6), 1013-1020.

18. Delavari, S.; Amin, N. A. S.; Mazaheri, H., Oxidative coupling of methane in a corona discharge plasma reactor using HY zeolite as a catalyst. *Reaction Kinetics, Mechanisms and Catalysis* **2014,** *113* (2), 557-573.

19. Pillai, U. R.; Sahle-Demessie, E., Corona-induced photoxidation of alcohols and hydrocarbons over TiO2 in the absence of a UV light source - a novel and environmentally friendly method for oxidation. *Chem Commun (Camb)* **2005,** (17), 2256-8.

20. Lee, R.; Coote, M. L., Mechanistic insights into ozone-initiated oxidative degradation of saturated hydrocarbons and polymers. *Phys. Chem. Chem. Phys.* **2016,** *18* (35), 24663-71.

21. Yehia, A.; Mizuno, A., Suppression of the Ozone generation in the positive and negative DC corona discharges. *International Journal of Plasma Environmental Science and Technology* **2008,** *2* (1), 44-49.

22. Yanallah, K.; Pontiga, F.; Fernández-Rueda, A.; Castellanos, A.; Belasri, A., Ozone generation by negative corona discharge: the effect of Joule heating. *J. Phys. D: Appl. Phys.* **2008,** *41* (19).

CHAPTER 5. FUNDAMENTALS AND EXECUTION OF REACTION ACCELERATION IN THE WET LAB

5.1 Introduction

The acceleration of chemical reactions in confined volumes has been under scrutiny for some time[1]. Reactions at interfaces or in confined volumes have been dominant in the field and such study is not confined to the field of mass spectrometry[2-4].

Sharpless et al.[5] reported multiple cases of the use of this idea for synthetic purposes, having arguably rediscovered the phenomenon after the work of Breslow *et al.*[6-7], documenting the acceleration of multiple reactions "on water". Sharpless showed that, when reagents were encapsulated in a water/oil emulsion, the reaction rate was accelerated.

In the field of mass spectrometry, accelerated reactions in charged microdroplets and thin films have taken root in the practice of ambient ionization[8]. Badu-Tawiah *et al.* first reported the acceleration of imine formations in thin films[9], while Augusti *et al.*[10] and Girod e*t al.* studied accelerated reactions in electrospray ionization (ESI) and desorption electrospray ionization (DESI) droplets[11] respectively.

Subsequently, accelerated reactions in electrospray droplets were reported by Thomas Müler[12]. The two reactions under study were the Claisen-Schmidt reaction and the Benzoin condensation. Not only was the acceleration of these reactive systems characterized by mass spectrometry, but also ultraviolet absorption spectroscopy. The Claisen-Schmidt reaction has since been considered to be a "standard measure" for new methods of reaction acceleration.

As the work progressed, the synthetic aspect moved towards more complex systems. Notably, the Hantzch synthesis of substituted pyridines[13], which was a step forward because of the fact that it involves reaction between three molecules/ions rather than just two, was developed for

electrospray. Fundamentally, the most important aspect of the Hantzch synthesis was the implication that longer droplet flight times facilitated longer reaction times; the longer the flight time, the greater the abundance of later stage intermediates and product.

Recently, the Leidenfrost effect, where a droplet is levitated on a cushion of its own vapor, has been demonstrated to be a useful tool for the acceleration of reactions[14]. These large droplets were shown to facilitate smaller acceleration factors than the highly disperse conditions of electrospray plumes, presumably due to the lower surface area to volume ratio. Volmer *et al.* have also demonstrated reaction acceleration in large, levitated droplets[15].

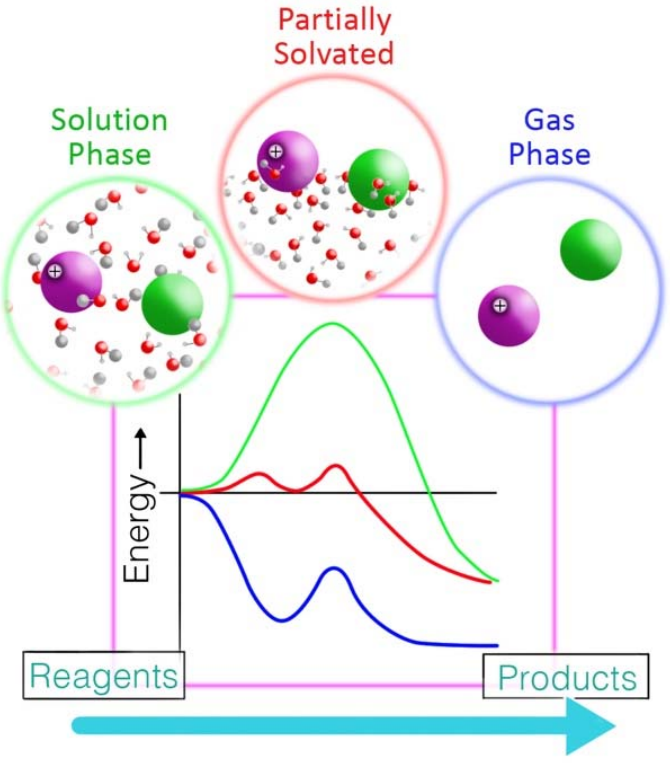

Figure 5.1 Illustration of the hypothetical energy diagram along the reaction coordinate compared to such diagrams for the solution and gas phase

It is theorized that three factors play a role in the acceleration of reaction rates; surface activity of the reagents, net charge in the system and concentration of the reagents in solution. All of these factors are thought to influence the presence or absence of reagents at the solution-air interface. The surface activity is a measure of the equilibrium of reactive species which exist in the bulk of the droplet vs. the reactive species which partition to the surface of the droplet[16]. The charge in the droplet can disturb this equilibrium, as can the concentration of reagents in the solution.

At the air/solvent interface, it is hypothesized that the solvation energy of the system approaches the gas phase energy landscape. This is illustrated in Figure 5.1. Interfacial effects, i.e. the nature of the interface and the effective interactions between the reagent and both phases may also help to secure reagents at a liquid/liquid or air/liquid interface to facilitate reaction acceleration. The former effect has recently been reported by Bain[17] and, separately, Yan *et al.*[18] in electrosprayed droplets. Evidence for the acceleration of the Suzuki reaction at the interface of chloroform/water, without the requirement of a phase-transfer catalyst is presented in the later part of this chapter.

5.2 Results and Discussion

5.2.1 Determination of the Phase of the Accelerated Fischer Indole Synthesis Induced by Electrospray

The Fischer indole synthesis (Scheme 5.1) has been studied in the low-pressure gas-phase in sector instruments[19] as well as under ambient pressure gas-phase conditions[20]. The chemistry includes a condensation reaction, a sigmatropic rearrangement and an elimination to form the final product.

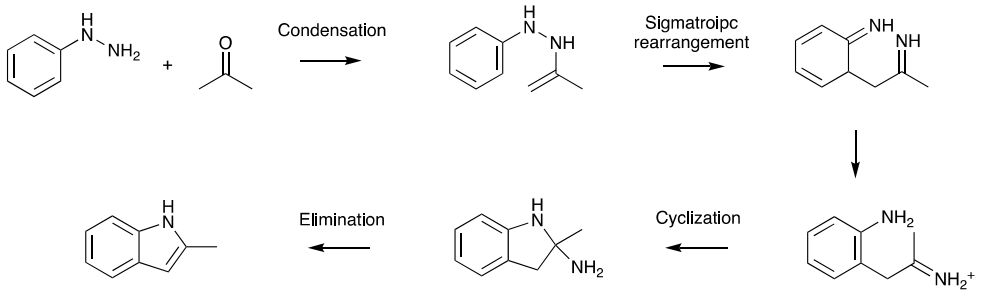

Scheme 5.1 Fischer indole synthesis

Glish *et al.* recorded the production of the final indole from the imine product under the conditions of CID[19], while Chen *et al.* recorded the formation of the indole as well as the formation of amino indole using an electrospray source and an extended, heated tube which was used to induce thermal dissociation[20]. This work will be revisited later and integrated into the discussion of the results.

With the convolution of energy pathways outlined in Figure 5.1 comes the potential for different reaction mechanisms. It is possible, for instance, that a general accelerated reaction is actually the product of efficient desolvation to produce gas phase ions, followed by a fast ion/molecule reaction in the gas phase. In order to probe this possibility, the Fischer indole synthesis was utilized. When a large excess of acetone is used, the solution-phase reaction proceeds not to the indole, but to the species which corresponds to a second acetone addition (Figure 5.2, structures 5 and 6). Even when under reflux, these are the only species that are produced and the traditional indole product is not observed[21].

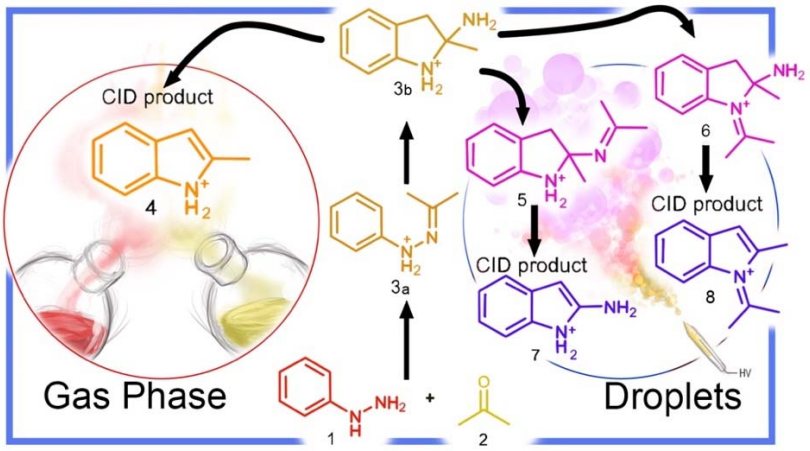

Figure 5.2 Overview of the experiment depicting the products of the solution phase reaction (right) and the gas phase reaction (left)

The reaction in electrosprayed droplets proceeds to the imine products 5 and 6 as a function of distance between the ion source and the inlet of the mass spectrometer (Figure 5.3).

The observation of the ions 5 and 6 in the mass spectrum confirm that the reaction proceeds via the solution phase mechanism. Indeed, these ions are simply not produced when the reagents are allowed to react in the vapor phase and subsequently passed through a corona discharge to facilitate ionization.

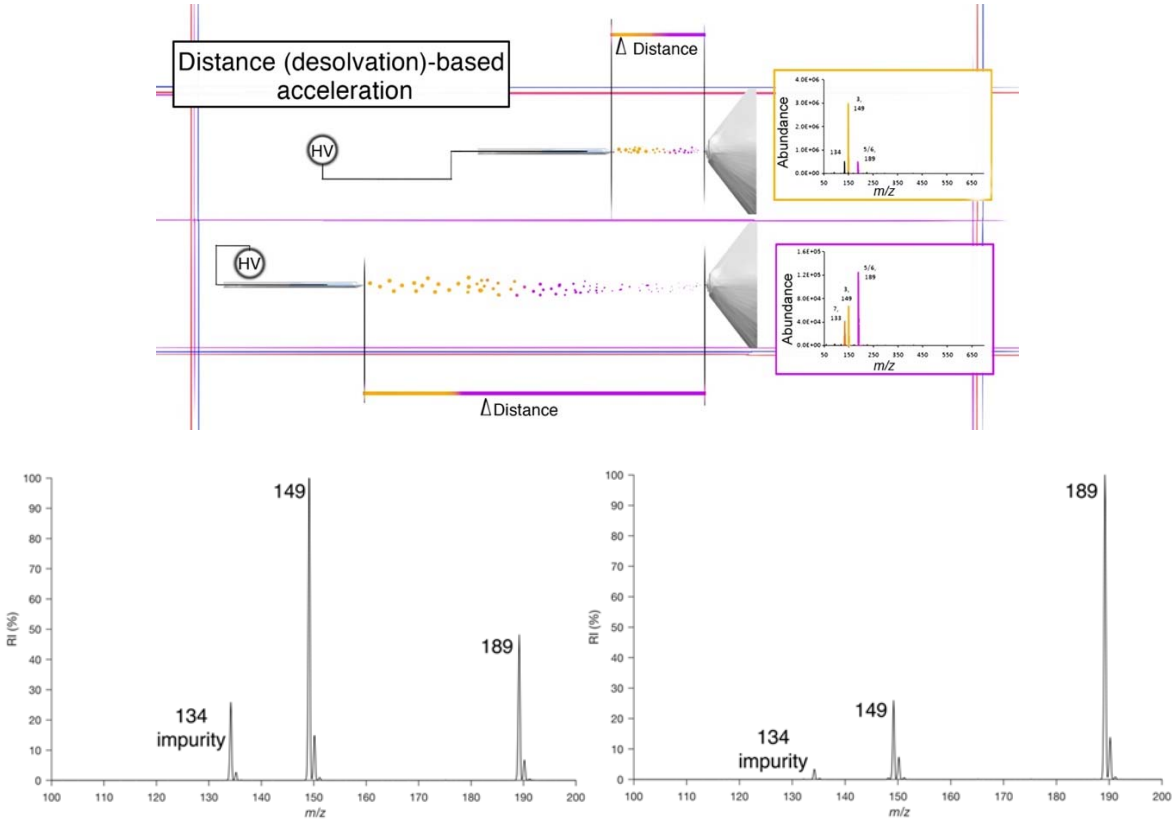

Figure 5.3 The effect of the distance of the ion source from the inlet of the mass spectrometer on the recorded mass spectra; Spectrum of the reaction mixture at 5 mm from the MS inlet (left) and at 7 cm (right)

The full scan mass spectrum is comprised of ions 3, 5, 6 and 7. The ratios of ions 5 and 6 (which are isobaric) to the ion, 3, was used as a measure of the progression of the reaction. There was also an impurity in the spectrum at *m/z* 134, which corresponds to the protonated acetone imine of aniline. This species was unreactive in the system and serves as a serendipitous internal standard. As the ion source was drawn away from the inlet of the mass spectrometer, the peak corresponding to 5 & 6 increased in intensity relative to the signal which represents the starting material. This phenomenon has been observed in other systems, most notably in a paper by Bain *et al.* which documents the accelerated Hantzch synthesis of pyridine in electrosprayed droplets as

a function of distance[13] and also work by Zare *et al.* which documents the effect of droplet flight time on protein unfolding[22].

The structures of the isobaric species which represent the product of the reaction were delineated via NMR and tandem mass spectrometry experiments. One of the products of fragmentation (observed in the CID spectrum) was aminoindole which was flanked by a signal corresponding to methylindole.

The fragmentation to methylindole is asserted to be the fragmentation of species 6, which loses ammonia followed by propene. The fragmentation to aminoindole was a particularly interesting observation, as it is a product which is apparently inaccessible in the solution phase. The rationale for this fragmentation is given in Scheme 5.2. The proposed 1,6 sigmatropic rearrangement is not dissimilar form the initial step in the reaction to form the cyclized structure. It would be favorable as it results in aromatization of the structure.

There is some overlap here with observations documented by Chen *et al.*[20]; they also recorded aminoindole, but in the full scan mass spectrum. The parallel is that that work was designed to study thermally-induced dissociation of electrosprayed ions before transmission into the mass spectrometer. This work suggests that the reagents in Chen's report were undergoing an accelerated reaction to generate the intermediate species, 5, which fragmented thermally to yield aminoindole before transmission into the ion trap of the mass spectrometer.

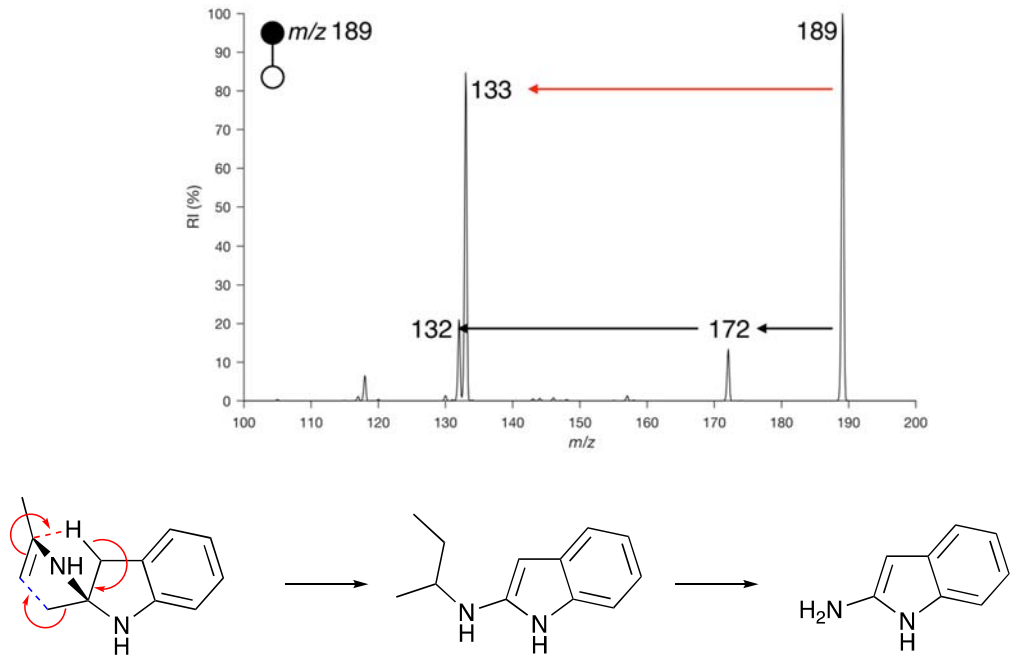

Scheme 5.2 CID product ion mass spectrum of *m/z* 189 – red arrow is fragmentation pathway shown in the scheme, black arrows are fragmentation pathway of the other isomer

5.2.2 Accelerated Reactions in a Rotary Evaporator

While charged microdroplets are not commonly encountered in the workflow of a synthetic organic chemist, thin films are. Thin films might form on the sides of flasks from which a solution has just been decanted, for instance. One of the most obvious places where thin films are encountered (in fact, they are intentionally generated) is in a flask connected to a rotary evaporator (roavap).

The low-pressure in a rotavap flask serves to remove the solvent quickly, so the solute becomes both highly concentrated and is transferred from a bulk-phase environment to a thin film environment (Figure 5.4).

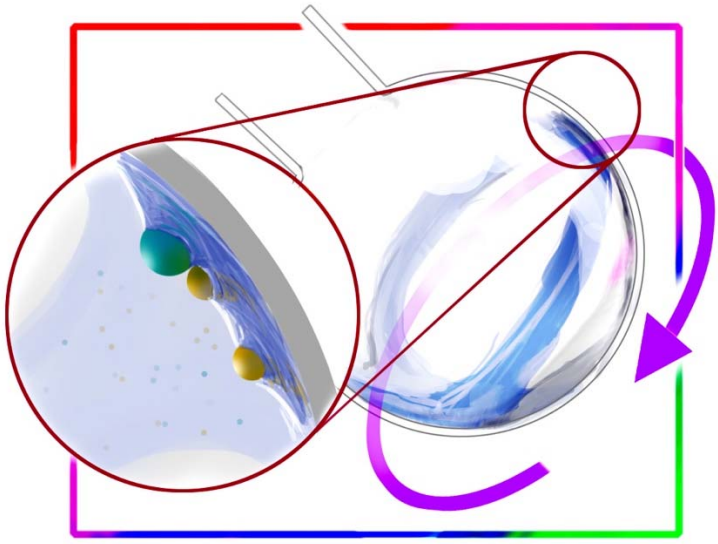

Figure 5.4 Thin films in a rotavap flask bringing partially solvated reagents into proximity

The study of accelerated reactions has largely been limited to small-scale applications. Synthetically useful accelerated reactions require scale-up. The solution to this problem has, thus far, been limited to the work of Sharpless *et al.*[5] and Bain *et al*[14]., where relatively large volumes of reaction solution were utilized. The large amount of material typically encountered in a rotavap flask and the generation of thin films in which reactions may accelerate constitutes a scale-up. In this section, the rapid synthesis of hundreds of milligrams of material in minutes is demonstrated. This section also illustrates that the accelerated reactions need not be confined to the niche; in fact, reaction acceleration may unwittingly be induced in synthetic organic chemistry laboratories everywhere, every day.

Claisen-Schmidt Condensation

Aldol reactions are of huge importance in organic synthesis[23]. The Claisen-Schmidt reaction constitutes an Aldol condensation, and since the first report of its acceleration by

electrospray[12], it has come to be considered a standard reaction to test for acceleration via new methods.

The general reaction scheme is shown in Figure 5.5. The substitution of the aldehyde has an enormous influence on the kinetics of the reaction[24]. Electron donating substituents slow the reaction significantly, while electron withdrawing substituents speed it up. This well-known effect is due to the differences in electron density at the aldehyde carbon due to conjugation or induction.

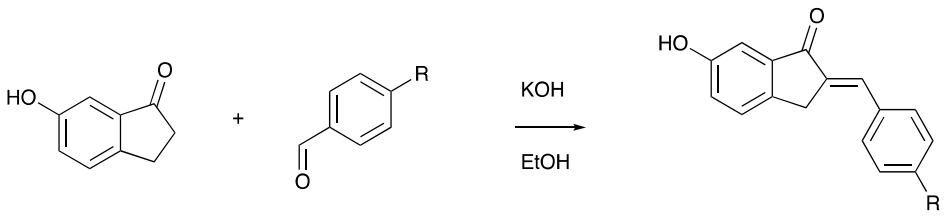

Figure 5.5 General reaction scheme for the base catalyzed Claisen-Schmidt condensation. In this work, R = H, OCH_3, $N(CH_3)_2$

Initially, benzaldehyde and 6-hydroxy-1-indanone were studied. Figure 5.6 shows the mass spectra recorded from the bulk reaction solution and from a solution which was dried under vacuum and subsequently diluted its initial concentration.

The spectrum from the bulk solution shows partial conversion to product. This could be the result of fast reaction in the electrosprayed droplets, or it could indicate the progression of the reaction in the bulk phase. The spectrum recorded of the reconstituted reaction mixture shows complete conversion of the starting material to product.

Figure 5.7 shows the bulk and rotavap reactions of hydroxyindanone with anisaldehyde to produce 2(*p*-methoxystyryl)-6-hydroxyindanone. In this case, the conversion is not as efficient as the previous case, but it is still excellent. The lower conversion efficiency can be explained by the fact that the methoxy group of anisaldehyde serves to slow the reaction.

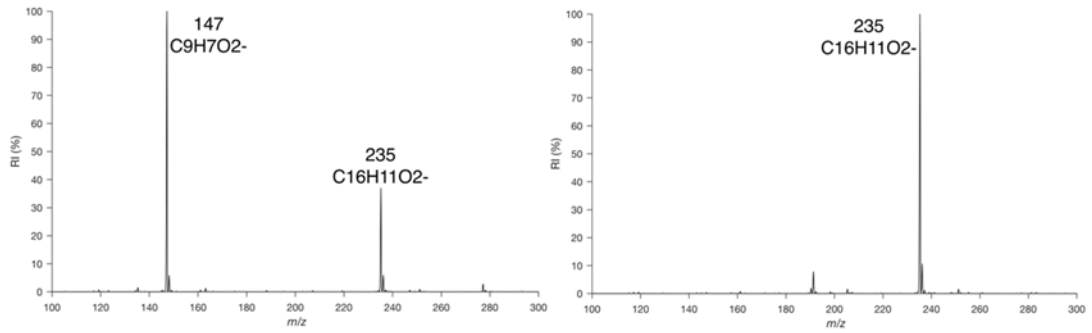

Figure 5.6 Spectrum from bulk reaction of 6-hydroxy-1-indanoe and benzaldehyde (left); Spectrum from reconstituted rotovap reaction (right)

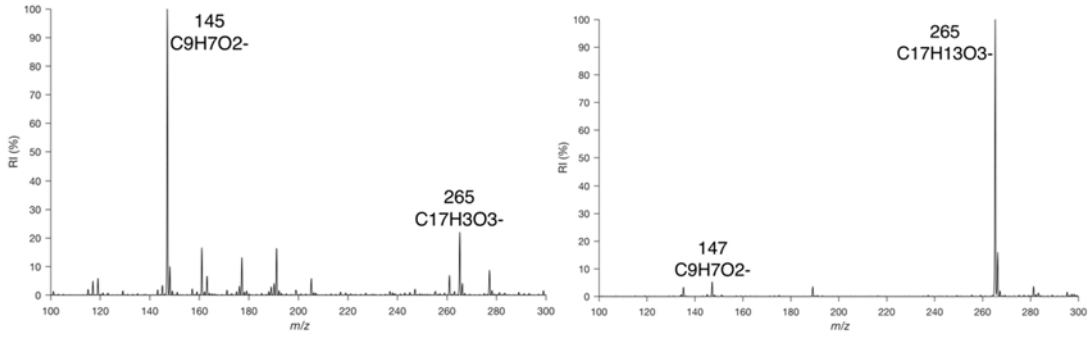

Figure 5.7 Spectrum from bulk reaction of 6-hydroxy-1-indanone and anisaldehyde (left); Spectrum from reconstituted rotovap reaction (right)

One further example is presented in Figure 5.8. There, the spectra from the bulk and rotavap reactions between hydroxyindanone and para-dimethylaminobenzaldehyde to produce 2(*p*-dimethylamino)-6-hydroxyindanone are shown. This system represents an unfavorable reagent pair, where the benzaldehyde is highly deactivated, more so than anisaldehyde. This is again represented by a greater population of starting material in the recorded spectrum form the reaction conducted in the rotavap relative to the analogous spectra from the other substrates.

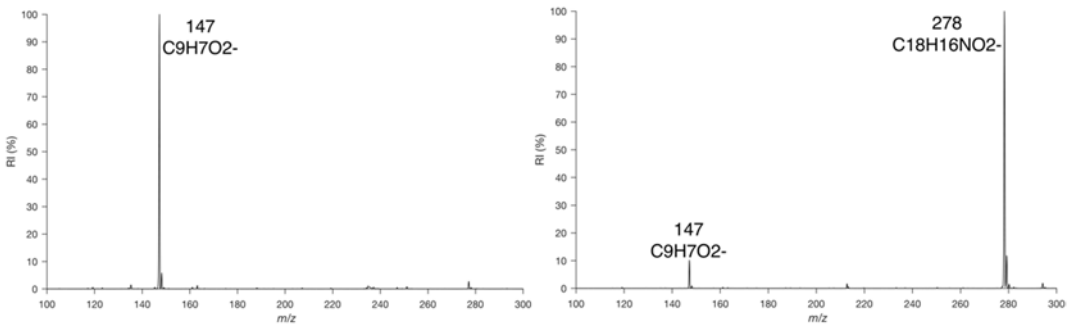

Figure 5.8 Spectrum from bulk reaction of 6-hydroxy-1-indanone with dimethylaminobenzaldehyde (left); Spectrum from the reconstituted rotavap reaction (right)

This method shows great promise in the ability to scale up reactions to produce material on the milligram scale. The reaction of 6-hydroxy-1-indanone and dimethylaminobenzaldehyde was scaled up to produce material on the order of five hundred milligrams.

A study of the acceleration as a function of solvent evaporation was conducted. The reaction of hydroxyindanone with *p*-dimethylaminobenzaldehyde was studied in this experiment. At every time point, a sample was taken and analyzed by mass spectrometry. Plotted on the ordinate is the ratio of the signal intensity in the mass spectrum of the product to the starting material. It can be seen that, over time, very little change is observed in the ratios until the last few samples, which demonstrate a remarkable change in speciation.

Interestingly, this curve closely follows the curve for concentration vs. evaporation if plotted assuming no loss of analyte to the gas phase (a sensible assumption in this case). Interestingly, the solid-phase Claisen-Schmidt reaction has been reported to occur quickly[25], as long as sufficient mixing is induced to ensure contact between the reagents and the catalyst. This experiment could, therefore, represent a way of efficiently bringing reagents into contact with one another before transferring them to the solid phase, where they quickly react, which is a paradigm not previously considered in the acceleration of reactions in thin films. This is asserted to be more

important than a highly concentrated solution phase system, as before extremely high concentration is achieved, the reagents precipitate from the solution. To control for this possibility, the solid reagents were added to a flask without active mixing and solvent was slowly added only until dissolution occurred, the spectral profile from that system matched the bulk phase reaction shown in Figure 5.8.

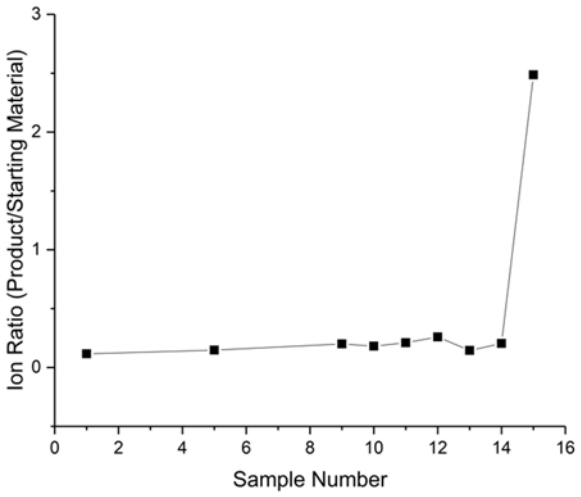

Figure 5.9 Ion ratio of product to starting material (dimethylaminobenzaldehyde) as a function of solvent evaporation (sample number represents 30 second intervals). The final sample was from dry material which was dissolved for analysis

To delineate the potential contribution of concentration, the reaction solution was evaporated almost to dryness, then left to react for 10 minutes, whereafter it was weighed, diluted and analyzed. The product/starting material ratio was 0.2. The flask was subsequently taken to dryness on the rotavap, weighed, diluted and analyzed. The product/starting material ratio was incalculable as a signal for the starting material was not recorded (as shown in Figure 5.8). The mass difference between the first and second reactions reported the amount of solvent present; 32.8 mg. This constituted a 10:1 molar ratio of solvent to total amount of reagents. Assuming the

only thing to evaporate was the solvent, the increase in concentration from the bulk reaction to the first sample was two orders of magnitude, and yielded only a little product. The concentration change from the first to the second sample was 4x, yet the reaction yielded product very efficiently, with a change in ratio of ion ratio of, apparently, orders of magnitude. This result suggests that the source of the acceleration is not concentration alone.

If concentration is not the major contributing factor to the observed conversion of starting materials to products, the remaining possibility is a change in the rate constant. The bulk-phase reaction was conducted and analyzed and, using the ion ratios (known to be a reliable source of information on relative concentration[24]) the rate constant was determined.

Using the rate equation for second order kinetics, the rate constant and initial concentration can be used to calculate the theoretical rate of consumption of starting material at a given starting concentration (Equation 5.1). The consumption of starting material, due to the stoichipmetry of the reaction, should be equivalent to the production of the product

$$rate = K \times [Indanone]^2$$

$$\frac{1}{[Indanone]} = Kt + \frac{1}{[Indanone]_0}$$

Equation 5.1 Calculation of moles produced per unit time for plot in Figure 5.10

The divergence illustrated in Figure 5.10 occurs at a mole ratio of solvent:reagent of approximately 10:1. It is not unreasonable to assume that 30 molecules of ethanol could represent a single solvent shell for the reagents, illustrating that in this case, the removal of the very last molecules of solvent initiates a change in the rate constant of the reaction, which is a remarkable result.

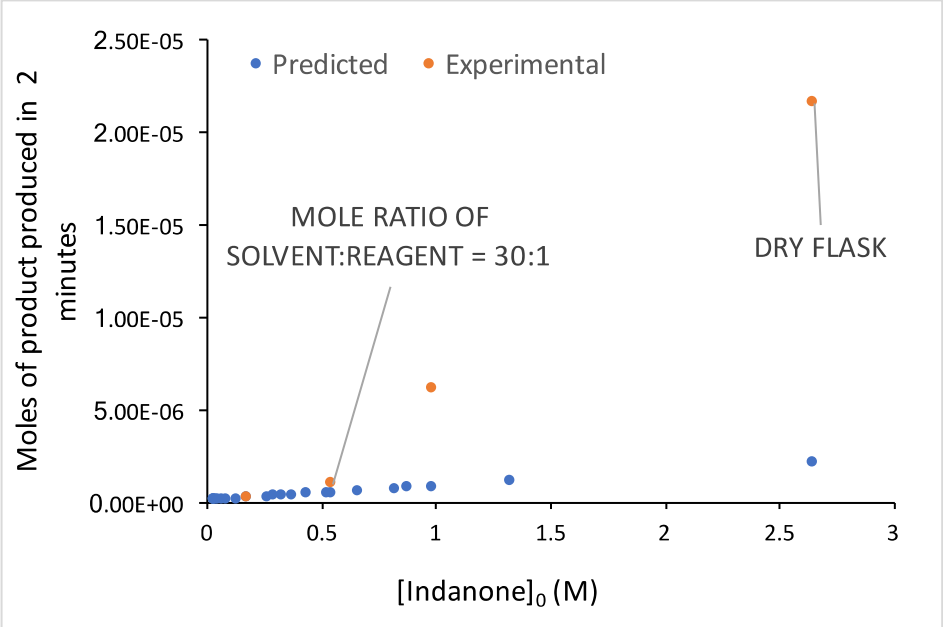

Figure 5.10 Plot of the moles of product produced over the course of 2 minutes against initial regent concentration based on the empirically determined rate constant

Imine Formation

Accelerated imine formation was initially reported by Badu-Tawiah *et al.*[9]. in that work, amines and carbonyl compounds were drop-cast onto a surface, re-dissolved and analyzed. The ratios of ions in the mass spectrum were compared to the spectrum from the bulk system and rapid C-N bond formation was revealed. One of the systems studied in that work is presented in Scheme 5.3, and was subsequently studied here.

The reaction of dimethylaminobenzaldehyde (*m/z* 150) and ethanolamine (*m/z* 62) forms an imine product (*m/z* 193) via the hydrated intermediate (*m/z* 211). The conversion to the product upon the removal of solvent is clear in Figure 5.11.

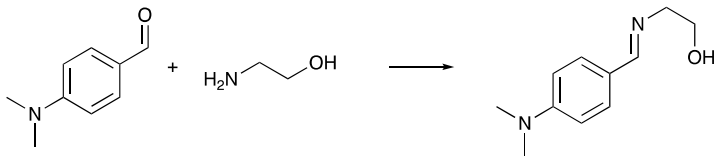

Scheme 5.3 General reaction scheme for the formation of an imine from dimethylaminobenzaldehyde and ethanolamine

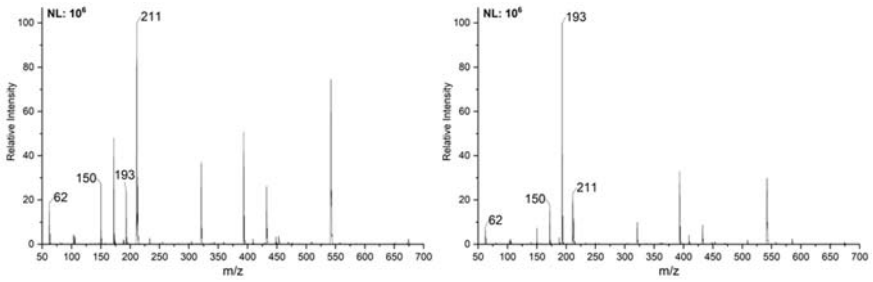

Figure 5.11 Spectrum from bulk Imine formation (left) and the reaction solution from the rotavap (right)

Imine formation is a so-called "click" reaction[26], meaning that the chemistry is favorable. To eliminate the consideration of concentration in the bulk-phase, the rotavap was modified to facilitate solvent addition to the flask under vacuum. This was accomplished by running a silica capillary through the vent of the rotavap and into the flask. When end of the capillary outside of the rotavap was dipped into a solvent, the draw through the line effectively pulled the liquid into the low-pressure environment of the flask. When the experiment was conducted in this way, a constant volume was maintained in the flask. Analysis of the solution from the rotavap flask relative to the bulk showed identical data to that presented in Figure 5.11, which implies that macro-scale increase in concentration was not required to accelerate this reaction.

Katritzky Reaction

The Katritzky reaction (Scheme 5.4) is the first reaction which was investigated for acceleration by paper spray ionization[27]. In the original work, it was shown that drying a solution of triphenylpyrilium and *p*-methoxyaniline on a paper substrate with a hydroxide catalyst facilitated fast reaction between the two reagents. The reaction is effectively a condensation reaction and the product is, conveniently, a pyridinium ion, which is particularly easy to detect by mass spectrometry.

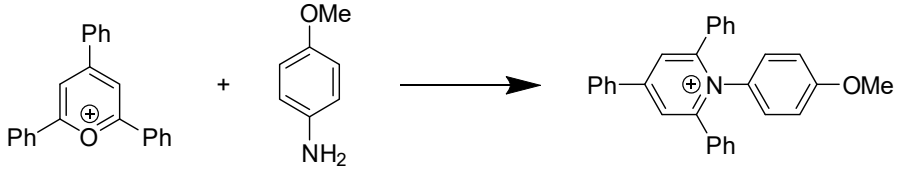

Scheme 5.4 General reaction scheme for the Katritzky Reaction

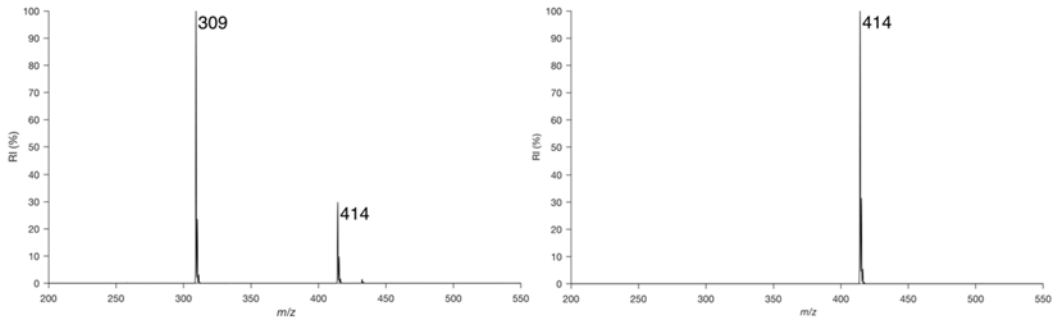

Figure 5.12 Spectrum from bulk Katritsky reaction (left); Spectrum from reconstituted rotavap reaction (right)

An aliquot of the bulk reaction mixture was dried under vacuum and subsequently reconstituted. The reconstituted solution was then analyzed by nanoelectrospray ionization and the spectrum in Figure 5.12 (right) was recorded. The only ion present in the spectrum was that of the product of the reaction, which dominated to the extent that the background was not observed.

The remaining bulk solution was then ionized by nanoelectrospray ionization (Figure 5.11, left) and the product of the reaction was observed at only 30% of the intensity of the starting material.

In the initial work, it was demonstrated that in order to convert the starting material to products as efficiently as this on paper, a hydroxide catalyst was required[27]. This may imply that in the case of the katritzky reaction, the solvent/low-pressure-air interface is more active than the solvent/ambient-pressure-air interface towards accelerating the reaction. This reaction was scaled to 500 milligrams, with 95% conversion, without a catalyst (confirmed by NMR, see experimental section).

Ester Hydrolysis

The hydrolysis of methyl cinnamate to produce cinnamic acid under basic pH (Scheme 5.5) was performed in the rotavap. This reaction, which could represent the de-protection of a molecule in a synthetic scheme[28], is the first example of its kind to be reported.

Figure 5.13 shows mass spectra recorded from the bulk solution and the aliquot of that solution dried under vacuum (and subsequently reconstituted). It was not possible to record signal for the product of the reaction from the bulk solution, but the reconstituted solution was dominated by the ion representing the product. In this case, the ester was not readily ionizable, which precluded the possibility of generating qualitative ion ratios for comparison.

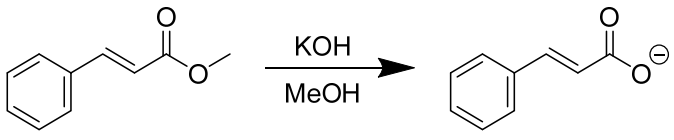

Scheme 5.5 Ester hydrolysis of methyl cinnamate under basic conditions

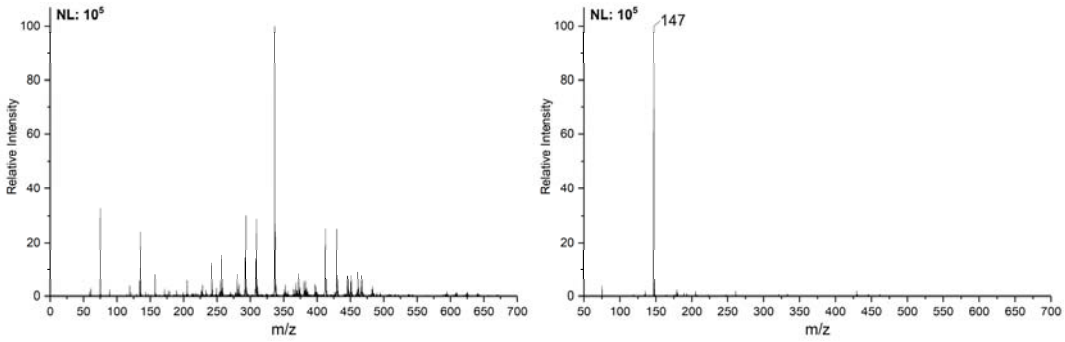

Figure 5.13 (Left) Spectrum from bulk ester hydrolysis of methyl cinnamate (Right) Spectrum from reconstituted rotovap reaction where *m/z* 147 corresponds to product

To facilitate the comparison of products and starting materials in the reaction, ethyl-4-pyridylacetate was exposed to the same conditions (Scheme 5.6). In the bulk-phase, no hydrolysis was recorded, while in the reaction mixture which was dried under vacuum, the product ion was dominant in the negative ion mode. In the positive ion mode, the starting material was also recorded but at a far lower level than in the bulk.

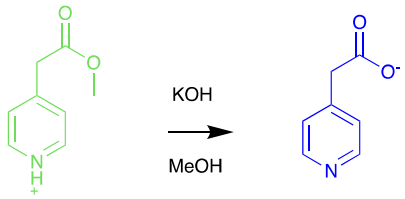

Scheme 5.6 Ester hydrolysis of ethyl-4-pyridylacetate under basic conditions

It was hypothesized that cycling this experiment may lead to greater conversion. Figure 5.14 demonstrates this experiment. Each cycle corresponds to the addition of solvent to the rotavap flask after it was taken to dryness. The data show that with each cycle, the starting material is depleted, while the product remains dominant in the spectrum.

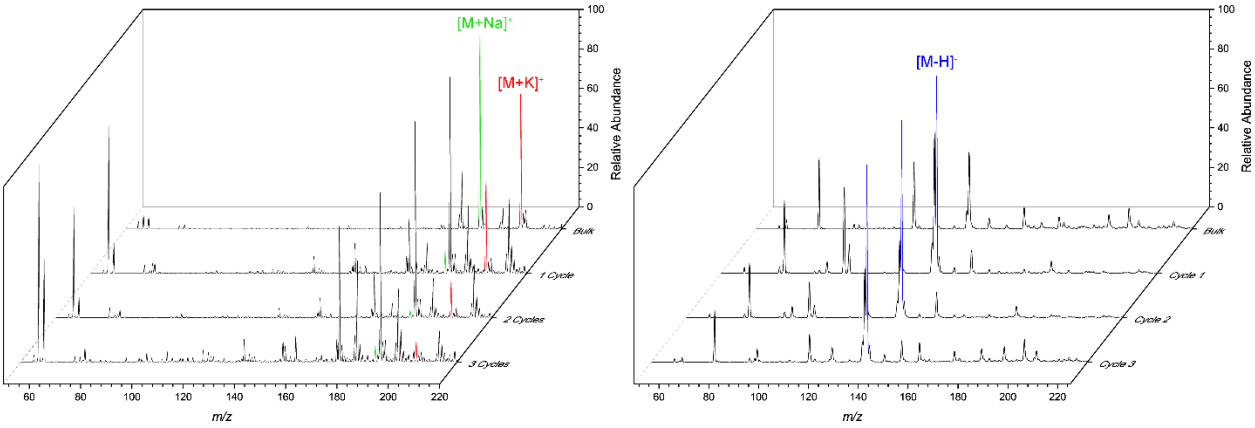

Figure 5.14 (Left) Positive mode spectrum of ethyl-4-pyridylacetate. Peaks in color correspond to metalated starting material. (Right) Spectrum from reconstituted rotovap reaction where the colored peak corresponds to the anion of the product carboxylic acid

5.2.3 Accelerated Suzuki Reaction in a Biphasic Mixture

The Suzuki reaction, an organometallic metathesis, is of vital importance to the pharmaceutical industry and was one of a few of its type to win the Nobel Prize in 2010[29]. Typically, these reactions are considered to be fast, going to completion within a couple of hours. Still, this timescale does not align with high throughput chemistry for either the purpose of screening or fast synthesis.

Before the study of accelerated reactions in charged droplets generated by ambient ionization source, Sharpless reported that reactions could be accelerated in emulsions[5]. Electrocyclization reactions featured prominently in the paper, which was termed the study of reactions “on water”.

The typical workflow of the organic chemist includes separation. Partitioning between an aqueous and organic phase is usually used to remove salts, acids or bases from the product, which remains in the organic phase. As part of a biphasic separation, the phases are mixed and a temporary emulsion is formed, which generates a very high surface-area-to-volume ratio for both phases. Such a high ratio increases the chance of reagents reacting at an interface between the two

phases. Presented here is preliminary work toward the acceleration of Suzuki reactions in simple biphasic solution.

The Suzuki reaction is catalyzed by palladium. There are now a number of water-stable palladium complexes. The performance of Suzuki reactions in water was recently reviewed by Chatterjee *et al.*[30]. XPhos Pd G3 is a commercially available palladium catalyst which is inert towards water and highly soluble in organic media. This makes the Suzuki reaction a target for acceleration in an emulsion wherein one phase is aqueous. Phase-transfer catalysis of Suzuki reacitons has previously been reported, and this work is closely related to that concept[31].

The first reaction probed in this work is outlined in Scheme 5.7. The pyridyl bromide (b) and the *p*-hydroxypehnylboronic acid (a) lend characteristics to the product (c) which facilitate detection in both negative and positive ion mode; the hydroxyl can be deprotonated and the pyridine heteroatom can readily be protonated.

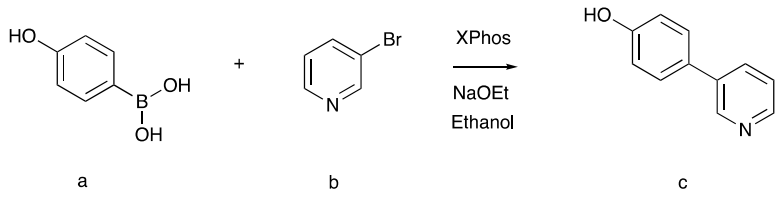

Scheme 5.7 The reagents and product of Suzuki coupling

Experimentally, the reagents and sodium ethoxide were mixed in stoichiometric equivalence, while the catalyst was used at 10% of the concentration. Four experiments were conducted to probe the effects of interfacial interactions between the solvent and a second phase on the rate of the reaction itself.

100 μL each of 10 mM stock solutions of the reagents and 100 μL of a 1 mM stock of the palladium catalyst were added to 1 mL of chloroform (1.4 mL total volume). The reaction solution

was mixed for 10 minutes, after which time, a 50 μL aliquot of the solution was diluted into 150 μL of 2:1 solution of ethanol:water with a spike of hydrochloric acid (3 mM). This final solution (referred to hereafter as the spray solution) was then analyzed by nanoelectrospray ionization. The resulting spectrum is shown in Figure 5.15.

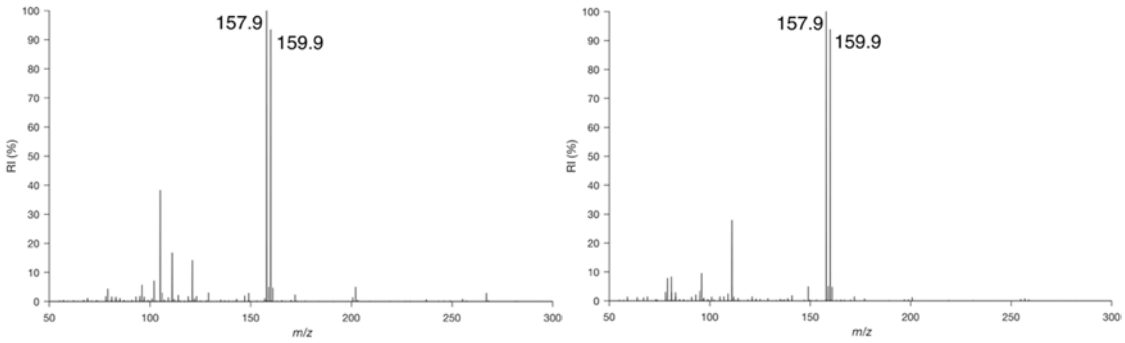

Figure 5.15 Full scan mass spectrum of the reaction solution after 10 minutes of reaction time in chloroform (left) and water (right)

The spectrum was dominated with the starting material 3-bromopyridine as well as some background signals at lower *m/z*. The experiment was repeated but instead of chloroform, water was used as the solvent. The spectrum recorded from that solution is also presented in Figure 5.15.

These control experiments show that there is no appreciable product formation over the course of 10 minutes in either solvent alone. The next experiments deal with the combination of both solvents in one flask. First, the experiment was conducted by adding to the reaction solution both chloroform and water. This generated a stationary, biphasic system with two, single, large volumes of solvent and so only one appreciable interface between the two phases existed.

It is important to note that the catalyst, reagents and the product did not migrate to the aqueous phase until the water was acidified at the end of the experiment (tested by mass

spectrometry), at which point the reagents and product move into the aqueous phase. Therefore, the last step after 10 minutes was to add a spike of acid to the biphasic mixture. Following this, the solution was agitated to encourage mixing of the individual phases and interfacial interaction, but not so vigorously so as to disrupt the organic phase and split it into small droplets. An aliquot of the aqueous phase was then added to a 1:1 solution of ethanol:water such that the final composition of that solution was essentially the same as the spray solvent described previously.

The spectrum recorded from this experiment is shown in Figure 5.16. A clear signal corresponding to the product was recorded. The reaction was allowed to progress over the same period of time as the previous two, single solvent control experiments, suggesting that the interface between the two solvents facilitated the reaction.

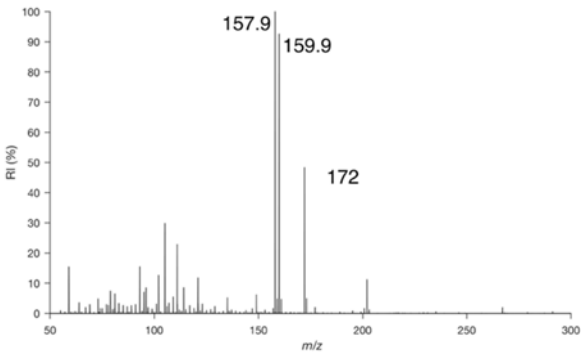

Figure 5.16 Full scan mass spectrum of the reaction solution after 10 minutes of reaction time in a biphasic system with only one large interface

The next experiment was designed to probe the effect of increasing the interfacial interactions between the two phases. By actively mixing the solutions, a temporary emulsion was formed, just as it does in a separating funnel. The biphasic solution was continually mixed to maintain the emulsion for ten minutes, after which time it was allowed to settle and separate (over the course of 10 seconds). The aqueous phase was then spiked with acid and diluted into a spray

solution as described in the previous experiment. The spectrum recorded from this experiment is presented in Figure 5.17. Also presented is the spectrum from the same experimental procedure, but the emulsion was maintained for 20 minutes.

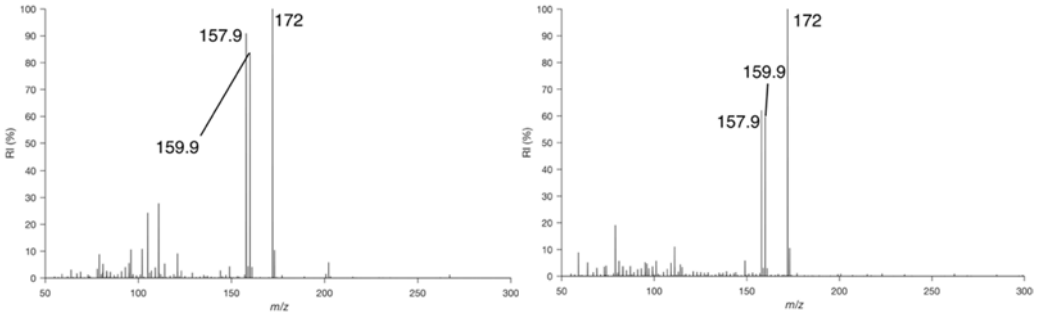

Figure 5.17 Full scan mass spectrum of the reaction solution after 10 minutes of reaction time in a mixed biphasic system (left) and after 20 minutes (right)

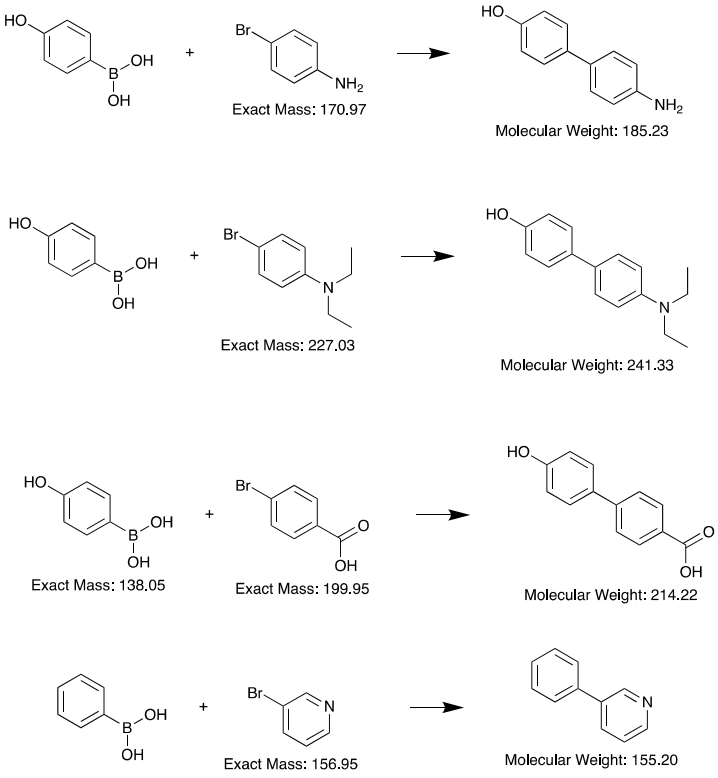

Scheme 5.8 Range of Suzuki reactions tested

These experiments illustrate the effect of the interface on the reaction. It is proposed that, because the reagents may strongly hydrogen bond, they are held at the interface of the organic phase by interactions with the aqueous phase. This hypothesis is founded in the work of Jung and Marcus which reports "dangling" O-H bonds into a phase immiscible with water[32]. This affects the solvation energy of the system, facilitating faster reaction. To assess this hypothesis, a series of reagents was tested. The pairs of reagents are illustrated in Scheme 5.8.

Bromoaniline reacted at a lower rate with hydroxyphenylboronic acid (HOPhBA). The mass spectrum of the reaction mixture after 20 minutes in bulk chloroform and 20 minutes in an emulsion of chloroform:water is given in Figure 5.18. Lower basicity of the aniline functional group relative to that of the pyridyl group is hypothesized to be the reason for the discrepancy; aniline was not held at the interface of chloroform:water as efficiently.

Even after 20 minutes of reaction time the conversion of reagent to product was far lower than that of the reaction between HOPhBA and bromopyridine. After 30 minutes, the intensity of the MS signal for the product had grown to 75% the intensity of the starting material. Two major factors could account for this; aniline has a lower proton affinity than pyridine and it also has the potential to chelate the catalyst.

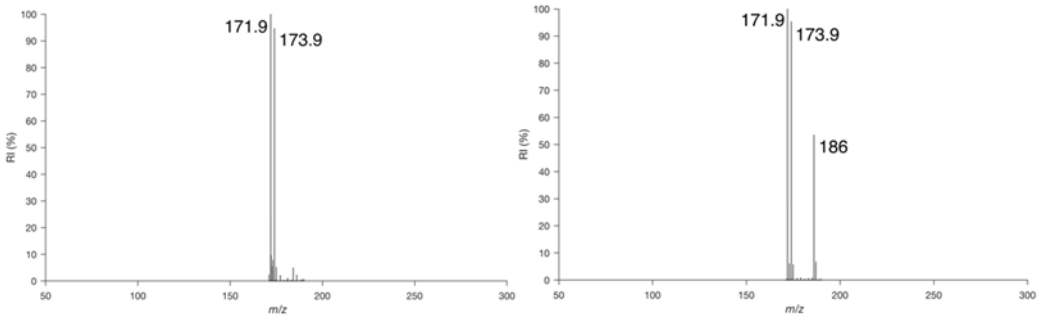

Figure 5.18 Reaction between HOPhBA and *p*-bromoaniline in emulsion (right) and bulk (left)

The addition of steric bulk to the amine in the system by ethylation was utilized to inhibit hydrogen bonding, increase the general lipophilicity of the molecule and inhibit potential catalyst chelation, hence, *p*-bromo-*N*,*N*-diethylaniline was tested as a coupling partner in the reaction.

After 20 minutes of reaction time in the emulsion, product was present at very low intensity relative to the starting materials and in the bulk, it was absent (Figure 5.19). This is taken as evidence to show that when the ability of the reagent to hydrogen bond is diminished, and when it is discouraged from interfacial interactions by virtue of its lipophilic nature, the magnitude of acceleration which can be achieved is diminished.

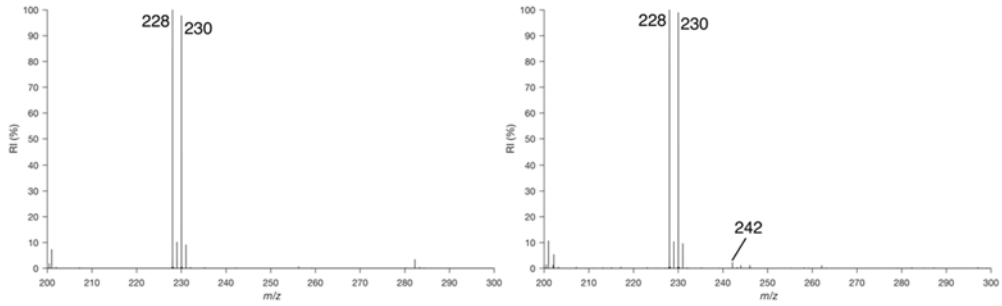

Figure 5.19 Full scan mass spectrum of the reaction between HOPhBA and *p*-bromo-*N*,*N*-diethylaniline after 10 minutes in bulk (left) and emulsion (right)

The complimentary reaction is to increase the hydrophilic nature of the reagent to the point that it is unlikely to associate with the organic phase. For this, *p*-bromobenzoic acid was tested. In this case, only a very small amount of product was observed in the spectrum (negative ion mode) relative to the starting material (Figure 5.20) after 20 minutes of reaction time. Presumably, the stoichiometric amount of base added to the reaction solution to scavenge the halide ion byproduct ensured that the carboxylic acid was ionized as the carboxylate in solution and therefore effectively partitioned into the aqueous phase. For this reason, the reaction was conducted in emulsion again

with a second equivalent of base, to ensure its interaction with the carboxylic acid did not quench the reaction. The results did not change.

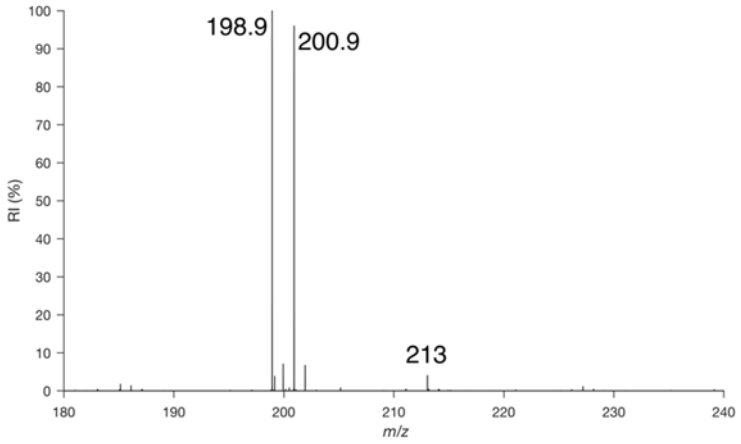

Figure 5.20 Full scan mass spectrum of the reaction mixture of HOPhBA and bromobenzoic acid after 20 minutes in an emulsion

Phenylboronic acid was reacted with bromopyridine in an emulsion of chloroform and water in order to test the effect of changing the boronic acid reagent. The mass spectrum of that reaction mixture is given in Figure 5.21. The ratio of starting materials to products in this case is approximately equivalent to the analogous reaction using HOPhBA acid (Figure 5.16), demonstrating that, at least in the limited number of cases studied here, this reagent has less of an effect on the progress of the reaction.

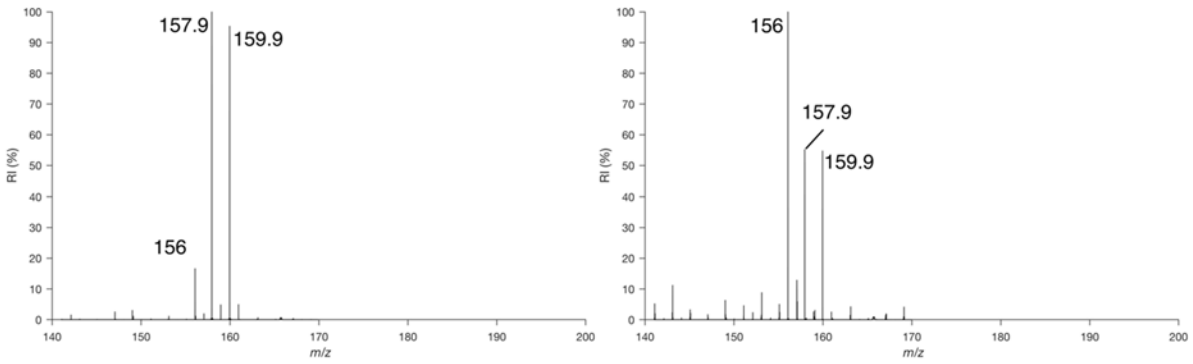

Figure 5.21 Mass spectrum of the reaction mixture of phenylboronic acid and 3-bromoaniline

These preliminary results appear to highlight how the nature of the interface as well as the properties of the reagents are key in the balancing act of designing accelerated reactions. It is also telling that the halogen bearing reagent seems to be the important one in the determination of reactivity, as the oxidative insertion of palladium into the C-X bond is considered to be the rate determining step of the Suzuki coupling[33]. The evidence suggests that oxidative insertion can be accelerated at the interface between water and chloroform without the requirement of a phase-transfer catalyst and the subsequent coupling reaction happens very rapidly after that.

5.3 Experimental

5.3.1 General Procedure for Analysis

Nanoelectrospray ionization emitters were pulled to a tip size of 10 μm using a micropipette tip puller (Sutter instruments inc.). The emitters were loaded with 10 μL of solution using gel-loading pipette tips (BioRad inc.) whereupon a steel electrode was inserted, which made contact with the solution. The emitter was positioned lwess than 1 cm away from the MS inlet and a 1.5 kV was applied to the electrode to generate an electrospray plume. The spectra were recorded on a hybrid LTQ-Orbitrap XL (Thermo Scientific).

5.3.2 Accelerated Fischer Indole Synthesis

To 200 μL of acetone was added phenylhydrazine (10 μL) and 1 M hydrochloric acid in methanol (50 μL). The solution was loaded into a nanoelectrospray emitter for analysis. The remaining solution was used as the standard "bulk" solution. A manually controlled 2D stage was used to hold the emitter and draw it back accurately in one dimension to perform distance-dependent experiments.

5.3.3 Accelerated Reactions in a Rotary Evaporator

Claisen-Schmidt reaction

6-hydroxy-1-indanone and the benzaldehyde substrate were prepared at a concentration of 52 mM in ehthanol. Potassium hydroxide was prepared at a concentration of 1.8 M in ethanol. 1mL of hydroxyindanone solution and 1 mL aldehyde solution were mixed and subsequently spiked with 40 μL of the potassium hydroxide solution. 1 mL of the reaction solution was dispensed into a rotavap flask and the solvent was removed under reduced pressure. After the reaction solution in the rotavap flask had been dried under vacuum, it was reconstituted and both the bulk and rotavap reaction solutions were analyzed by nanoelectrospray ionization.

To generate the data for the plot in Figure 5.10, the reaction vessel was flushed with air before it had completely dried.

Ester hydrolysis

Stock solutions of the esters (10 mM) in 10 mL of ethanol were prepared. A stock solution of potassium hydroxide (0.15 M) was prepared in ethanol. 2 mL of ester solution was spiked with 40 μL of the potassium hydroxide solution. 1 mL of the reaction solution was dispensed into a rotavap flask and the solvent was removed under reduced pressure. This experiment was cycled

by reconstituting what remained in the flask with 1 mL of ethanol and then removing the solvent again under reduced pressure. The remaining 1 mL of reaction solution was treated as the standard bulk reaction solution. After the reaction solution in the rotavap flask had been dried under vacuum, it was reconstituted and both the bulk and rotavap reaction solutions were analyzed by nanoelectrospray ionization.

Imine formation

Stock solutions of dimethylaminobenzaldehyde and ethanolamine were prepared in ethanol (10 mM). These solutions to 10 mL of ethanol was added an aliquot (1 mL) of each reagent. 5 ml of the solution was then transferred to the rotavap flask and the solvent was removed under reduced pressure. The remaining 5 mL of solution was treated as the standard bulk reaction. After the reaction solution in the rotavap flask had been dried under vacuum, it was reconstituted and both the bulk and rotavap reaction solutions were analyzed by nanoelectrospray ionization.

Katritzky reaction

Stock solutions of triphenylpyrillium and *p*-anisidine (100 mM in acetonitrile) were mixed at stoichiometric equivalence into a round bottomed (rotavap) flask. A small volume (about 500 μL) was dispensed into a scintillation vial to serve as the bulk standard. After the reaction solution in the rotavap flask had been dried under vacuum, a small sample was dissolved in acetonitrile, and a second small sample was dissolved in deuterated methanol for NMR. reconstituted and both the bulk and rotavap reaction solutions were analyzed by nanoelectrospray ionization. At this scale, the reaction yielded 80% conversion (Figure 5.22).

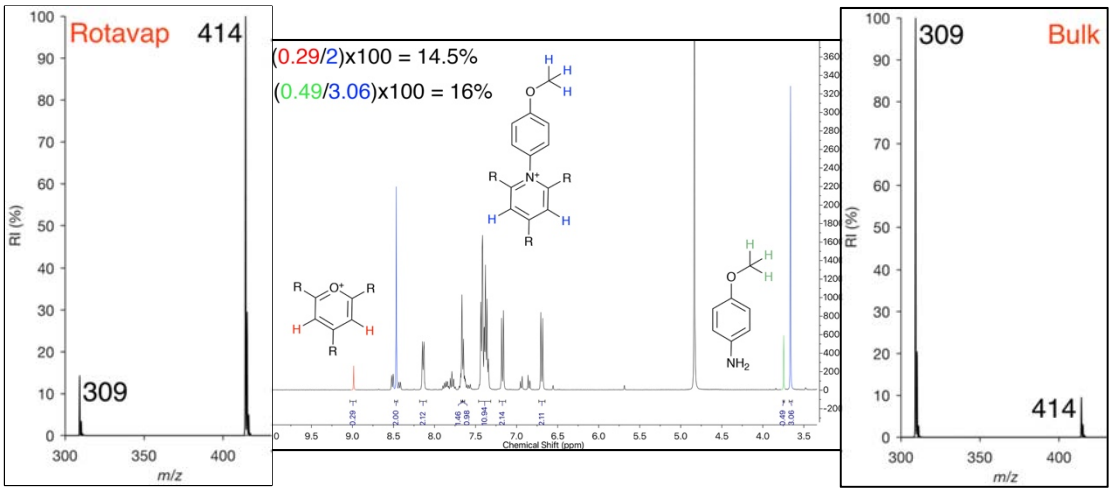

Figure 5.22 NMR spectrum of product of Katritzky reaction from a rotavap flask at a scale of 510 mg; Left – full scan mass spectrum of reaction from the rotavap; - Right – full scan mass spectrum of the bulk reaction

5.3.4 General Procedure for Conducting Suzuki Reactions

Stock solutions of the boronic acid and halogeno aromatic compounds were prepared in ethanol at a concentration of 10 mM. 100 µL of each solution spiked into 1 mL of chloroform. For biphasic reactions, 1 mL of wager was subsequently added.

After the predetermined reaction time, 10 µL of 1M hydrochloric acid in methanol was added to the biphasic solution to induce extraction of the amine-bearing starting materials/products. 10 µL of the aqueous phase was then diluted into 10 µL of ethanol and directly by nanoelectrospray ionization.

The bulk phase reactions were not acidified initially, instead, 10 mL of the solution was diluted into a mixture of 10 µL of ethanol and 10 µL of water, with a 1 µL spike of aM hydrochloric acid in methanol. This solvent composition facilitated the dissolution of chloroform into a solvent which was essentially the same across all analyses.

5.4 References

1. Yan, X.; Bain, R. M.; Cooks, R. G., Organic Reactions in Microdroplets: Reaction Acceleration Revealed by Mass Spectrometry. *Angew. Chem. Int. Ed. Engl.* **2016,** *55* (42), 12960-12972.

2. Fleder, D.; Leung, D. H.; Bergman, R. G.; Raymond, K., Selective Molecular Recognition, C-H Bond Activation, and Catalysis in Nanoscale Reaction Vessels. *Acc. Chem. Res.* **2005,** *38*, 349-358.

3. Li, Q.; Simon, S. L., Curing of Bisphenol M Dicyanate Ester under Nanoscale Constraint. *Macromolecules* **2008,** *41*, 1310-1317.

4. Koh, Y. P.; Simon, S. L., Kinetic study of trimerization of monocyanate ester in nanopores. *J. Phys. Chem. B* **2011,** *115* (5), 925-32.

5. Narayan, S.; Muldoon, J.; Finn, M. G.; Fokin, V. V.; Kolb, H. C.; Sharpless, K. B., "On water": unique reactivity of organic compounds in aqueous suspension. *Angew. Chem. Int. Ed. Engl.* **2005,** *44* (21), 3275-9.

6. Breslow, R.; Maitra, U.; Rideout, D., Selective Diels-Alder Reactions in Aquaous Solutions and Suspensions. *Tetrahedron Lett.* **1983,** *24*, 1901-1904.

7. Rideout, D.; Breslow, R., Hydrophobic Acceleration of Diels-Alder Reactions *J. Am. Chem. Soc.* **1980,** *102*, 7816-7817.

8. Espy, R. D.; Wleklinski, M.; Yan, X.; Cooks, R. G., Beyond the flask: Reactions on the fly in ambient mass spectrometry. *TrAC, Trends Anal. Chem.* **2014,** *57*, 135-146.

9. Badu-Tawiah, A. K.; Campbell, D. I.; Cooks, R. G., Accelerated C-N bond formation in dropcast thin films on ambient surfaces. *J. Am. Soc. Mass. Spectrom.* **2012,** *23* (9), 1461-8.

10. Augusti, R.; Chen, H.; Eberlin, L. S.; Nefliu, M.; Cooks, R. G., Atmospheric pressure Eberlin transacetalization reactions in the heterogeneous liquid/gas phase. *Int. J. Mass spectrom.* **2006,** *253* (3), 281-287.

11. Girod, M.; Moyano, E.; Campbell, D. I.; Cooks, R. G., Accelerated bimolecular reactions in microdroplets studied by desorption electrospray ionization mass spectrometry. *Chem. Sci.* **2011,** *2* (3), 501-510.

12. Muller, T.; Badu-Tawiah, A.; Cooks, R. G., Accelerated carbon-carbon bond-forming reactions in preparative electrospray. *Angew. Chem. Int. Ed. Engl.* **2012,** *51* (47), 11832-5.

13. Bain, R. M.; Pulliam, C. J.; Cooks, R. G., Accelerated Hantzsch electrospray synthesis with temporal control of reaction intermediates. *Chem Sci* **2015,** *6* (1), 397-401.

14. Bain, R. M.; Pulliam, C. J.; Thery, F.; Cooks, R. G., Accelerated Chemical Reactions and Organic Synthesis in Leidenfrost Droplets. *Angew. Chem. Int. Ed. Engl.* **2016,** *55* (35), 10478-82.

15. Crawford, E. A.; Esen, C.; Volmer, D. A., Real Time Monitoring of Containerless Microreactions in Acoustically Levitated Droplets via Ambient Ionization Mass Spectrometry. *Anal Chem* **2016,** *88* (17), 8396-403.

16. Cech, N. B.; Enke, C. G., Practical implications of some recent studies in electrospray ionization fundamentals. *Mass Spectrom. Rev.* **2001,** *20* (6), 362-87.

17. Bain, R. M.; Sathyamoorthi, S.; Zare, R. N., "On-Droplet" Chemistry: The Cycloaddition of Diethyl Azodicarboxylate and Quadricyclane. *Angew. Chem. Int. Ed. Engl.* **2017**.

18. Yan, X.; Cheng, H.; Zare, R. N., Two-Phase Reactions in Microdroplets without the Use of Phase-Transfer Catalysts. *Angew. Chem. Int. Ed. Engl.* **2017,** *56* (13), 3562-3565.

19. Glish, G. L.; Cooks, R. G., The Fischer Indole Synthesis and Pinacol Rearrangement in the Mass Spectrometer. *J. Am. Chem. Soc.* **1978,** *100*, 6720-6735.

20. Chen, H.; Eberlin, L. S.; Nefliu, M.; Augusti, R.; Cooks, R. G., Organic reactions of ionic intermediates promoted by atmospheric-pressure thermal activation. *Angew. Chem. Int. Ed. Engl.* **2008,** *47* (18), 3422-5.

21. Bain, R. M.; Ayrton, S. T.; Cooks, R. G., Fischer Indole Synthesis in the Gas Phase, the Solution Phase, and at the Electrospray Droplet Interface. *J. Am. Soc. Mass. Spectrom.* **2017,** *28* (7), 1359-1364.

22. Lee, J. K.; Kim, S.; Nam, H. G.; Zare, R. N., Microdroplet fusion mass spectrometry for fast reaction kinetics. *Proc Natl Acad Sci U S A* **2015,** *112* (13), 3898-903.

23. Heravi, M. M.; Zadsirjan, V.; Dehghani, M.; Hosseintash, N., Current applications of organocatalysts in asymmetric aldol reactions: An update. *Tetrahedron: Asymmetry* **2017,** *28* (5), 587-707.

24. Bain, R. M.; Pulliam, C. J.; Yan, X.; Moore, K. F.; Müller, T.; Cooks, R. G., Mass Spectrometry in Organic Synthesis: Claisen–Schmidt Base-Catalyzed Condensation and Hammett Correlation of Substituent Effects. *J. Chem. Educ.* **2014,** *91* (11), 1985-1989.

25. Rahman, A. F.; Ali, R.; Jahng, Y.; Kadi, A. A., A facile solvent free Claisen-Schmidt reaction: synthesis of alpha,alpha'-bis-(substituted-benzylidene)cycloalkanones and alpha,alpha'-bis-(substituted-alkylidene)cycloalkanones. *Molecules* **2012,** *17* (1), 571-83.

26. Kolb, H. C.; Finn, M. G.; Sharpless, K. B., Click Chemistry: Diverse Chemical Function from a Few Good Reactions *Angewandte Chemie International Edition* **2001,** *40*, 2004-2021.

27. Yan, X.; Augusti, R.; Li, X.; Cooks, R. G., Chemical Reactivity Assessment Using Reactive Paper Spray Ionization Mass Spectrometry: The Katritzky Reaction. *ChemPlusChem* **2013,** *78* (9), 1142-1148.

28. Romanski, J.; Nowak, P.; Kosinski, K.; Jurczak, J., High-pressure transesterification of sterically hindered esters. *Tetrahedron Lett.* **2012,** *53* (39), 5287-5289.

29. Heravi, M. M.; Hashemi, E., Recent applications of the Suzuki reaction in total synthesis. *Tetrahedron* **2012,** *68* (45), 9145-9178.

30. Chatterjee, A.; Ward, T. R., Recent Advances in the Palladium Catalyzed Suzuki–Miyaura Cross-Coupling Reaction in Water. *Catal. Lett.* **2016,** *146* (4), 820-840.

31. Oehme, G.; Paetzold, E., Efficient two-phase Suzuki reaction catalyzed by palladium complexes with water-soluble phosphine ligands and detergents as phase-transfer reagents *Journal of Molecular Catalysis A: Chemical*
2000, *152*, 69-79.

32. Jung, Y.; Marcus, R. A., On the Theory of Organic Ctalysis "on Water". *J. Am. Chem. Soc.* **2007,** *129*, 5492-5502.

33. Smith, G. B.; Dezeny, G. C.; Hughes, D. L.; King, A. O.; Verhoeven, T. R., Mechanistic Studies of the Suzuki Cross-Coupling Reaction. *J. Org. Chem.* **1994,** *59*, 8151-8156.

VITA

Stephen Ayrton was born in Sheffield, UK, in 1991 to parents Francis Stephen Ayrton and Nicola Kay Ayrton. He spent six years there before moving to Leeds, UK, where he attended St. Margaret's primary school and subsequently Horsforth secondary school, where he studied Art, Maths and Chemistry towards the end of his secondary education.

After secondary school, Stephen attended the University of Bradford where, under the guidance of Dr. Richard Bowen, he developed a love of organic synthesis and mass spectrometry. During his undergraduate studies, Stephen studied the ion chemistry of halogenostyrylbenzoxazoles, an ongoing research interest of Dr. Bowen. During his subsequent MChem. coursework, Stephen studied the ion chemistry of indoles, during the course of which, he observed an interesting oxidative coupling reaction which appeared to be induced by electrospray.

During the presentation of this work at a joint RSC/BMSS conference in honour of Drs Kieth Jennings and Jim Scrivens, Stephen met Dr. R. G. Cooks. This interaction inspired Stephen to apply to Purdue University to undertake a Ph.D. in Dr. Cooks' lab.

Stephen has been fortunate enough to have started a family during his Ph.D. career, and his daughter, Isabelle, has served as an incredible source of inspiration and motivation throughout.

PUBLICATIONS

1. Ayrton, S. T., Jones, G. R., Couce, D. S., Morris, M. R., Cooks, R. G., Uncatalyzed, Regioselective Oxidation of Saturated Hydrocarbons in an Ambient Corona Discharge. *Angew. Chem. Int. Ed.*, Accepted
2. Ayrton, S. T., Chen, X., Bain, R. M., Pulliam, C. J., Achmatowicz, M., Flick, T. G., Ren, D., Cooks, R. G., Gas-Phase Ion Chemistry to Determine isoAspartate in a Peptide. In preparation
3. Bain, R. M.‡, Ayrton, S. T.‡, Cooks, R. G., Fischer Indole Synthesis in the Gas Phase, the Solution Phase, and at the Electrospray Droplet Interface. *J. Am. Chem. Soc.* **2017,** *28*, 1359-1364.
4. Ayrton, S. T., Cooks, R. G., Pugia, M., Molecular labels for analysis of amines and diols by spray based ionization-mass spectrometry. *Analyst* **2016,** *141*, 5398-5403.
5. Bain, R. M., Pulliam, C. J., Ayrton, S. T., Bain, K., Cooks, R. G., Accelerated Hydrazone Formation in Charged Microdroplets. *Rapid Comm. Mass Spec.* **2016,** *30*, 1875-1878.
6. Bain, R. M., Yan, X., Raab, S. A., Ayrton, S. T., Flick, T. G., Cooks, R. G., On-line chiral analysis using the kinetic method, *Analyst* **2016,** *141*, 2441-2446.
7. Baird, Z., Pirro, V., Ayrton, S. T., Hollerback, A., Hanau, C., Marfurt, K., Foltz, M., Cooks, R. G., Pugia, M., Tumor Cell Detection by Mass Spectrometry Using Signal Ion Emission Reactive Release Amplification, *Anal Chem* **2016**, *88*, 6971-6975.

‡ Authors contributed equally

A Journal of the Gesellschaft Deutscher Chemiker
Angewandte
GDCh
International Edition
Chemie
www.angewandte.org

Accepted Article

Titl Uncatalyzed, Regioselective Oxidation of Saturated Hydrocarbons in an Ambient Corona Discharge

thors: Stephen T Ayrton, Gareth Rhys Jones, David Douce, Mike Morris, and R Graham Cooks

To be cited as: *Angew Chem. Int. Ed.* 10.1002/anie.201711190
Angew Chem. 10.1002/ange.201711190

Link to VoR: http://dx.doi.org/10.1002/anie.201711190
http://dx.doi.org/10.1002/ange.201711190

WILEY-VCH

Angewandte Chemie International Edition 10.1002/anie.201711190

WILEY-VCH

COMMUNICATION

Uncatalyzed, Regioselective Oxidation of Saturated Hydrocarbons in an Ambient Corona Discharge

S. T. Ayrton[a], G. R. ones[b], D. S. Douce[b], M. R. Morris[b], R. G. Cooks*[a]

Abstract: Atmospheric pressure chemical ionization (APCI) in air or in nitrogen with just traces of oxygen is shown to yield regioselective oxidation, dehydrogenation and fragmentation of alkanes. Ozone is produced from ambient oxygen in-situ and is responsible for the observed ion chemistry, which includes partial oxidation to ketones and C-C cleavage to give aldehydes. The mechanism of oxidation is explored and relationships between ionic species produced from individual alkanes is established. Unusually, dehydrogenation occurs via water loss. Competitive incorporation into the hydrocarbon chain of nitrogen vs oxygen as a mode of ionization is also demonstrated.

Saturated hydrocarbons are notoriously difficult substrates for chemical reactions. Classical reactions are not site selective and partial oxidation is not achievable in satisfactory yields without the use of specialized catalysts[1]. Neither the C-H nor the C-C bonds are easy targets for chemical reaction as the literature of catalysis makes clear[2]. Saturated hydrocarbons are similarly difficult substrates for analysis by mass spectrometry. Electron ionization gives neither molecular weight information, nor specific structural information, unless used in conjunction with molecular beam cooling[3]. So resistant is this problem to solution by mass spectrometry that, in spite of modern atmospheric pressure ionization and electrospray methods[2c, 4], including specialized methods like reactions with metal ions[5], the decades-old technique of field ionization is still favored by many for the determination of alkane molecular weight distributions[6]. Nevertheless, low-powered atmospheric pressure plasmas are of increasing interest as ionization sources in commercial mass spectrometers because they generate molecular weight diagnostic $[M–H]^+$ ions[4c, 7]. In this paper, we demonstrate controlled addition of N and O to hydrocarbons using ion/molecule reactions. This provides both a method of chemical analysis and forms the basis for small-scale collection of oxidized molecules.

This study builds on the previous observation of nitrogen atom insertion into saturated hydrocarbons during paper based ionization to generate imines, observed as $[M+N]^+$ ions.[8] This involves indiscriminate N atom insertion along the carbon backbone.

Somewhat related plasma-induced ambient reactions include oxygen addition to benzene to form phenol[9] and oxygen-for-CH substitution to form pyrylium from benzene[ ]. More closely related is the formation of $[M+O–3H]^+$ ions from alkanes in an atmospheric pressure microplasma[ ], the mechanism of which has not been established. The mechanism of nitrogen atom insertion has previously been elucidated[8b]. Here, we set out to understand some of the complex oxidation processes that occur in ambient plasmas.

Standard APCI sources have not previously been shown to give oxygen or nitrogen addition products of alkanes. However, oxidized species were observed in the APCI mass spectra of saturated hydrocarbons when air was intentionally introduced into the ion source region (Fig.1, for more examples see SI sections 6 and 7). Fig. 1B and C show the molecular ion region of *n*-nonane when ionized using a commercial APCI system in a nitrogen atmosphere containing traces of oxygen, which were introduced through a fused silica capillary (Fig. A). The major peaks correspond, as shown by exact mass measurements, to $[M+O-5H]^+$, $[M+O-3H]^+$, $[M+O-H]^+$, $[M+N-2H]^+$, and $[M+N]^+$. By modifying the plasma conditions, it is possible to select for either oxygen or nitrogen insertion (Figs. B, C). When ionization takes place in a nitrogen atmosphere with traces of oxygen at low corona current, nitrogen addition is strongly favored over oxygen addition. At higher currents, the opposite is true.

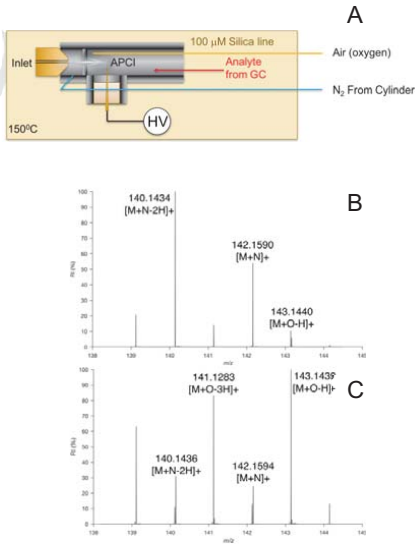

Figure 1. Molecular ion region of the mass spectrum of *n*-nonane ionized by APCI apparatus (a) to produce; b) products of N-fixation and c) products of oxidation (QToF data)

[a] S. T. Ayrton and R. G. Cooks,
Department of Chemistry
Purdue University
560 Oval Drive
E-mail: cooks@purdue.edu
[b] G. R. Jones, D. S. Douce and M. R. Morris
MS Research
Waters Corporation
Wilmslow, UK

Supporting information for this article is given via a link at the end of the document.

These observations led to offline experiments to determine the structures of the oxidized ions. The APCI ion source was removed from the mass spectrometer and operated with an external power supply and *n*-nonane was introduced into the ionization region in the gas phase via a fused silica capillary leading from a heated vial (Fig. c). The plasma was struck and, without the suction of the instrument to pneumatically guide the resulting ions, they were deposited onto the grounded surface of the ionization source. After 3 h, the ion source was washed with hexane and the washings were analyzed by GC-MS. Comparison of retention times (SI Section 2) indicated that the major product was 3-nonanone. Comparison to full scan APCI MS spectra (which under these conditions yielded characteristic fragment ions) of ketone standards (Figure 2) confirmed that the oxidation was regioselective, producing 3-nonanone as the major product. The data also suggest a minor proportion of 5-nonanone but no 2- or 4-nonanone, as discussed in the SI (Section 2).

The only reasonable primary sources of the added oxygen are water and dioxygen. Intentional introduction of water into the ionization region (SI Section 3) showed that this was not the oxygen source. By increasing the air flow into the ionization region, or flowing in pure oxygen, oxidation became incrementally more favorable (SI section 4). Oxygen is known to produce ozone in corona discharges[ ] and is likely responsible for the oxidation processes reported here. Ozone is a known reagent for the oxidation of saturated hydrocarbons.[1]

Probe APCI experiments, where pure nonane was applied directly to the APCI needle, yielded the same ions as the GC-APCI experiment, with the notable addition of a series of O adducts (Fig. A), which are apparently too fragile to survive in analytically useful abundance unless relatively high concentrations of hydrocarbon are present. Equivalent data for heptane is presented in Fig. S5.1. The adducts corresponded to the protonated ([M+O +H]$^+$) and the hydride abstracted ([M+O -H]$^+$) forms of the ozone adduct. The former is likely to be the product of the neutral-neutral interaction documented by Lee *et al.*[a] , which is subsequently protonated, while the latter is interpreted as the product of the ion-molecule interaction between M-H$^+$ and neutral O . Evidence for this comes from the heavier

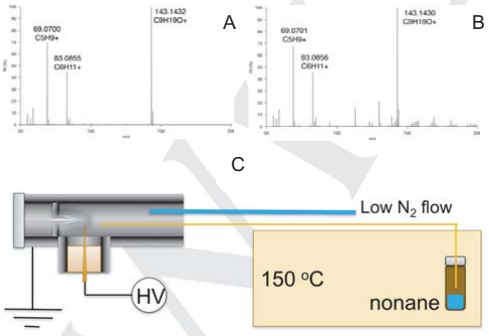

Figure 2. Full scan APCI mass spectra of a) major collected product of n-nonane APCI; b) authentic -nonanone; c) illustration of the apparatus used to collect the oxidation product (QToF data)

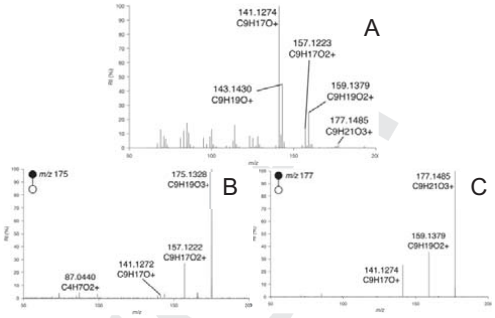

Figure 3. a) full scan probe APCI MS of nonane; b) CID product ion mass spectra of nonane+O -H$^+$ produced by probe APCI; c) nonane+O +H$^+$ (bottom) produced by probe APCI (Orbitrap data)

hydrocarbon substrates, which appear to sterically inhibit the reaction between the [M-H]$^+$ ion and ozone neutral and so exhibit strong [M-H]$^+$ signals in their spectra (Fig. S6.7).

The fragile ozone adducts fragmented upon isolation in the ion trap. The CID fragmentation spectra (Fig. B, 3C) recoded for [M+O -H]$^+$ and [M+O +H]$^+$ contained the major species under study in this report ([M+O-3H]$^+$, [M+O -H]$^+$,etc.), proving the key link between the ozone adducts and the oxygen-bearing products.

As already noted, the major ions typically produced from saturated hydrocarbons in APCI sources are hydride abstracted cations, [M–H]$^+$[4c, 7]. Rapid, intramolecular ,2 -hydride shifts should effectively mobilize this charge. Interaction of this ion with ozone would be stabilized through carbocation/dipole interactions (Scheme 1) and the observed regioselectivity of O addition is explained by preference for this interaction to occur at the end of the chain, where steric resistance would be lowest. The observed regioselectivity with preference for formation of -nonanone as well as dehydrogenated propionaldehyde formation is exactly matched by the proposed interaction. Note that the primary product of the proposed ion/molecule reaction (after structural rearrangement) is the protonated hydroperoxide, The [M+O–H]$^+$

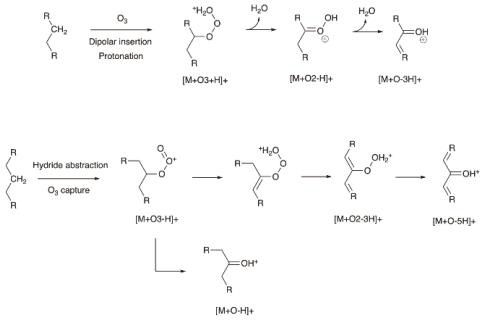

Scheme 1. Mechanisms (truncated) for the production of ketones via the ion/molecule and molecule/molecule reaction pathways.

Angewandte Chemie International Edition

10.1002/anie.201711190

WILEY-VCH

COMMUNICATION

species is closely related to the equivalent neutral pathway which was computed to undergo O-O bond cleavage and rearrangement to generate the ketone or C-C bond heterolysis to give the smaller chain aldehyde[a] . Mechanisms are presented in Scheme 1 while a more detailed scheme is given in the SI (Section 5). A particularly striking feature of the MS/MS data of the ozone adducts (Fig. B, C) is the loss of water as the route to the dehydrogenated ketones. This route contrasts with the more usual dehydrogenation by superoxide, recently reported in the case of amine dehydrogenation in a corona discharge.[15]

To investigate the regioselectivity of oxidation in more detail, two forms of reflux condensers were constructed (Figure 4). The first condenser (Fig. 4A) incorporated a pin-barrel corona discharge module in the neck of a simple reflux condenser to facilitate interaction between vapor-phase hydrocarbon and the discharge.

After refluxing *n*-heptane for two hours followed by *n*-nonane for another two hours in the same vessel, the residual liquid (trapped between the steel barrel and the neck of the reflux condenser) was dissolved in methanol and analyzed by nano electrospray ionization-MS (nESI-MS, Figure 5A). The observed species in the spectra corresponded to the dehydrogenated, oxidized compounds, viz. nonenone and heptenone.

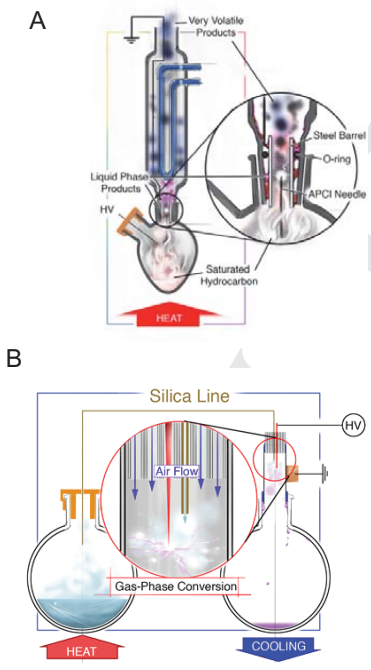

Figure 4. A. Reflux apparatus designed to maximize expose of hydrocarbon vapor to corona discharge but with inefficient trapping of volatile products B. Second reflux and vapor phase corona discharge apparatus with efficient trapping of volatile, fragmented and oxidized products.

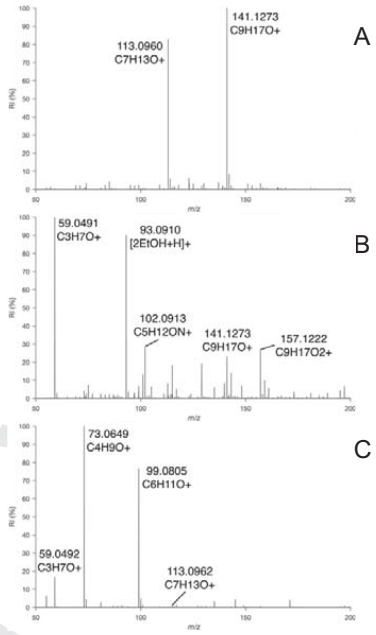

Figure 5. Products of oxidation of mixture of n-heptane and n-nonane generated in reflux apparatus of Fig. 4A (A); Collected fragmented products using second reflux apparatus (Fig.4B) with nonane (B) and heptane (C). (nESI-Orbitrap data)

The dehydrogenation products are readily observed in all mass spectra recorded using an APCI ion source (such as in Figure 1), but they are typically flanked by ions which are not dehydrogenated ($[M+O-H]^+$), as well as doubly-dehydrogenated ($[M+O-5H]^+$) ions. The experiments using the apparatus in Fig. 4A were performed off-line from the MS and using a different APCI setup from that used for MS and the chemical selectivity clearly favors the single dehydrogenation of the ketone, i.e. $[M+O-3H]^+$. The balance between this product (also reported by Nie et al.[ ]) and the deprotonated ketone $[M+O-H]^+$ is clearly condition-dependent.

During the experiment with the condenser in Fig. 4A odor was emitted from the top of the reflux condenser, which suggested that inefficient condensation was occurring and some material was escaping. In order to identify these vapors, a second apparatus was designed to transfer the vapor-phase chemicals from a hot vessel to a chilled vessel via an APCI discharge source (Fig. 4B). In this latter experiment, *n*-nonane was boiled in the first flask which forced it through the silica transfer line and into the region of corona discharge. The nESI-MS of the collected material showed a dominant ion with the chemical formula C H_7O (Fig. 5B). This observation parallels the GC-MS based assignment of the major product of nonane oxidation in the corona discharge as -nonanone. The interpretation of this data is that upon exposure to the corona discharge, the small amount of material that was transferred was efficiently oxidized and also fragmented to yield

propionaldehyde, a process known to be associated with the oxidation of hydrocarbons by ozone[a] .

The experiment was repeated with *n*-heptane and two prominent ions were observed. These ions had the molecular formulae, C_4H_9O and C_6H O (Fig. 5C). In this case, as with nonane, the recorded structures indicate the position of oxidation in the chain. The formulae of the two ions indicated that, as in the case of nonane, the positions of oxidation were separated by a methylene unit.

At low flow rates of hydrocarbon vapor (as in the initial GC-MS experiment), the chemistry that occurs in the APCI ion source is apparently very efficient. This is demonstrated by the fact that no appreciable signal was observed for residual nonane after the collection initial experiment was completed (using the apparatus in Fig. 2C), i.e. all the hydrocarbon was converted efficiently, which is illustrated by the GC trace which showed no signal at the retention time of *n*-nonane (ca. 4.2 min., Figure S .1). Clearly, there is a dependence of conversion efficiency on the plasma flux and the volume of hydrocarbon vapor allowed to flow through it.

The use of commercial APCI sources with the simple addition of a silica line to feed air into the ionization region allows selection between two types of chemical derivatization; oxygen or nitrogen insertion. This was demonstrated further using a range of hydrocarbon substrates, including nonane, tetradecane, octadecane and a polywax standard (a mixture of saturated *n*-alkanes of even chain lengths in the range of C -C_{80}). At low corona current, nitrogen fixation was recorded while at high current, oxidation was recorded. (SI Section 6). Oxygen insertion is associated with ketone formation as well as C-C cleavage and aldehyde formation. Nitrogen insertion occurs with C-C insertion; it is better suited to the determination of molecular weight, especially in mixtures, because it gives spectra that are largely free of fragment and adduct ions.

Regioselective oxidation of saturated hydrocarbons without a catalyst, evidenced by the GC-MS experiments and the selective production of aldehyde fragments, has been demonstrated by exposure to a corona discharge in air. Evidence has been provided of a complex mechanism of oxidation and of interrelationships between ionic species leading to oxidized materials. The simple methodology by which hydrocarbons can be selectively derivatized in a corona discharge is noteworthy. The standard petrochemical industry response to the complexity of naturally occurring hydrocarbons [4] has been to convert their alkane components catalytically into small oxidized and/or dehydrogenated molecules. There might be merit in further exploration of the ketone and aldehyde production processes described here.

Acknowledgements

The authors gratefully acknowledge helpful conversations with Ryan M. Bain and Andreas Kaerner. This material is based in part upon work supported by the U.S. Department of Energy, Office of Science, Office of Basic Energy Sciences, Separations and Analysis Program (DE-FG02- 6ER15807). This work was also supported by the Eli Lilly LRAP (17045108) program.

Keywords: Oxidation, Ion molecule reactions, saturated hydrocarbon, mass spectrometry

[1] a) A. E. Shiov, G. B. Shul'pin, Chem. Rev. 1997, 97, 2879-2893; b) X. H. Li, J. S. Chen, X. Wang, J. Sun, M. Antonietti, J. Am. Chem. Soc. 2011, 133, 8074-8077.

[2] a) H. Schwarz, Angew. Chem. Int. Ed. Engl. 2011, 50, 10096-10115; b) H. Schwarz, Catal. Sci. Technol. 2017, 7, 4302-4314; c) U. R. Pillai, E. Sahle-Demessie, Chem. Commun. (Camb) 2005, 2256-2258.

[3] A. B. Fialkov, A. Gordin, A. Amirav, J. Chromatogr. A 8, 1195, 127-135.

[4] a) C. Wu, K. Qian, M. Nefliu, R. G. Cooks, J. Am. Soc. Mass. Spectrom. 2010, 21, 61-267; b) D. Zhan, J. B. Fenn, Int. J. Mass spectrom. , 194, 197-208; c) C. Jin, J. Viidanoja, M. Li, Y. Zhang, E. Ikonen, A. Root, M. Romanczyk, J. Manheim, E. Dziekonski, H. I. Kenttamaa, Anal. Chem. 6, 88, 10592-10598.

[5] a) P. Duan, M. Fu, D. S. Pinkston, S. C. Habicht, H. I. Kenttamaa, J. Am. Chem. Soc. 2007, 129, 9266-9267; b) L. I. Grace, A. Abo-Riziq, M. S. deVries, J. Am. Soc. Mass. Spectrom. 2005, 16, 437-440.

[6] a) Z. Linang, C. S. Hsu, Energy Fuels 1998, 12, 637-643; b) C. S. Hsu, M. Green, Rapid Commun. Mass Spectrom. 2001.

[7] N. Hourani, N. Kuhnert, Rapid Commun. Mass Spectrom. 2012, 26, 2365-2371.

[8] a) G. Li, X. Li, Z. Ouyang, R. G. Cooks, Angew. Chem. Int. Ed. 2013, 52, 1040-1043; b) X. Li, X. Yan, R. G. Cooks, Int. J. Mass spectrom. 2017, 418, 79-85.

[9] N. Na, Y. Xia, Z. Zhu, X. Zhang, R. G. Cooks, Angew. Chem. Int. Ed. Engl. 2009, 48, 2017-2019.

[10] S. P. Badal, T. D. Ratcliff, Y. You, C. M. Breneman, J. T. Shelley, J. Am. Soc. Mass. Spectrom. 2017, 28, -1020.

[11] X. Xie, Z. Wang, Y. Li, L. Zhan, Z. Nie, J. Am. Soc. Mass. Spectrom. 2017, 28, 1036-1047.

[12] a) A. Yehia, A. Mizuno, Int. J. Plasma Environ. Sci. Tech. 2008, 2, 44-49; b) K. Yanallah, F. Pontiga, A. Fernández-Rueda, A. Castellanos, A. Belasri, J. Phys. D: Appl. Phys. 2008, 41.

[13] a) R. Lee, M. L. Coote, Phys. Chem. Chem. Phys. 2016, 18, 24663-24671; bC. Clarence, S. J. Schubert, R. N. Pease, J. Am. Chem. Soc. 1956, 78, 2044- 48.

[14] A. G. Marshall and Ryan P. Rodgers, Acc. Chem. Res. , *37*, 53 -59

Angewandte Chemie International Edition

10.1002/anie.201711190

WILEY-VCH

COMMUNICATION

Atmospheric pressure corona discharge ionization (APCI) in air or in the presence of traces of oxygen is shown to yield regioselective oxidation, dehydrogenation and fragmentation. The chemistry of oxidation is explored and relationships between ionic species produced from single analytes is established. Ozone is produced from ambient oxygen in-situ and dehydration is responsible for the observed dehydrogenated ketones.

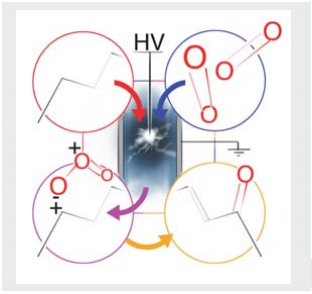

*S. T. Ayrton, G. R. Jones, D. S. Douce, . R. Morris, R. G. Cooks**

ge No. – Page No.

ncatalyzed, Regioselective xidation of Saturated Hydrocarbons in an Ambient Corona Discharge